HYBRID METHOD OF SINGLE SIDEBAND SIGNAL GENERATION

Sugihono Kadarisman

NAVAL POSTGRADUATE SCHOOL
Monterey, California

THESIS

HYBRID METHOD OF
SINGLE SIDEBAND SIGNAL GENERATION

by

Sugihono Kadarisman

December 1974

Thesis Advisor: G.D. Ewing

Approved for public release; distribution unlimited.

UNCLASSIFIED

SECURITY CLASSIFICATION OF THIS PAGE (When Data Entered)

REPORT DOCUMENTATION PAGE

READ INSTRUCTIONS BEFORE COMPLETING FORM

1. REPORT NUMBER	2. GOVT ACCESSION NO. / 3. RECIPIENT'S CATALOG NUMBER
4. TITLE (and Subtitle) Hybrid Method of Single Sideband Signal Generation	5. TYPE OF REPORT & PERIOD COVERED Engineer's Thesis; December 1974 6. PERFORMING ORG. REPORT NUMBER
7. AUTHOR(s) Sugihono Kadarisman	8. CONTRACT OR GRANT NUMBER(s)
9. PERFORMING ORGANIZATION NAME AND ADDRESS Naval Postgraduate School Monterey, California 93940	10. PROGRAM ELEMENT, PROJECT, TASK AREA & WORK UNIT NUMBERS
11. CONTROLLING OFFICE NAME AND ADDRESS Naval Postgraduate School Monterey, California 93940	12. REPORT DATE December 1974 13. NUMBER OF PAGES 176
14. MONITORING AGENCY NAME & ADDRESS (if different from Controlling Office) Naval Postgraduate School Monterey, California 93940	15. SECURITY CLASS. (of this report) Unclassified 15a. DECLASSIFICATION/DOWNGRADING SCHEDULE

16. DISTRIBUTION STATEMENT (of this Report)

Approved for public release; distribution unlimited.

17. DISTRIBUTION STATEMENT (of the abstract entered in Block 20, if different from Report)

18. SUPPLEMENTARY NOTES

19. KEY WORDS (Continue on reverse side if necessary and identify by block number)

Single Sideband Signal Generation

20. ABSTRACT (Continue on reverse side if necessary and identify by block number)

The Hybrid SSB-signal generation method is introduced. It is a combination of phase-shift and filter methods in SSB-signal generation. The motivation is to design a high degree of unwanted signal suppression with less complexities. Computer analysis is used to determine the correct time-constants to achieve high degree phase-shift accuracy. The way is open for designing an even higher degree of performance by increasing

(20. ABSTRACT Continued)

the all-pass network order or the number of Chebyshev function poles within a reasonable practicality. Due to effective utilization of the phase-shift method, the hybrid-method has a significant advantage in the low audio frequency range and helps the burdens of the demodulation process. The hybrid SSB-signal generation technique may find its greatest potential for multichannel sound transmission over international telecommunication paths. Inductorless realization makes it attractive and compatible with miniaturization.

Hybrid Method of

Single Sideband Signal Generation

by

Sugihono Kadarisman
Lieutenant Commander, Indonesian Navy
B.A.Sc., University of British Columbia, 1961
M.S., Naval Postgraduate School, 1974

Submitted in partial fulfillment of the
requirements for the degree of

ELECTRICAL ENGINEER

from the

NAVAL POSTGRADUATE SCHOOL
December 1974

The[illegible]

ABSTRACT

The Hybrid SSB-signal generation method is introduced. It is a combination of phase-shift and filter methods in SSB-signal generation. The motivation is to design a high degree of unwanted signal suppression with less complexities. Computer analysis is used to determine the correct time-constants to achieve high degree phase-shift accuracy. The way is open for designing an even higher degree of performance by increasing the all-pass network order or the number of Chebyshev function poles within a reasonable practicality. Due to effective utilization of the phase-shift method, the hybrid-method has a significant advantage in the low audio frequency range and helps the burdens of the demodulation process. The hybrid SSB-signal generation technique may find its greatest potential for multichannel sound transmission over international telecommunication paths. Inductorless realization makes it attractive and compatible with miniaturization.

TABLE OF CONTENTS

ACKNOWLEDGMENTS

The author wishes to express his utmost gratitude to Prof. Dr. G.D. Ewing, whose continuous guidance and assistance in making this thesis possible have helped bridge the gap between theoretical knowledge which the author has gained while being an officer student at the U.S. Naval Postgraduate School and application of this knowledge to actual design of a system in the real world.

I. INTRODUCTION

Single-sideband (SSB) signals and their techniques of production and reproduction have long been known and implemented. It is widely applied in frequency multiplex signal transmission in telecommunications and may become potentially applicable for future stereophonic broadcasting systems, in the context of conserving the frequency spectrum. The specifications regarding this matter are recommended by an international organization called the International Telegraph and Telephone Consultative Committee (CCITT).

It is foreseen that in the future the application of SSB signals will still be widespread. While SSB signaling itself is not new, its generation continues to offer challenges in devising new techniques. Because of the rapid advancement in electronic technology, the performance requirements of SSB equipments recommended by CCITT change from time to time. One of the most important requirements involves the ability of a filtering system to pass signals in the desired frequency band and suppress signals outside the band in an "abrupt" way. In more popular terms this means that the system must have a "sharp cutoff" or "steep skirt" characteristic. A measure of this characteristic is the dB sideband suppression, which is the ratio expressed in dB of the desired sideband level to the undesired sideband level.

It is this dB requirement which has become more and more severe as the signal reproduction demands ever increasing quality. The sharper the passband characteristic curve at cutoff, the closer adjacent information channels may be allocated within the frequency spectrum, thus more efficient utilization of the frequency spectrum is achieved. Sharp cutoff characteristic together with the use of SSB techniques increase this efficiency even more. However, the provision of guard bands between adjacent channels must be included to suppress the effect of crosstalk between them. Recommendations regarding this matter are also made by CCITT.

Modern SSB-communication systems demand large suppression level between the passband and the rejection band. A 50 dB suppression level within 4 kHz guard band for a 2-channel communication system with up to 15 kHz (high fidelity) signals have been considered adequate in the past, but today, with more sophisticated technology this level requirement becomes more stringent, and in the future it certainly will become even more so. At present time several manufacturers claim to have been able to reach as high as 95 dB suppression level.

In SSB generation, a filter may be employed to suppress (reject) the unwanted sideband after translation of the information (audio frequency) band to an intermediate band. Note that frequency translations and filterings are generally carried out via intermediate frequency band(s) before reaching

the final operating frequency stage. This technique is to make the filtering process easier, more accurate and better designed with a given complexity of the filter.

There are several known types of filter which can serve this purpose. These are LC-filters, mechanical (magnetostrictive)-filters, crystal-filters and active-filters. Typical operating frequency range of LC-filters is between 1 kHz to 500 kHz and their suppression characteristics are good. One disadvantage of LC-filters are their relatively large size. Mechanical (magnetostrictive)-filters have typical operating frequency range between 100 kHz to 500 kHz and crystal-filters have typical operating frequency range between 10 kHz to as high as 10 MHz. Filters of these two types are categorized as medium sized. A suppression level of 50 dB is typical of them. When there is a need of filters in miniaturized equipments, active-filters are used. Because their size can be made small, they are compatible with integrated circuits. In addition, active-filters have another advantage over filters of the preceding types in the low frequency range. Typical operating frequency range of active-filters for SSB application is between several Hertz to about 500 kHz.

In the synthesis of filters, the method of approximation using Butterworth or Chebyshev functions may be employed in the design. The number of poles in the filter's polynomial (transfer) function determines the steepness of the "skirt".

The more poles it has, the steeper the skirt. Since this method is an approximation one, errors can not be avoided. These errors take the form of amplitude ripples oscillating in the passband as well as in the rejection band (Chebyshev approximation). With more poles in the transfer function, the ripple amplitude becomes smaller. In later discussions, it will be evident that the tolerable level of these ripples and the desired suppression level within a specified frequency range determine the required number of poles.

Theoretically, a filter designed using these techniques can meet the high suppression level requirement, simply by providing enough poles in its transfer function. However, the implementation may not be easy. Complexities caused by the crowded poles arise. One might be able to construct a filter meeting the high degree of performance level specified, but he must also pay more (expensive). Economics also play an important role in the design process.

Another method of SSB generation which has also long been known is the phase-shift method. In this method filters are not employed; instead, a sideband cancellation technique is utilized. However, this method needs a high degree of accuracy in the audio phase-shift circuit. The incoming audio signal is split into two. In the operating audio frequency range these two signal components must be maintained at exactly the same amplitude and at 90° phase difference. While the amplitude requirement is not very hard to meet,

the phase requirement is crucial. In order to perform (alone) as a sideband suppressor effectively, the phase-shift deviation from 90° must be less than 1°. Indeed, a difference of only 0.5° in the phase-shift error causes a considerable difference (in the order of 4 dB) in the sideband suppression level. If the phase-shift method alone were to carry out a 95 dB sideband suppression, a formidable task would be encountered. This difficult task involves difficulties in the design process and the provision of very highly accurate (very small tolerance) circuit components. In addition, the fact that a wide operating frequency range is desired for high fidelity adds to this complexity. For these reasons, the phase-shift method has not been very successful in the past. Although one might be able to construct a system with a sideband suppression level of the order of 95 dB throughout 30 Hz to 15 kHz frequency range, the cost would be enormous, because of the many precision higher order all-pass circuits required. A more important reason for this difficulty is the fact that in the design process the circuit parameters are very difficult to determine with such a high degree accuracy of the phase-shift. The condition, i.e., the values of many time constants (or conversely cutoff frequencies) must be searched such that the maximum phase-shift error is minimum throughout the specified operating frequency range. The wider the specified frequency range, the larger the number of time constants required and hence the optimum condition search becomes more difficult.

Fortunately, with the aid of digital computers today, this design burden can be relieved and the very time-consuming computation efforts become much reduced. It is the purpose of the following discussions, therefore, to revive the phase-shift method and put it back into focus.

Theoretically, the phase-shift error can be made smaller and smaller by increasing the order of the all-pass functions, but as a consequence, the complexity as well as the cost also increase.

Having been introduced to the two methods of SSB generation, and also important, having recognized the complexities and economic considerations involved, one starts thinking of combining the two and hopes that the combination will provide a less complex and expensive system, yet still performs as desired. In the following discussions the two methods will be analyzed one after another and then the combination or the "hybrid"-method of SSB generation will be presented. After determining the necessary equations and simplifying them in order to be able to carry out their realization, proposals regarding how one could build the hybrid SSB generator are also presented. It is interesting to observe that only R-C and active circuit components are involved in the realization (Inductorless).

II. SIDEBAND SUPPRESSION METHODS

The following discussions deal with methods of how one could generate single-sideband signals. As has been mentioned earlier, the phase-shift and filter methods have long been known. A combination of the two may be called a "Hybrid" method. The discussion of the hybrid method cannot be undertaken without first discussing the previous two. Therefore, the emphasis is really on the analysis of the phase-shift and filter methods, their realization, the supporting theory, etc. The combination of the two methods or hybrid is primarily motivated by sharing the burdens or limitations borne by the two methods such that the design and hopefully the cost could be offered more moderately.

A. PHASE-SHIFT METHOD

1. Functional Analysis

The principle involved in the generation of single-sideband signal by phase-shift method is shown by the block diagram in Fig. 1. It is centered about two separate simultaneous modulation processes and the combination of the modulation products. The audio (baseband) signal is split into two components that are identical except for a phase difference of 90° throughout the baseband frequency range. The output of the carrier frequency oscillator (L.O.) which may be at the operating frequency or usually at a fixed

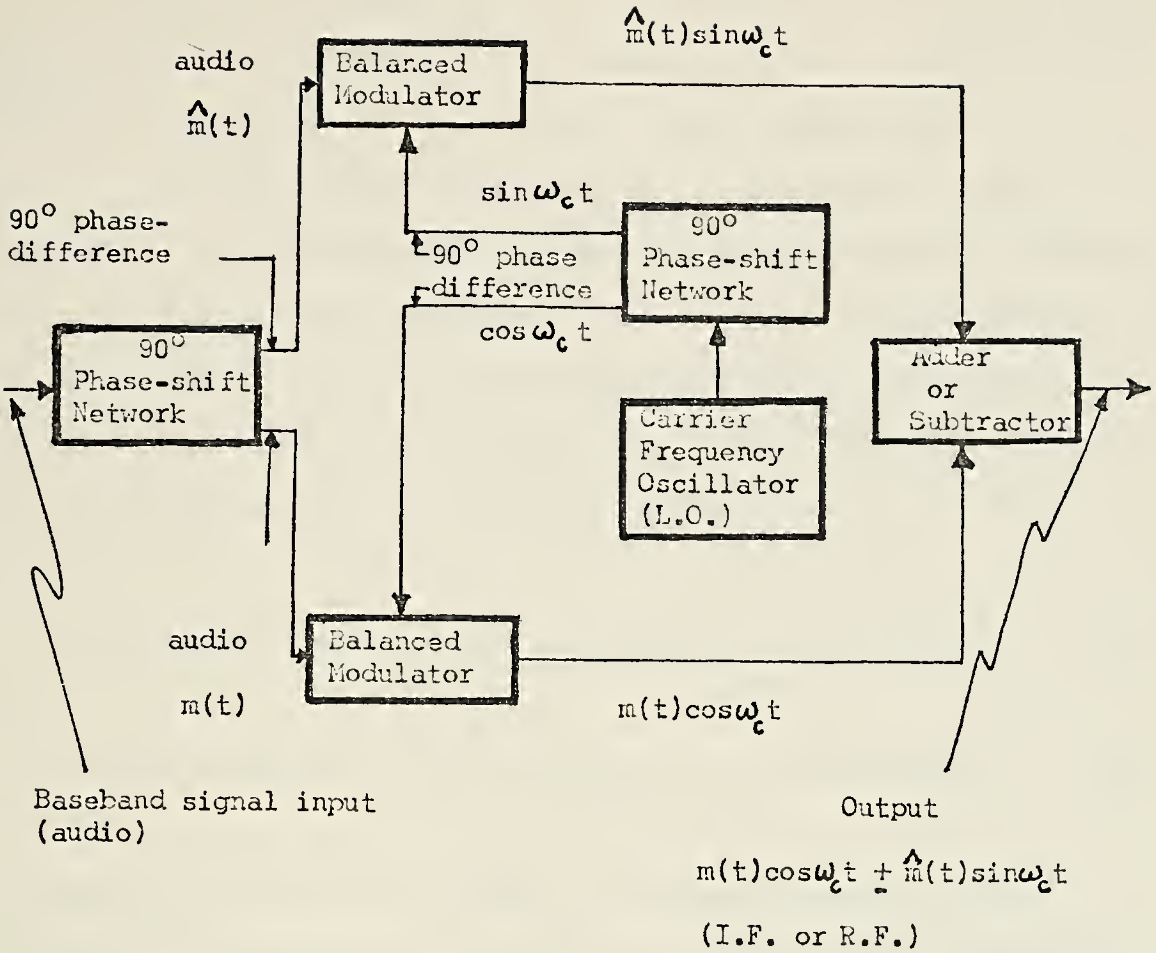

FIG. 1. Phase-Shift Method for Generating SSB Signals

intermediate frequency, is also split into two separate components having a 90° phase difference. One carrier frequency and one audio component are combined in each of two separate balanced modulators. The carrier is suppressed in the modulators, and the relative phases of the sidebands are such that one sideband is balanced out while the other sideband is accentuated in the combined output. If the output from the balanced modulator is of sufficient amplitude,

such a sideband generator can work directly into the antenna, the baseband of a microwave or cable system. The power can also be increased in a following linear amplifier.

To see analytically how the arrangement in Fig. 1 operates, let the baseband signal be sinusoidal and appears at the input to one modulator as $\cos \omega_m t$ and hence as $\sin \omega_m t$ at the other. Also, let the carrier be $\cos \omega_c t$ at one modulator and hence $\sin \omega_c t$ at the other. Then the outputs of the balanced modulators (multipliers) are

$$\cos \omega_m t \cos \omega_c t = \frac{1}{2} [\cos(\omega_c - \omega_m)t + \cos(\omega_c + \omega_m)t] \tag{1}$$

$$\sin \omega_m t \sin \omega_c t = \frac{1}{2} [\cos(\omega_c - \omega_m)t - \cos(\omega_c + \omega_m)t] \tag{2}$$

If these waveforms are added, the lower sideband (LSB) results; if subtracted, the upper sideband (USB) appears at the output. Hence in this case,

$$\text{LSB:} \quad \cos(\omega_c - \omega_m)t \tag{3}$$

$$\text{USB:} \quad \cos(\omega_c + \omega_m)t \tag{4}$$

In general, if the modulation m(t) is given by

$$m(t) = \sum_{i=1}^{m} A_i \cos(\omega_i t + \theta_i) \tag{5}$$

then, using Fig. 1 it is seen clearly that the output of the SSB modulator is, in general

$$m(t)\cos\omega_c t \pm \hat{m}(t)\sin\omega_c t \qquad (6)$$

where

$$m(t) \equiv \sum_{i=1}^{m} A_i \sin(\omega_i t + \theta_i) \qquad (7)$$

2. <u>All-Pass Networks</u>

The success of the phase-shift method lies almost entirely on the audio (baseband) phase-shift circuit. The reasons for this have been mentioned earlier. It is the requirement of highly accurate 90° phase difference in the split baseband signals in a wide frequency spectrum (in the following design a spectrum of 30 Hz to 17 kHz is required) which consitutes the main concern in the design process. As for the other components, namely the balanced modulators, the adder/subtractor and the carrier phase-shift circuit, they do not present much difficulty. The carrier phase-shift circuit has only to operate at a fixed frequency.

Therefore, the theory of the phase-shift method is practically centered in the theory of building an audio (baseband) phase-shift circuit. It is evident that networks which are able to offer these characteristics, namely same amplitude and constant phase shift of the two outputs in a frequency range, are All Pass Networks. Depending on the required frequency range, several all-pass networks may be cascaded to obtain the desired characteristics.

Consider the following second order transfer function in the s-domain,

$$H(s) = \frac{(s-s_1)(s-s_1^*)}{(s-s_2)(s-s_2^*)} \tag{8}$$

where the zeros are conjugates and so are the poles; furthermore s_1 is the image of s_2 and s_1^* is the image of s_2^*. Equation (8) can then be written as

$$H(s) = \frac{(s-s_1)(s-s_1^*)}{(s+s_1)(s+s_1^*)} \tag{9}$$

The pole-zero configuration of H(s) in the s-plane is shown in Fig. 2. Note that such a function, which has zero(s) in the right hand side of the s-plane is also referred to as a non-minimum transfer function. A minimum transfer function has no zero(s) in the right hand side of the s-plane.

For $s = j\omega$ the value of $H(j\omega)$ and the argument of $H(j\omega)$ can be evaluated graphically. Since $|s+s_1^*| = |s-s_1|$ and $|s+s_1| = |s-s_1^*|$ for all ω, it is quite obvious that $|H(j\omega)|$ is always constant (unity) for all frequencies; therefore, H(s) is also called an All-Pass Function.

To investigate the phase response of $H(j\omega)$, the numerator and denominator of H(s) are called $F_a(s)$ and $F_b(s)$ respectively,

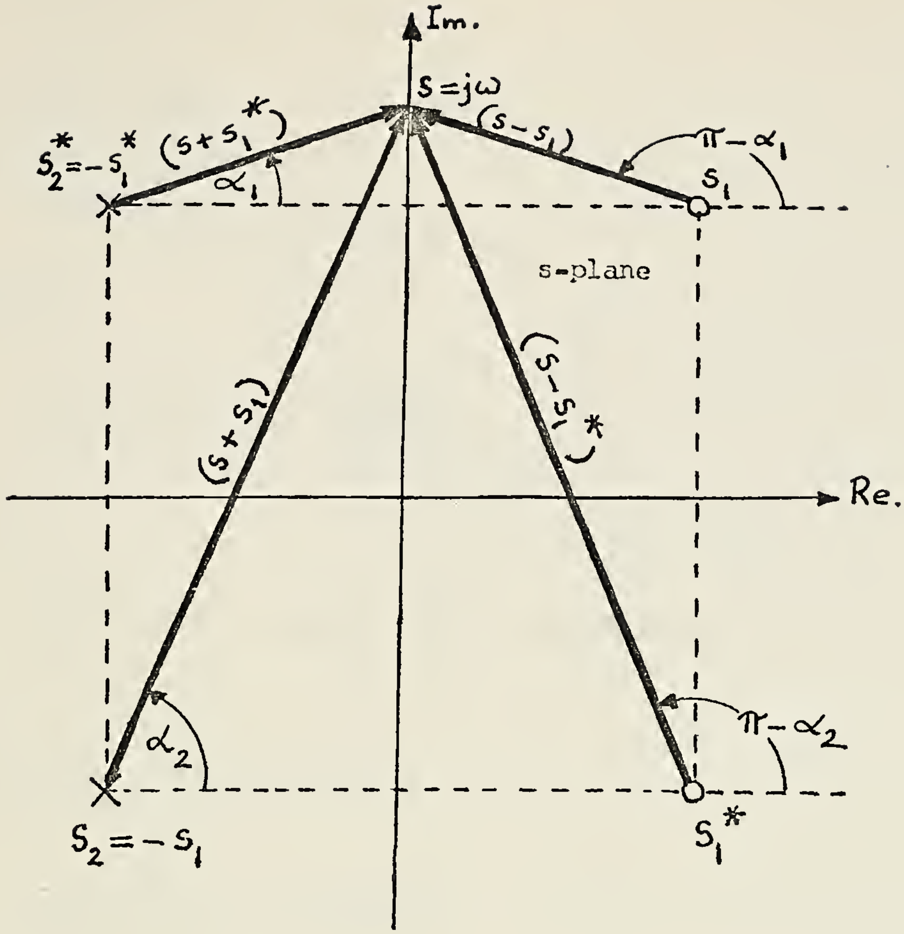

FIG. 2. Pole-zero Configuration of a Second Order All-Pass Transfer Function

$$F_a(s) = (s-s_1)(s-s_1^*) \tag{10a}$$

$$F_b(s) = (s+s_1)(s+s_1^*) \tag{10b}$$

For $s = j\omega$,

$$\arg F_a(j\omega) = (\pi-\alpha_1) + (\pi-\alpha_2) = 2\pi - (\alpha_1+\alpha_2) \tag{11}$$

and since an angle of 2π may be replaced by an angle of 0, i.e., no change of sign involved, Eq. (11) becomes

$$\arg F_a(j\omega) = -(\alpha_1+\alpha_2) \tag{12}$$

On the other hand,

$$\arg F_b(j\omega) = (\alpha_1+\alpha_2) \tag{13}$$

Therefore,

$$\arg H(j\omega) = \arg \frac{F_a(j\omega)}{F_b(j\omega)}$$

or

$$\arg H(j\omega) = \arg F_a(j\omega) - \arg F_b(j\omega) \tag{14}$$

and from Eqs. (12) and (13),

$$\arg H(j\omega) = -2(\alpha_1+\alpha_2) \tag{15}$$

The angles α_1 and α_2 depend on the frequency ω and it is well understood in circuit theory that the phase response (Bode phase plot) of $H(j\omega)$, or in other words, the plot of $\arg H(j\omega)$ versus frequency ω of Eq. (15) should look like one shown in Fig. 3. In this case ω_c is the cutoff frequency of the all-pass circuit which is equal to the magnitude of the distance from the origin to one of the poles on the s-plane; and ζ is the damping factor determined by the relative pole conjugate pair locations in the s-plane.

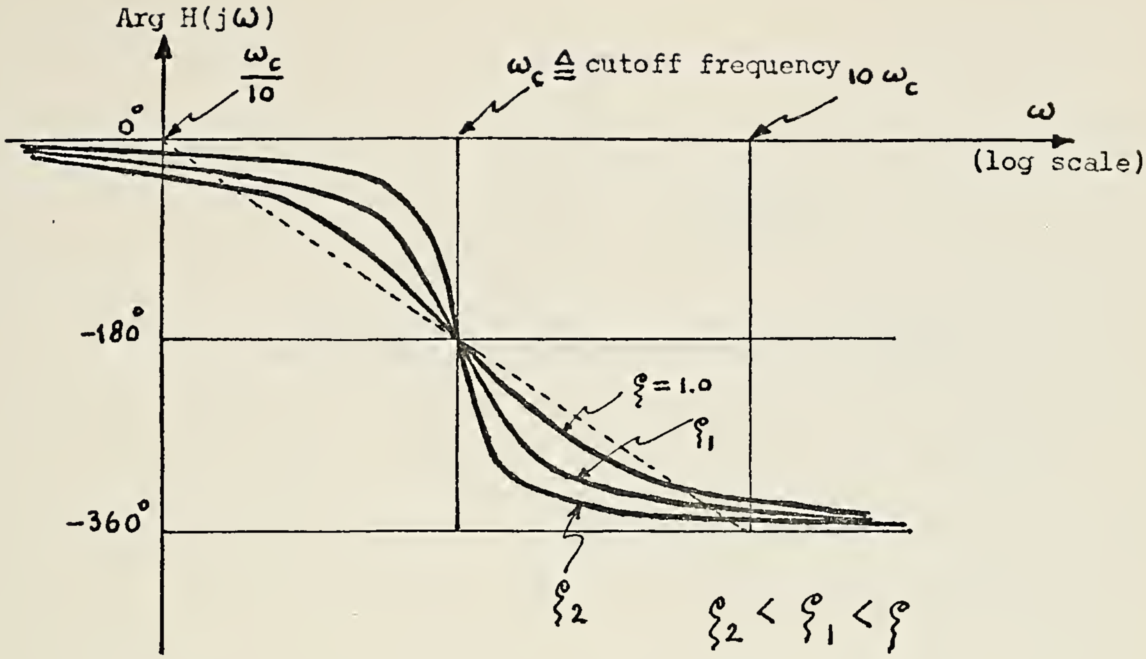

FIG. 3. Bode Phase Plot of a Second Order All-Pass Circuit

Figure 4 shows how, in a second order system, one can vary the damping factor,

$$\zeta = \cos\theta \tag{16}$$

to obtain the pole conjugate pair locations. The pole pair will travel along a semicircle as ζ is varied. The extreme cases occur at $\zeta = 0$ or $\theta = 90°$ when the system starts to oscillate (pole pair at points a and b) and at $\zeta = 1$ or $\theta = 0$ when the system is critically damped, i.e., the two conjugate poles coincide each other. At this point it is worthwhile to note that transfer functions referred to as second order systems are those with $0 \leq \zeta \leq 1$. Those with $\zeta > 1$ are not,

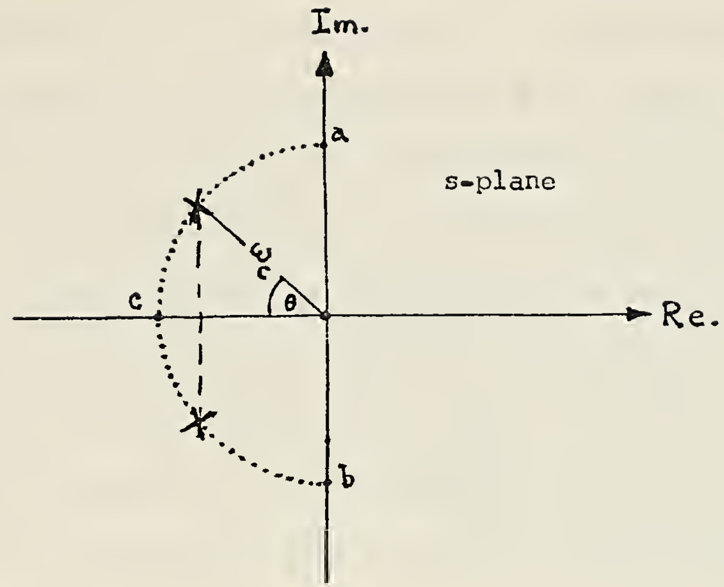

FIG. 4. Conjugate Pole Pair of a Second Order System

and may be considered as two first order systems in cascade, although they all may have a quadratic expression in the denominator of their transfer functions.

As it will be evident in the following discussions, the fact that the phase response of $H(j\omega)$ is almost linear in the frequency range portion between $\omega_c/10$ and $10\omega_c$ (Fig. 3) really offers about the only technique making use of this for building a constant phase-shift network in a band of frequencies. The most logical choice of ζ is obviously $\zeta = 1$ (network is critically damped), since it offers the longest "linear" portion of the phase response curve, in other words it makes the phase curve closest to linear in the widest possible frequency range compared to that if

smaller values of ζ were chosen. Linearity in the phase response is desirable in the shaping of the phase-shift circuit. This means that one of the poles is right on top of its conjugate on the negative real axis of the s-plane. Surprisingly, this situation gives rise to another blessing; as it will be evident later the realization of an all-pass network is simpler with the case where this situation is met, rather than with the case where the poles of the transfer function are conjugate pair with imaginary components ($\zeta < 1$). Note that these coincident poles are also called double or non-simple poles.

Consider now two all-pass functions $H_1(j\omega)$ and $H_2(j\omega)$ whose time constants, or cutoff frequencies, are shifted such that the phase response of $H_1(j\omega)$ differs from the phase response of $H_2(j\omega)$ by 90° throughout the frequency range. In this frequency region both response curves show considerable linearity as shown in Fig. 5. The damping factor of the two functions were taken the same and unity ($\zeta = 1$). The 90° phase-shift takes place in the region between points p and q, in which the frequency separation is less than one decade ($\approx$ 0.5 decade).

Therefore, to form a phase-shift circuit operating from 30 Hz to 15 kHz for example, one would require about six such networks cascaded if the phase-shift error is to be minimum in that frequency range.

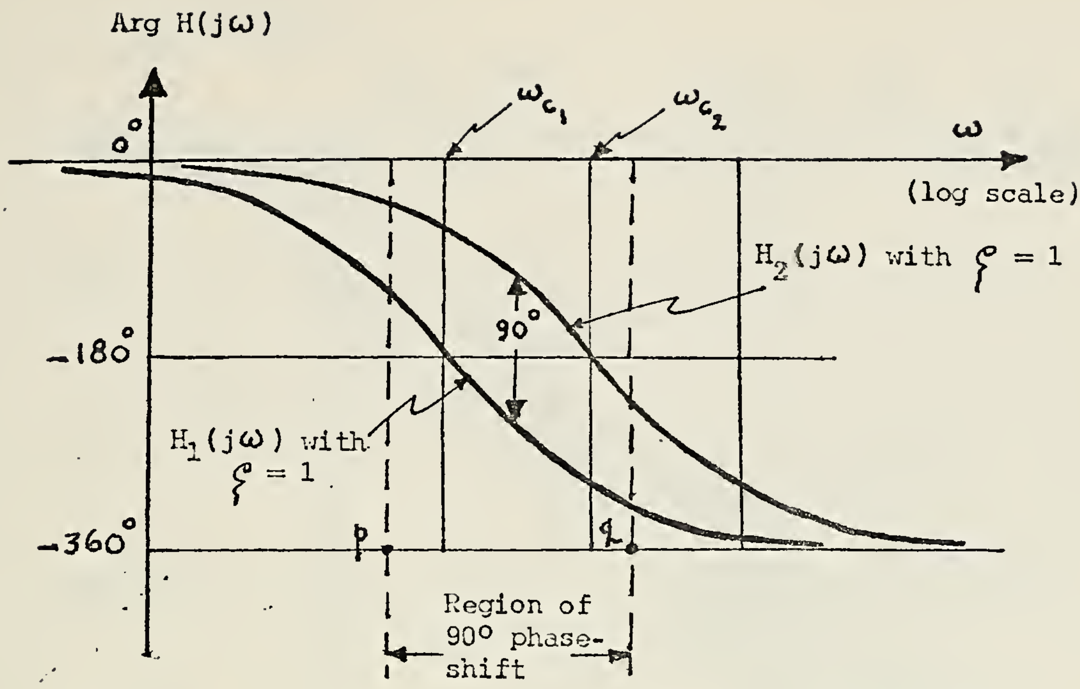

FIG. 5. Two Second Order All-Pass Functions $H_1(j\omega)$ and $H_2(j\omega)$ phase-shifted 90° apart ($\zeta = 1$)

To illustrate how the overall phase response looks, consider only two such cascade arrangements as shown in Fig. 6. It is clearly shown that the presence of 90° phase-shift error (ripples) as the frequency varies can not be avoided. This is caused by the fact that in the p-q region the phase response curves are not perfectly linear and especially in the region where the two function pairs are joined together to form the desired constant phase-shift between them. Thus, one would like to make the arrangement in such a way that this error is minimized or at least less than the tolerance value.

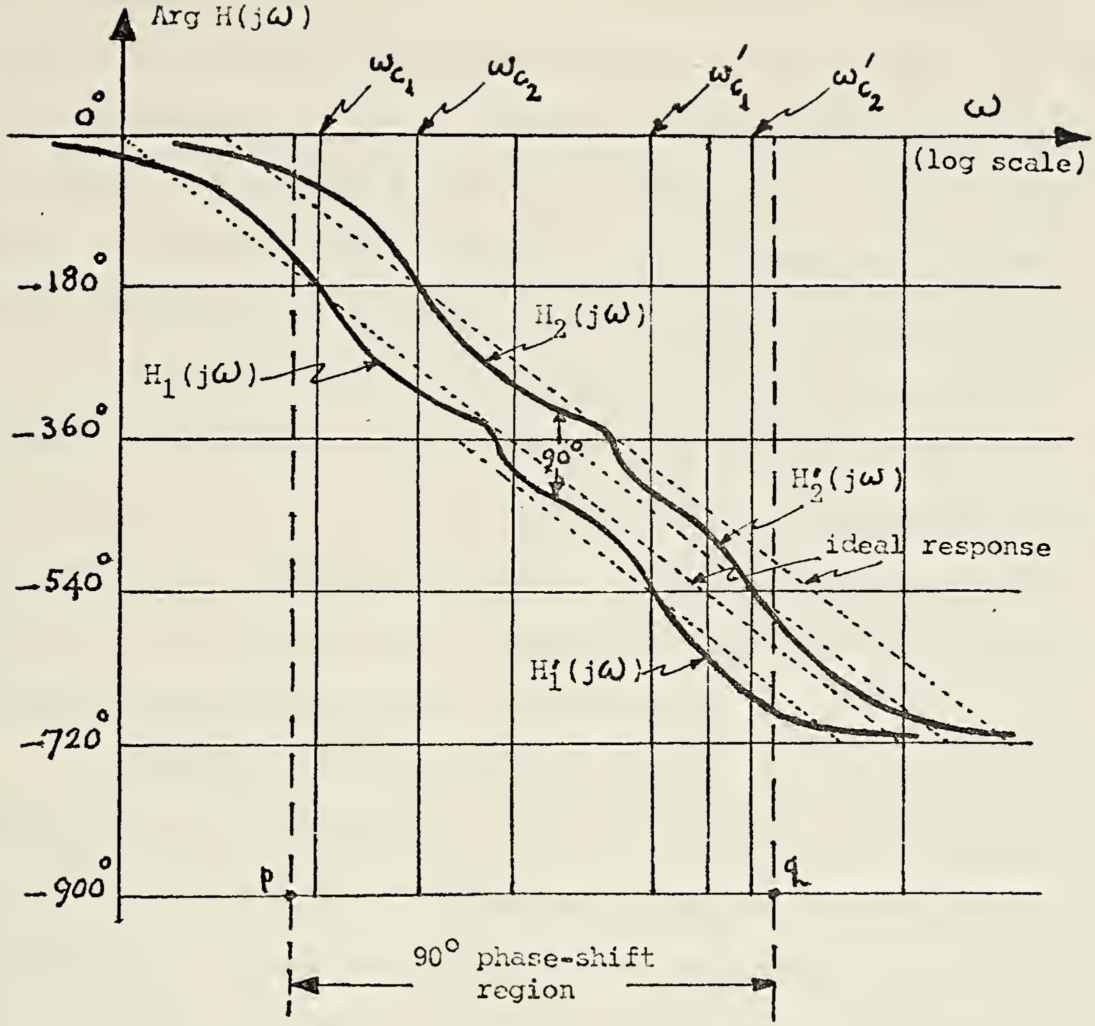

FIG. 6. Two Second Order (ζ = 1) All-Pass Networks in Cascade

Note the wide frequency coverage of p-q region where the phase-shift is 90°, compared to that in Fig. 5. Also note that the second pair cutoff frequencies do not lie on the ideal response lines. This is in order to obtain smaller phase-shift ripples (error) in the new (broader) p-q region.

The efforts to carry out this arrangement is very time consuming. It involves varying the time constants (or cutoff frequencies) hence the poles of the all-pass functions. For example in Fig. 6 one would have to vary four different cutoff frequencies for the two pairs of

of functions individually and independently. Therefore, without the aid of computers this task seems almost impossible to be carried out, especially with such a high degree of phase-shift accuracy required (of the order of up to 2°). While determining the correct cutoff frequencies for two pairs of functions like in Fig. 6 might not be very tedious, to do the same thing with six pairs of such functions is indeed a formidable task. Each of the twelve cutoff frequencies must be varied individually, independently (in both frequency change directions with different frequency rates) to yield an overall phase response which meets the severe phase-shift accuracy requirement.

This very time consuming effort in circuit parameter computation is believed to have been a major stumbling block in the past and why the phase-shift method has not been popular. In addition, circuit components are required to be of very high precision. However, today a precision in component values of less than 1% is quite normal.

In Fig. 6, it is seen that in order to obtain the desired characteristics over a wide frequency region, many network pairs are required, because in order to achieve smaller phase-shift error the cutoff frequencies following the first pair must be shifted toward the left (down frequency) from the ideal response lines. This explains why a high degree of phase-shift accuracy and wide frequency range specifications of the system require more all-pass networks

in cascade (hence more expensive) compared to that if the specifications were not so stringent.

So far, the network functions (or transfer functions) discussed have been of second order types. This approach is quite normal, because in network analysis second order systems (whose characteristics are known and well established) are often taken as a model to analyze other (arbitrary) types of network.

A first order system may then be considered as a special case of a second order system with $\zeta > 1$ if the definition of a second order system were extended for cases where $\zeta > 1$ (the poles have passed the "break-away" point in the root locus of the system). A higher order system may be looked at as a cascade of second order systems.

At this point, a question may arise as to what role the order of the system plays in the phase-shift error reduction in all-pass network design. To analyze this, the best illustration can be done by comparing the phase responses of a first order and a second order all-pass network. The later with $\zeta = 1$ however, i.e., it has double or non-simple poles.

Figure 7 shows the s-plane configuration of a first order all-pass network. The equation of its transfer function is

$$H(s) = \frac{(s-s_2)}{(s+s_1)} = \frac{(s-s_1)}{(s+s_1)} \tag{17}$$

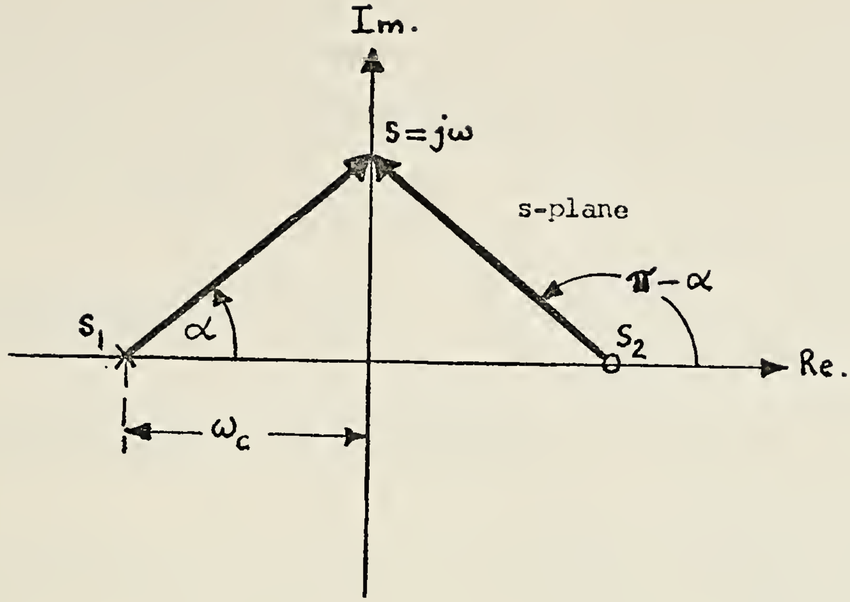

FIG. 7. s-Plane Configuration of a First Order All-Pass Network

since the zero is an image of the pole. Furthermore, since $|s-s_1| = |s-s_2| = |s+s_1|$, it is quite obvious that $|H(j\omega)|$ is constant (unity) for all frequencies (all-pass). To find the equation of the phase response,

$$\arg H(j\omega) = (\pi-\alpha-\alpha) = (\pi-2\alpha) \tag{18a}$$

or

$$\arg H(j\omega) = \pi - 2 \arctan \frac{\omega}{\omega_c} \tag{18b}$$

A π factor emerges here which causes a discontinuity of the phase-response. At $\omega = 0$ and at $\omega = \infty$ the phase curve changes sign. Therefore at $\omega = 0$ the transfer function must be inverted. Inverting the sign of the function has the simple interpretation of changing one of the references

(excitation or response) in the network. Since the procedure may be necessary only in the transfer function, the change of one reference is not serious problem in its realization. Eq. (18b) then becomes

$$\arg H(j\omega)_{f.o.} = -2\alpha \tag{19a}$$

or

$$\arg H(j\omega)_{f.o.} = -2 \arctan \frac{\omega}{\omega_c} \tag{19b}$$

where the subscript f.o. is an abbreviation of first order. This problem of sign change will be shown more clearly in later discussions on the network realization.

Next, consider a second order all-pass function ($\zeta = 1$) whose pole-zero configuration is shown in Fig. 8. Its transfer function is

$$H(s) = \frac{s^2 - 2ss_2 + s_2^{\,2}}{s^2 + 2ss_1 + s_1^{\,2}} \tag{20a}$$

or since $\zeta = 1$, and s_1 is the image of s_2,

$$H(s) = \frac{(s-s_1)^2}{(s+s_1)^2} \tag{20b}$$

Again, because $|s-s_1| = |s-s_2| = |s+s_1|$, $|H(j\omega)|$ is constant (unity) for all ω and thus $H(j\omega)$ is an all-pass function.

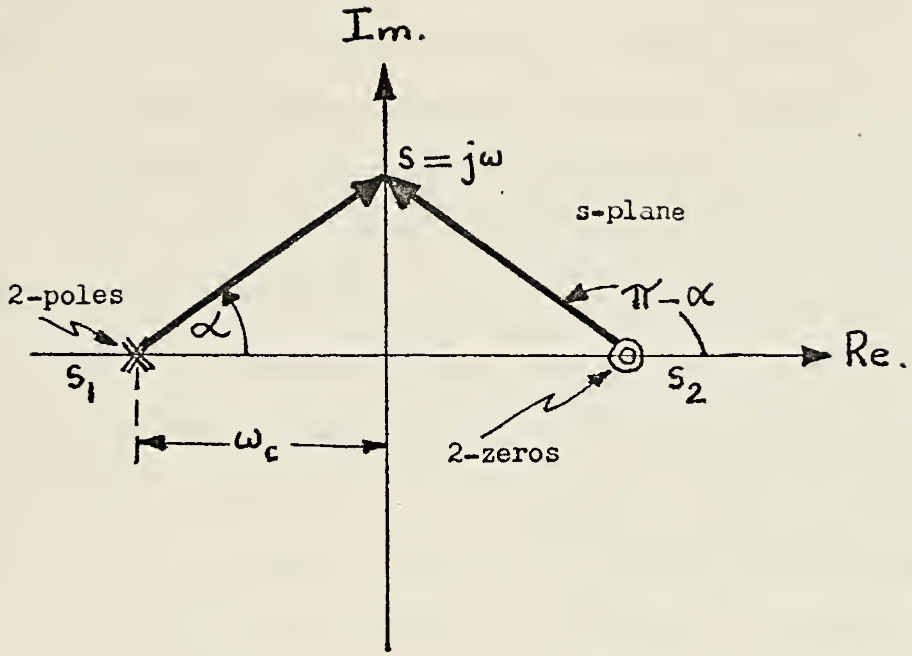

FIG. 8. s-Plane Configuration of a Second Order All-Pass Function (with $\zeta = 1$)

The phase response

$$\arg H(j\omega) = 2(\pi-\alpha) - 2\alpha = 2\pi - 4\alpha \tag{21a}$$

or

$$\arg H(j\omega) = -4\alpha = -4 \arctan \frac{\omega}{\omega_c} \tag{21b}$$

The 2π factor in Eq. (21b) causes no sign change problem and Eq. (21a) may always be written as Eq. (21b). This is an advantage of second order over first order case, but it is not a significant one as previously stated.

The difference between the two cases, namely the difference on the effect of phase-shift error (ripple) reduction can be appreciated when the phase response curves for the two are drawn, one superimposed on the other as shown in Fig. 9. A pair of all-pass functions $H_1(j\omega)$ and $H_2(j\omega)$ shifted 90° apart in the "linear" p-q region is shown for both first and second order cases. While the "linear" p-q region is approximately the same in both cases, the second order case shows a smaller 90° deviation in its phase-shift (ripples). This is caused primarily by the following reasons:

a. Although the "linear" p-q regions are about the same, in the second order case the length of linearity in the phase curve is greater than that in first order case, i.e., the length of 3-4 curve is greater than the length of 1-2 curve in Fig. 9. This is desirable in reducing the phase-shift error.

b. The two phase curves are closer to each other in the second order case, i.e. their cutoff frequency distance $\Delta\omega_2 < \Delta\omega_1$, hence they make the phase-shift error reduction even better.

Therefore, the second order arrangement is logically preferable. This statement was supported by computer simulation results done for both cases with 7 pairs of such networks cascaded to meet the 30 Hz to about 17 kHz frequency range specification. With first order case, the best (min.max) phase-shift error was found to be ~ 3.7°, while with second order case this value was found to be ~ 2.0°. Despite the

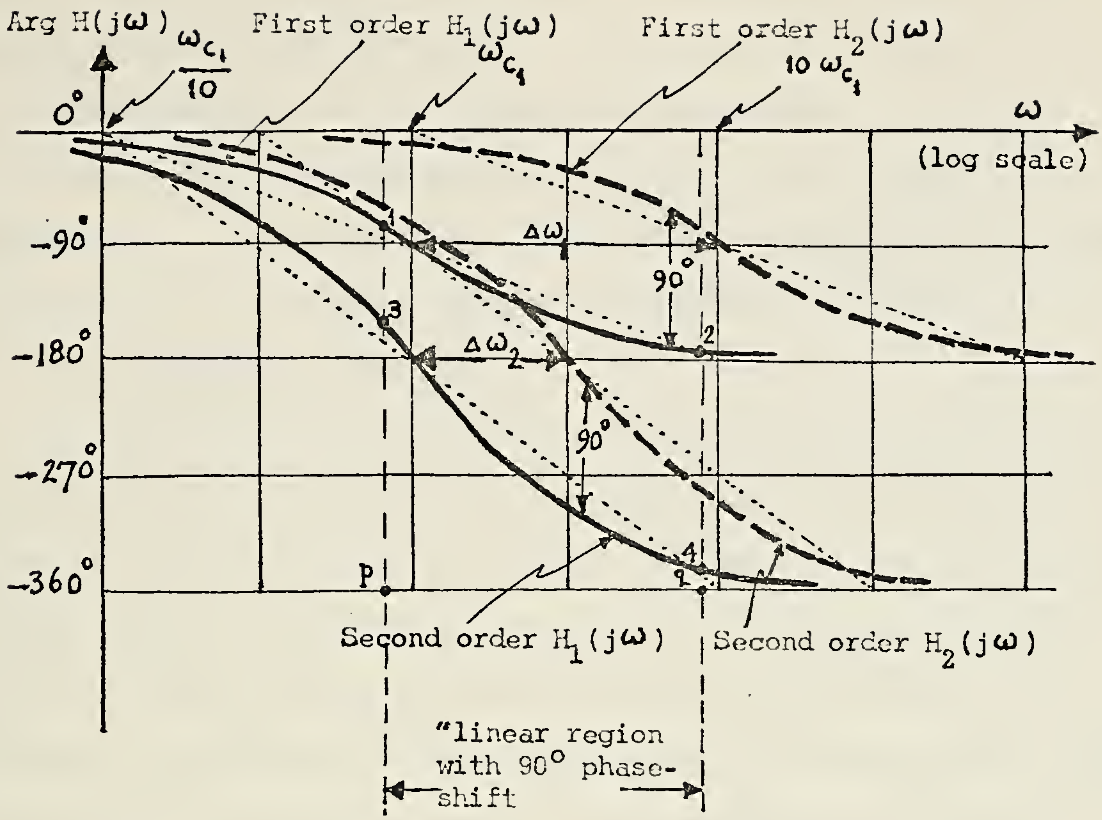

FIG. 9. All-Pass Functions $H_1(j\omega)$ and $H_2(j\omega)$ Shifted 90° Apart for Both First and Second Order Cases

fact that building a first order phase-shift circuit would be less complex and less expensive relatively (because only half of the components, plus an inverter if the number of poles is odd, are required with respect to second order case), the performance however, is far from satisfactory. Thus, a second order system would be more appropriate to satisfy the desired specifications. Of course, one could go to a higher order system by putting triple or even multiple instead of double (non-simple) poles and zeros on the s-plane in order to achieve a much better phase-shift error (much less than 1°),

but at the same time the network would become more complex and certainly more expensive. Again, economics play an important role in the design considerations. What one is looking for here is a modest design of the sideband suppressor. The hybrid system where the phase-shift circuit is a part of (subsystem) seems to offer this modesty.

3. Performance Analysis

The main concern here is to determine the effect of the 90° phase-shift error in the passband on the unwanted sideband signal attenuation level relative to the passband signal level. Although an unbalance in amplitude between the two phase-shifted signal components also affects the sideband suppression level, practically the phase-shift error constitutes the major factor in the sideband suppression level determination. In practice, an amplitude unbalance can be corrected somewhere in the circuit, but phase-shift error cannot be avoided; it is fixed by the design of the circuit. A direct relationship between the phase-shift error and the sideband suppression level exists and will be shown in the following discussions. To do this, let Fig. 1 be redrawn as shown in Fig. 10. Note that α and β networks are designated such that they should be 90° out of phase throughout the passband.

First, a qualitative analysis is conducted using the phasor relationship of the carrier and the sideband voltages in the circuit in Fig. 10. The concept of stationary carrier

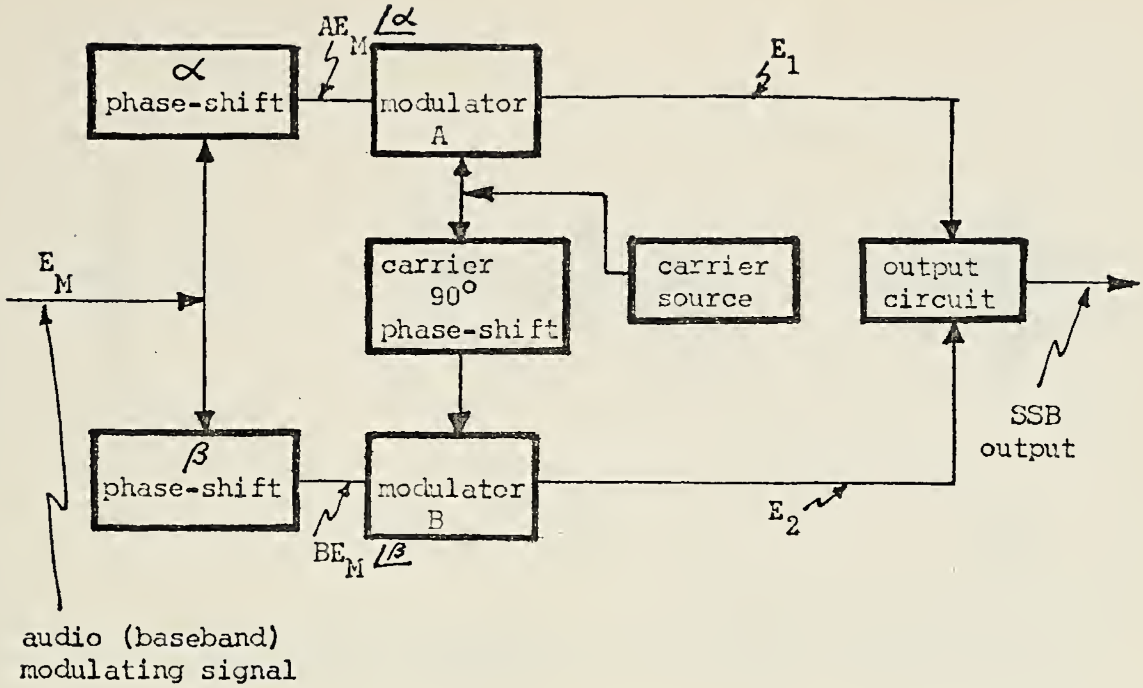

FIG. 10. FIG. 10. Phase-Shift SSB Generator

phasor with single-frequency sideband phasors rotating about its tip is used in Fig. 11(c). In Fig. 11(a) the phasors are shown in a relative position corresponding to the crest of the modulation cycle. The phasor corresponding to the USB component rotates faster than the carrier, making its relative motion with respect to the carrier phasor counter-clockwise. Conversely, the LSB component with respect to the carrier phasor appears to rotate clockwise because it is a lower frequency than the carrier. In Fig. 11(b) the carrier phase is retarded 90°, again with the audio phase such that the modulated envelope is at crest value. If a 90° delay is introduced into the audio frequency input to the modulator associated with the output in Fig. 11(b), then the sideband

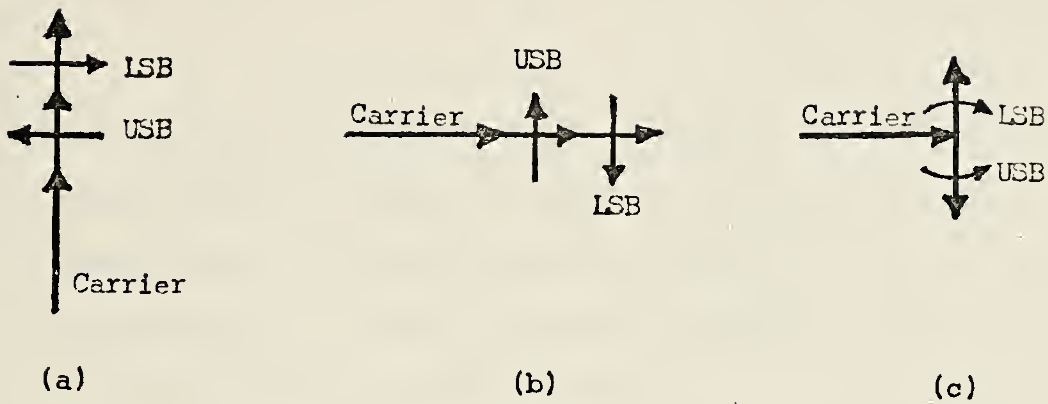

FIG. 11. Phasor Diagrams Showing Sideband Selection by Phase-Shift Method

phasors are rotated to positions shown in Fig. 11(c). Addition of the DSB (double sideband) phasors in Figs. (a) and (c) will result in reinforcement of the lower and cancellation of the upper sideband components.

Second, a quantitative analysis is conducted using the following trigonometric manipulations. A carrier and a signal input are impressed on each modulator as given below:

Input to modulator A,

$$E_c \cos 2\pi f_c t = \text{carrier} \tag{22}$$

$$A \cos(2\pi f_s t+\alpha) = \text{signal through } \alpha\text{-network} \tag{23}$$

Input to modulator B,

$$E_c \cos(2\pi f_c t-90°+\Delta) = \text{carrier after } -90° + \Delta \text{ phase-shift} \tag{24}$$

$$B \cos(2\pi f_s t+\beta) = \text{signal through } \beta\text{-network} \tag{25}$$

Substituting $\beta = \alpha-90°+\delta$ gives

$$B \cos(2\pi f_s t+\alpha-90°+\delta) = \text{signal through } \beta\text{-network} \tag{26}$$

where

A = amplitude of signal through α-network

α = phase-shift of signal through α-network

B = amplitude of signal through β-network

β = phase-shift of signal through β-network

Δ = error in carrier phase from 90°

δ = error in signal phase from 90° difference between α and β networks

f_s = signal frequency

f_c = carrier frequency

E_c = carrier amplitude

The output from modulator A, if complete carrier balance is assumed, is

$$\begin{aligned} E_{AO} &= E_c \cos 2\pi f_c t[A \cos(2\pi f_s t+\alpha)] \\ &= \frac{1}{2} E_c A\{\cos[2\pi(f_c+f_s)t + \alpha] + \cos[2\pi(f_c-f_s)t - \alpha]\} \end{aligned} \tag{27}$$

and the output from modulator B, if complete carrier balance is assumed, is

$$E_{BO} = E_c \cos(2\pi f_c t - 90° + \Delta)[B \cos(2\pi f_s t + \alpha - 90° + \delta)]$$

$$= \frac{1}{2} E_c B\{\cos[2\pi(f_c+f_s)t + \alpha - 90° - 90° + \Delta + \delta]$$

$$+ \cos[2\pi(f_c-f_s)t - \alpha - 90° + 90° + \Delta - \delta]\}$$

$$= \frac{1}{2} E_c B\{-\cos[2\pi(f_c+f_s)t + \alpha + \Delta + \delta]$$

$$+ \cos[2\pi(f_c-f_s)t - \alpha + \Delta - \delta]\} \qquad (28)$$

Then the total output from both modulators is

$$E_O = E_{AO} + E_{BO}$$

$$= \frac{1}{2} E_c\{A \cos[2\pi(f_c+f_s)t + \alpha] + A \cos[2\pi(f_c-f_s)t - \alpha]$$

$$- B \cos[2\pi(f_c+f_s)t + \alpha + \Delta + \delta]$$

$$+ B \cos[2\pi(f_c-f_s)t - \alpha + \Delta - \delta]\} \qquad (29)$$

At this point, it is quite clear by inspection of Eq. (29) that if equal signal amplitude ($A = B$) is assumed as well as phase errors Δ and δ equal to zero, the above expression indicates cancellation of the upper sidebands (f_c+f_s) and addition of the lower sidebands (f_c-f_s). Rearranging terms, the total output becomes

$$E_0 = \frac{1}{2} E_c \Big\{ \quad A^2+B^2+2AB\cos(\Delta-\delta) \cdot \sin[2\pi(f_c-f_s)t - \alpha + $$

$$+ \tan^{-1} \frac{A+B\cos(\Delta-\delta)}{B \sin(\Delta-\delta)}]$$

$$+ \quad A^2+B^2-2AB\cos(\Delta+\delta) \cdot \sin[2\pi(f_c+f_s)t + \alpha -$$

$$- \tan^{-1} \frac{A+B\cos(\Delta+\delta)}{B \sin(\Delta+\delta)}] \Big\} \qquad (30)$$

The degree of sideband suppression is related to the equality of the coefficients of the upper and lower sidebands in the formula given above:

$$\text{Sideband Suppression} = 10 \log \frac{A^2+B^2+2AB\cos(\Delta-\delta)}{A^2+B^2-2AB\cos(\Delta+\delta)} \qquad (31)$$

It is fairly simple to adjust signal amplitude at the proper value to ensure that A = B for a single frequency. When equal signal amplitudes are fed into the two balanced modulators, Eq. (31) becomes

$$\underset{(A=B)}{\text{Sideband Suppression}} = 10 \log \frac{1 + \cos(\Delta-\delta)}{1 - \cos(\Delta-\delta)} \qquad (32)$$

In practice, to adjust A = B and the carrier phase-shift error $\Delta = 0$ is quite easily done; therefore the sideband suppression becomes

$$\underset{(A=B;\ \Delta=0)}{\text{Sideband Suppression}} = 20 \log \cot \frac{\delta}{2} \qquad (33)$$

Eq. (33) is the performance equation that is pursued. It is one related to the phase-shift inaccuracy (only) in the passband. Other similar relations regarding inaccuracy due to $A \neq B$ and $\Delta \neq 0$ have been ignored. In practice, to adjust $A = B$ and $\Delta = 0$ can be done, but to set $\delta = 0$ is almost impossible; it is fixed for a particular design.

To get a clear picture of the above analysis, the following example is presented. Suppose in a phase-shift SSB system, the phase-shift at the audio frequency of 500 Hz is only 88°. To determine to what extent this frequency be present in the unwanted lower sideband, first let

$$\delta = 90° - 88° = 2°$$

Assuming audio signal levels are exactly the same in the passband and no phase-shift error in the carrier, using Eq. (33),

$$\begin{aligned}\text{Sideband suppression level} &= 20 \log \cot \frac{2°}{2} \\ &= 35.16 \text{ dB}\end{aligned}$$

B. FILTER METHOD

1. Functional Analysis

The filter method for SSB generation uses a band-pass filter having sufficient selectivity to pass one sideband and reject the other.

The analysis is best illustrated by a straight forward example of generating an SSB signal using this method as shown in Fig. 12. The frequency specifications are not those used in the actual design which will be undertaken, however, the idea is the same. In this figure, the voice frequency of 300 - 3000 Hz (baseband signal) and a carrier are applied to a balanced modulator. The output of the balanced modulator bears both the upper and the lower sideband signals. One or the other of these signals is then selected by a (sideband) filter. The filter is a bandpass filter whose passband encompasses the frequency range of the sideband selected. The filter must have a cutoff sharp enough to separate the selected sideband from the other sideband. The frequency separation of the sidebands is twice the frequency of the lowest frequency spectral components of the baseband signal. Altogether, then, the sideband filter in Fig. 12 has a passband which, measured from f_c, extends from about 300 to 3000 Hz and in which range its response is quite flat. Outside this passband the response falls off sharply, being down at least 40 dB at 4000 Hz and rejecting the unwanted sideband also by at least 40 dB.

Suppose generation of an SSB signal with a carrier of, say 10 MHz is desired. Then a passband filter is required, with a selectivity that provides 40 dB of attenuation within 600 Hz (frequency separation between the sidebands) at a

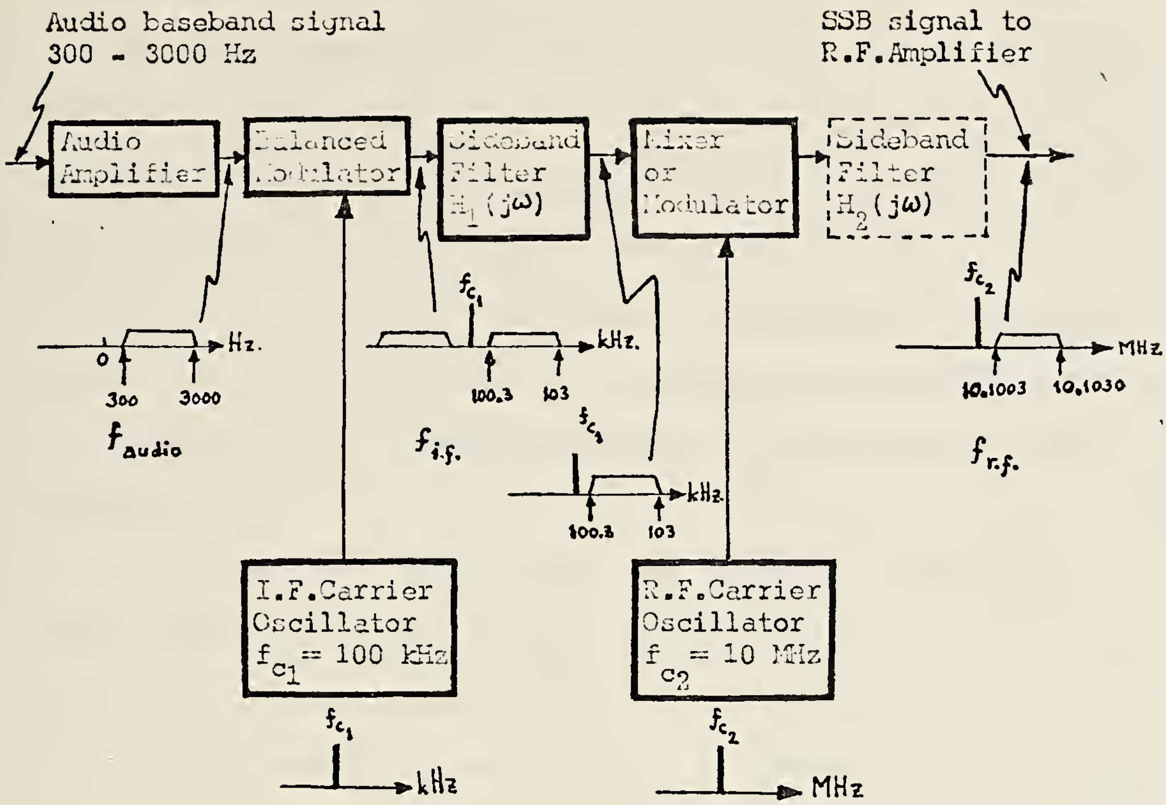

FIG. 12 An Example of Filter Method for SSB Generation

frequency of 10 MHz, a percentage frequency change of 0.006 %. Filters with such sharp selectivity are very elaborate and difficult to construct. For this reason, it is customary to perform the translation of the baseband signal to the final carrier frequency in several stages. Two such stages of translation are shown in Fig. 12. The first carrier has been selected to be of 100 kHz frequency. The upper sideband, say, of the output of the balanced modulator ranges from 100.3 to 103 kHz. The filter following the balanced modulator which selects the upper sideband need now exhibit a selectivity of only a hundredth of the selectivity (40 dB

in 0.6% frequency change) required in the case of a 10-MHz carrier. Now let the filter output be applied to a second balanced modulator, supplied this time with a 10-MHz carrier. Again, let the upper sideband is to be selected. Then the second filter must provide 40 dB of attenuation in a frequency range of 200.6 kHz (the frequency separation between the sidebands now), which is nominally 2% of the carrier frequency.

It has been noted that the simplest physical frequency-translating device is a mixer, while a balanced modulator is a balanced arrangement of two mixers. A mixer, however, has the disadvantage that it presents at its output not only sum and difference frequencies but the input frequency as well. Still, when it is feasible to discriminate against these input signals, there is a merit of simplicity in using a mixer rather than a modulator. In the present case, if the second frequency-translating device (Fig. 12) were a mixer rather than a modulator, then in addition to the upper and lower sidebands, the output would contain a component encompassing the range 100.3 to 103 kHz as well as the 10-MHz carrier. Fortunately, the range 103.3 to 103 kHz is well outside the 10,100,300 to 10,103,000 Hz. Moreover, it is realistic to design a filter which will suppress the 10-MHz carrier, since the carrier frequency is separated from the lower edge of the upper sideband (10,100,300 Hz) by nominally a 1% frequency change.

In summary, it has been noted that when a single-sideband (SSB) signal is to be generated which has a carrier in the megahertz or tens of megahertz range, the frequency translation is to be done in more than one stage - frequently two but not uncommonly three. If the balanced signal has spectral components in the range of hundreds of hertz or lower (as in an audio signal), the first stage invariably employs a balanced modulator, while succeeding stages may use mixers.

2. Filter Synthesis - Approximations - Butterworth & Chebyshev Filters

In the sideband suppression using filter-method, obviously the sideband filter(s) is the heart of the system. The following discussion is an analysis of the network synthesis which leads to the design procedures in building filters. The problem of network synthesis seldom starts with a given rational function (driving point or transfer function). In many cases the desired response is given in the form of a curve or in tabular form, and the first task is to find the appropriate transfer function for the desired network. This stage in synthesis is the approximation problem, and can be stated briefly as follows:

Given ideal specifications (versus ω), find the best realizable function that approximates the ideal one according to some error criterion. The adjective "ideal" is used to emphasize the fact that the function shall eventually be found and will only give an approximation to the given

(ideal) response. Also, to speak of the "best" approximation follows only after it has been decided upon an error criterion by which this approximation will be judged. Obviously, an approximation that is judged the best by one error criterion will not necessarily be the best one by a different error criterion.

It is thus seen that the approximation problem is the first step in network synthesis. In the following, only approximations in the frequency domain will be discussed. That is, ideal specifications of magnitude, phase, real and imaginary parts will be given as functions of ω.

a. Butterworth (maximally flat) approximation

The prototype ideal characteristic that shall be discussed is of an ideal low-pass filter. As shown in Fig. 13, it is of constant magnitude (scaled to 1) from $\omega = 0$ to $\omega = \omega_c$, the cutoff frequency (scaled to 1), and is zero from the cutoff frequency onward. That is,

$$|Z_{12}|^2 = \begin{cases} 1 & 0 < |\omega| < 1 \quad \text{(the passband)} \\ 0 & |\omega| > 1 \quad \text{(the stopband)} \end{cases} \tag{34}$$

This prototype is not so restricted as it may seem. By suitable transformations, it is easily adaptable to high-pass, band-pass and band-stop characteristics.

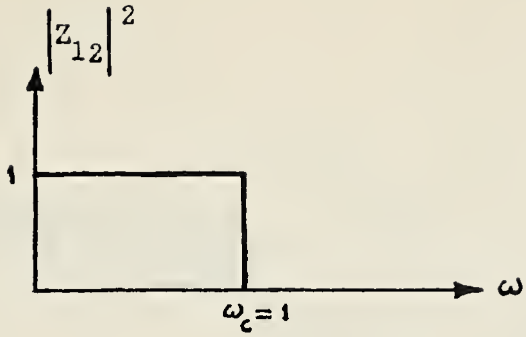

FIG. 13 Ideal Characteristic of a Low-pass Filter

A rational function approximation that suggests itself is of the form

$$|\tilde{Z}_{12}|^2 = \frac{1}{1 + g_n(\omega^2)} \tag{35a}$$

where $g_n(\omega^2)$ is a function of ω^2 satisfying

$$g_n(\omega^2) \ll 1 \quad \text{when } \omega < 1 \tag{35b}$$

and

$$g_n(\omega^2) \gg 1 \quad \text{when } \omega > 1 \tag{35c}$$

The tilde (˜) on Z_{12} is used to indicate the approximating function. Since $|\tilde{Z}_{12}|^2$ is to be an even function, g_n is chosen as a function of ω^2 rather than of ω.

A special form of Eq. (35a) known as the n^{th}-order Butterworth function is given by [6]

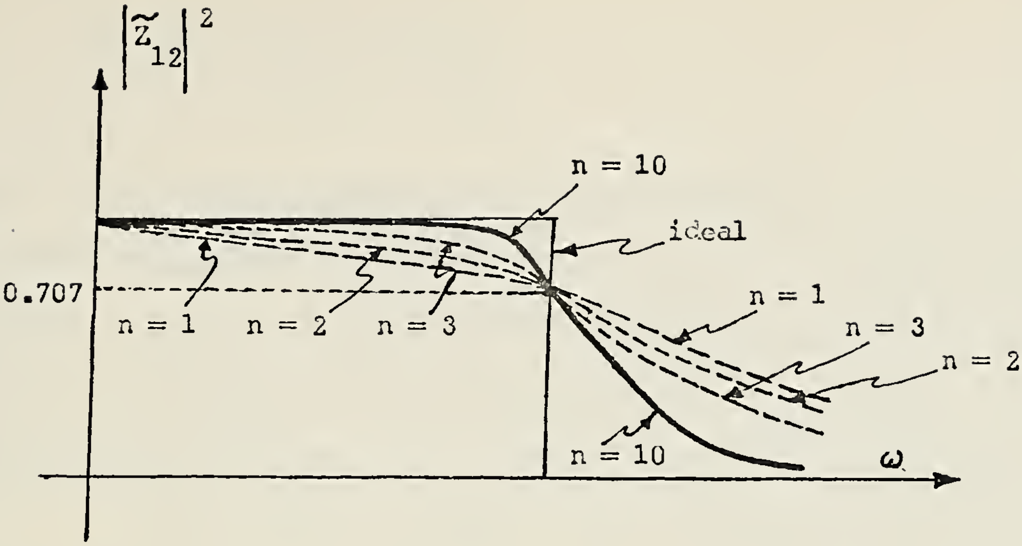

FIG. 14 Several Butterworth Functions

$$|\tilde{Z}_{12}|^2 = \frac{1}{1 + \omega^{2n}} \tag{36}$$

and its plot is shown in Fig. 14 for n = 1,2,3 and 10.

The power series expression of $|\tilde{Z}_{12}|^2$ near the origin gives

$$|\tilde{Z}_{12}|_{\omega\to 0} = (1 + \omega^{2n})^{\frac{1}{2}}_{\omega\to 0}$$

$$= 1 - \frac{1}{2}\omega^{2n} + \frac{1.3}{2.4}\omega^{4n} - \frac{1.3.5}{2.4.6}\omega^{6n} + \ldots. \tag{37}$$

and therefore its first (2n - 1) derivatives with respect to ω vanish at $\omega = 0$. For this reason, the Butterworth approximation is sometimes known as "maximally flat". The error of this approximation is

$$E(\omega^2) = |Z_{12}| - |\tilde{Z}_{12}| \tag{38}$$

and is seen to be maximally flat too. That is, at $\omega = 0$, the error function as well as its first $(2n - 1)$ derivatives are zero. Such an approximation emphasizes one single point (here, $\omega = 0$) where it is excellent, and not a range of frequencies (it is known as the Taylor type of approximation).

The single parameter that specifies the Butterworth function is n. Having chosen it, $\tilde{Z}_{12}(s)$ must be found next. There is a little algebraic manipulation to come to the desired form of equation. When a magnitude of rational (ratio of polynomials) function $|F(j\omega)|$ is given, its square can be written as

$$|F(j\omega)|^2 = \left|\frac{P(j\omega)}{Q(j\omega)}\right|^2 = \left|\frac{P(s)}{Q(s)} \cdot \frac{P(-s)}{Q(-s)}\right|_{s=j\omega}$$

$$= \frac{C(\omega^2)}{B(\omega^2)} \tag{39}$$

and a method of obtaining F(s) suggests itself immediately, i.e. given $|F(j\omega)|$, square it and form

$$|F(j\omega)|^2 = F(s)\cdot F(-s)\big]_{s=j\omega} = \frac{C(-s^2)}{B(-s^2)}\Big]_{s=j\omega} \tag{40}$$

The function $C(-s^2)/B(-s^2)$ has poles and zeros in quadrantal symmetry.

Now, since in the case considered

$$\tilde{Z}_{12}(s)\cdot\tilde{Z}_{12}(-s)]_{s=j\omega} = \frac{1}{1+\omega^{2n}} \tag{41a}$$

then

$$\tilde{Z}_{12}(s)\cdot\tilde{Z}_{12}(-s)]_{s=j\omega} = \frac{C(-s^2)}{B(-s^2)}\bigg]_{s=j\omega} \tag{41b}$$

and therefore,

$$B(-s^2) = 1 + (-1)^n s^{2n} \tag{41c}$$

The roots of $B(-s^2) = 0$ are all located on the unit circle with quadrant symmetry, as shown in Fig. 15 for $n = 4$. Roots in the left hand plane (note that they never lie on the $j\omega$-axis) are taken as the poles of $\tilde{Z}_{12}(s)$, and the resulting $\tilde{Z}_{12}(s)$ is

$$\begin{aligned}\tilde{Z}_{12}(s) &= \frac{1}{(s-s_1)(s-s_2)(s-s_3)\ \ldots} \\ &= \frac{1}{s^n + a_{n-1}s^{n-1} + a_{n-2}s^{n-2} + \ldots + a_1 s + 1}\end{aligned} \tag{42}$$

where

$$s_{2k+1} = -\sin(2k+1)\frac{\pi}{2n} + j\cos(2k+1)\frac{\pi}{2n} \qquad k = 0,1,2,\ldots,n-1 \tag{43}$$

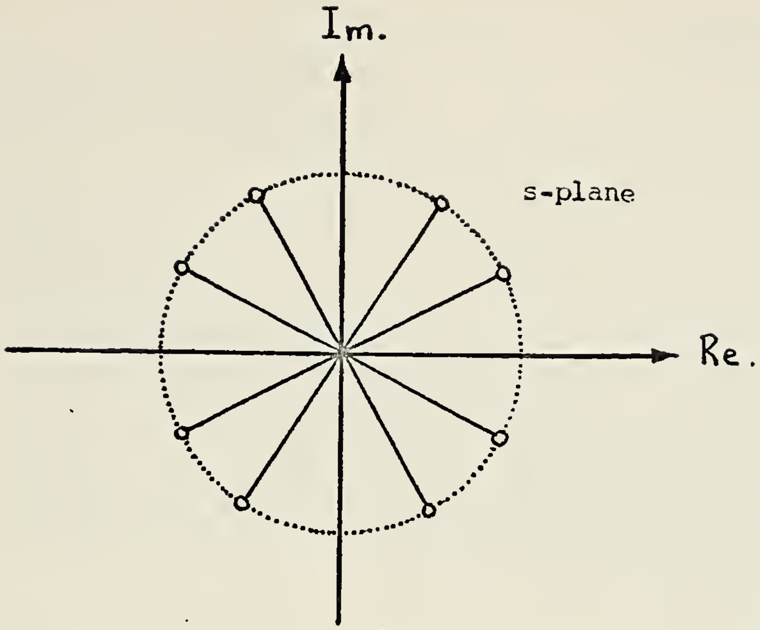

FIG. 15 Roots of $B(-s^2) = 0$ for a fourth-order Butterworth function

So, given the desired number of poles n, one can use Eq. (43) to determine their locations in the s-plane, which are needed in carrying out the realization.

Table 1 shows the denominator of Butterworth approximation function being factorized to at the most 2^{nd}-order degree for different n's. This table helps locate the poles for different n's.

To clarify how one would go about following the steps in the design of a Butterworth filter, for example it is required to find a Butterworth function to approximate the low-pass magnitude characteristic such that for $\omega >> 4\omega_c$

Table-1 Poles of $\tilde{Z}_{12}(s)$, Butterworth Approximation

n	Factors of Denominator
1	$(s+1)$
2	$(s^2+1.414s+1)$
3	$(s^2+s+1)(s+1)$
4	$(s^2+0.765s+1)(s^2+1.848s+1)$
5	$(s+1)(s^2+0.618s+1)(s^2+1.618s+1)$
6	$(s^2+0.518s+1)(s^2+1.414s+1)(s^2+1.932s+1)$
7	$(s+1)(s^2+0.445s+1)(s^2+1.247s+1)(s^2+1.802s+1)$
8	$(s^2+0.390s+1)(s^2+1.111s+1)(s^2+1.663s+1)(s^2+1.962s+1)$

(four times the cutoff frequency and beyond), it does not deviate more than 3% from its value in the passband. To solve this, first parameter needed is n. From the given specifications

$$\left|\tilde{Z}_{12}\right|_{\omega=4} = \left.\frac{1}{1+\omega^{2n}}\right|_{\omega=4} \leq 0.03$$

Therefore,

$$1 + 4^{2n} >> \frac{10^4}{9}$$

or $4^{2n} >> 1110$

Hence, n = 3 will do. The Butterworth function is then,

$$\left|Z_{12}\right|^2 = \frac{1}{1+\omega^6}$$

At this point, it is felt that the discussion on Butterworth approximation function has sufficed, since it was only intended to be a prelude to the Chebyshev (equiripple) approximation function which will be discussed next and adopted as the type of the filter subsystem later.

b. Chebyshev (equiripple) Approximation

As mentioned earlier, the Butterworth approximation is excellent at one point ($\omega = 0$) at the expense of the rest of the passband. Consider again Eq. (35) and seek a polynomial g_n (rather than a single term ω^n) that satisfies Eq. (35b) in an oscillatory manner (rather than the monotonic manner of ω^n). Such characteristics are displayed by the Chebyshev polynomials.

The Chebyshev polynomial of the first kind is defined as follows:

$$T_n(\omega) = \cos(n \cos^{-1}\omega) \tag{44a}$$

Let $$\cos \phi = \omega \tag{44b}$$

then $$T_n(\omega) = \cos n\phi \tag{44c}$$

It is easily verified that $T_n(\omega)$ is a finite polynomial in ω if the following identity [6] is used, namely

$$\cos n\phi = 2^{n-1}\cos^n\phi - \frac{n}{1!} 2^{n-3}\cos^{n-2}\phi + \frac{n(n-3)}{2!} 2^{n-5}\cos^{n-4}\phi - \frac{n(n-4)(n-5)}{3!} 2^{n-7}\cos^{n-6}\phi + \dots \tag{45}$$

or, alternately, the identity

$$2 \cos n\phi = (\cos \phi + j \sin \phi)^n + (\cos \phi - j \sin \phi)^n \quad (46)$$

For example, the first three Chebyshev polynomials of the first kind are

$$T_o(\omega) = \cos 0 = 1 \quad (47a)$$

$$T_1(\omega) = \cos \phi = \cos(\cos^{-1} \omega) = \omega \quad (47b)$$

$$T_2(\omega) = \cos 2\phi = 2 \cos^2\phi - 1 = 2\omega^2 - 1 \quad (47c)$$

Two useful recursion formulas can be derived by using familiar trigonometric relations for the cosine functions. These are:

$$2 \cos m\phi \cos n\phi = \cos(n+m)\phi + \cos(n-m)\phi \quad (48a)$$

and

$$\cos(n+1)\phi = 2 \cos n\phi \cos \phi - \cos(n-1)\phi \quad (48b)$$

yielding

$$2T_m(\omega)\, T_n(\omega) = T_{n+m}(\omega) + T_{n-m}(\omega) \quad , \quad n \geq m \quad (49a)$$

and

$$T_{n+1}(\omega) = 2\omega T_n(\omega) - T_{n-1}(\omega) \quad (49b)$$

respectively. With these relationships, the following Chebyshev polynomials are constructed in addition to Eqs. (47):

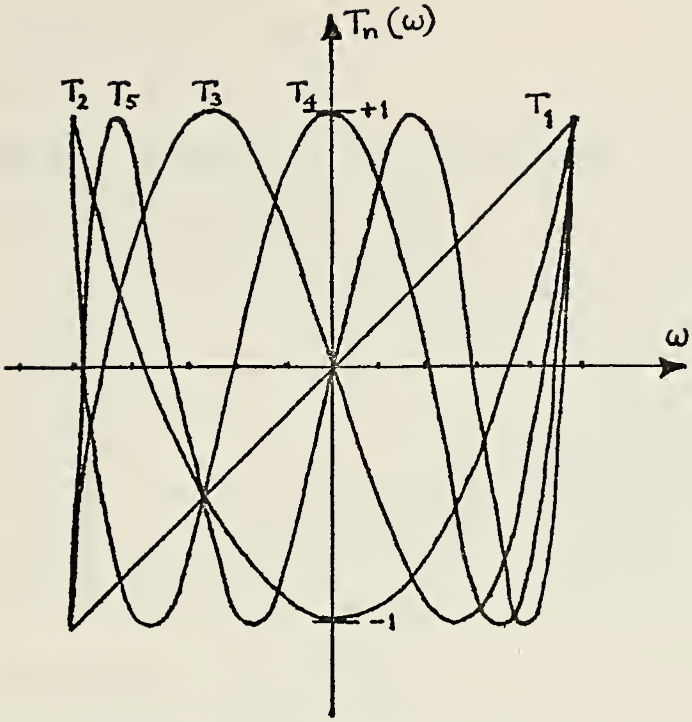

FIG. 16. Plots of Chebyshev Polynomials

$$T_3(\omega) = 4\omega^3 - 3\omega$$

$$T_4(\omega) = 8\omega^4 - 8\omega^2 + 1 \qquad (49c)$$

$$T_5(\omega) = 16\omega^5 - 20\omega^3 + 5\omega$$

and their plots are shown in Fig. 16. Higher order $T_n(\omega)$ may be constructed in a similar way as before; they are listed in Table-2.

From this discussion, the following properties of $T_n(\omega)$ can be listed:

a. T_n is odd when n is odd, and even when n is even.

$T_o = 1$ for all ω.

Table-2 Coefficients of a Chebyshev Approximation

(a) 0.5-db ripple ($\epsilon = 0.349$, $\epsilon^2 = 0.122$)

n	b_7	b_6	b_5	b_4	b_3	b_2	b_1	b_0
1								2.863
2							1.426	1.516
3						1.253	1.535	0.716
4					1.197	1.717	1.025	0.379
5				1.172	1.937	1.309	0.752	0.179
6			1.159	2.172	1.589	1.172	0.432	0.095
7		1.151	2.413	1.869	1.648	0.756	0.282	0.045
8	1.146	2.657	2.149	2.184	1.148	0.573	0.152	0.024

(b) 1-db ripple ($\epsilon = 0.509$, $\epsilon^2 = 0.259$)

n	b_7	b_6	b_5	b_4	b_3	b_2	b_1	b_0
1								1.965
2							1.098	1.102
3						0.989	1.238	0.491
4					0.953	1.454	0.743	0.276
5				0.937	1.689	0.974	0.580	0.123
6			0.928	1.931	1.202	0.939	0.307	0.069
7		0.923	2.176	1.429	1.357	0.549	0.214	0.031
8	0.920	2.423	1.655	1.837	0.447	0.448	0.107	0.017

(c) 2-db ripple ($\epsilon = 0.765$, $\epsilon^2 = 0.585$)

n	b_7	b_6	b_5	b_4	b_3	b_2	b_1	b_0
1								1.307
2							0.804	0.823
3						0.738	1.022	0.327
4					0.716	1.256	0.517	0.206
5				0.705	1.499	0.693	0.459	0.082
6			0.701	1.745	0.867	0.771	0.210	0.051
7		0.698	1.994	1.039	1.144	0.383	0.166	0.020
8	0.696	2.242	1.212	1.579	0.598	0.359	0.073	0.013

Table-2 (continued)

(d) 3-db ripple ($\epsilon = 1$, $\epsilon^2 = 1$)

n	b_7	b_6	b_5	b_4	b_3	b_2	b_1	b_0
1								1.002
2							0.645	0.708
3						0.597	0.928	0.251
4					0.581	1.169	0.405	0.177
5				0.575	1.415	0.549	0.408	0.063
6			0.571	1.663	0.691	0.699	0.163	0.044
7		0.568	1.911	0.831	1.052	0.300	0.146	0.016
8	0.567	2.161	0.972	1.467	0.472	0.321	0.056	0.011

Poles of a Chebyshev Approximation

(a) 0.5-db ripple ($\epsilon = 0.349$, $\epsilon^2 = 0.122$)

$n = 1$	2	3	4	5	6	7	8
−2.863	−0.713 $\pm j1.004$	−0.626	−0.175 $\pm j1.016$	−0.362	−0.078 $\pm j1.008$	−0.256	−0.044 $\pm j1.005$
		−0.313 $\pm j1.022$	−0.423 $\pm j0.421$	−0.112 $\pm j1.011$	−0.212 $\pm j0.738$	−0.057 $\pm j1.006$	−0.124 $\pm j0.852$
				−0.293 $\pm j0.625$	−0.290 $\pm j0.270$	±0.160 $\pm j0.807$	−0.186 $\pm j0.570$
						−0.231 $\pm j0.448$	−0.220 $\pm j0.200$

(b) 1-db ripple ($\epsilon = 0.509$, $\epsilon^2 = 0.259$)

$n = 1$	2	3	4	5	6	7	8
−1.965	−0.549 $\pm j0.895$	−0.494	−0.139 $\pm j0.983$	−0.289	−0.062 $\pm j0.993$	−0.205	−0.035 $\pm j0.996$
		−0.247 $\pm j0.966$	−0.337 $\pm j0.407$	−0.089 $\pm j0.990$	−0.170 $\pm j0.727$	−0.046 $\pm j0.995$	−0.100 $\pm j0.845$
				−0.234 $\pm j0.612$	−0.232 $\pm j0.266$	−0.128 $\pm j0.798$	−0.149 $\pm j0.564$
						−0.185 $\pm j0.443$	−0.176 $\pm j0.198$

Table-2 (continued)

(c) 2-db ripple ($\epsilon = 0.765$, $\epsilon^2 = 0.585$)

$n = 1$	2	3	4	5	6	7	8
−1.307	−0.402 $\pm j0.813$	−0.369	−0.105 $\pm j0.958$	−0.218	−0.047 $\pm j0.982$	−0.155	−0.026 $\pm j0.990$
		−0.184 $\pm j0.923$	−0.253 $\pm j0.397$	−0.067 $\pm j0.973$	−0.128 $\pm j0.719$	−0.034 $\pm j0.987$	−0.075 $\pm j0.839$
				−0.177 $\pm j0.602$	−0.175 $\pm j0.263$	−0.097 $\pm j0.791$	−0.113 $\pm j0.561$
						−0.140 $\pm j0.439$	−0.133 $\pm j0.197$

(d) 3-db ripple ($\epsilon = 1$, $\epsilon^2 = 1$)

$n = 1$	2	3	4	5	6	7	8
−1.002	−0.322 $\pm j0.777$	−0.299	−0.085 $\pm j0.946$	−0.177	−0.038 $\pm j0.976$	−0.126	−0.021 $\pm j0.987$
		−0.1493 $\pm j0.904$	−0.206 $\pm j0.392$	−0.055 $\pm j0.966$	−0.104 $\pm j0.715$	−0.028 $\pm j0.983$	−0.061 $\pm j0.836$
				−0.144 $\pm j0.597$	−0.143 $\pm j0.262$	−0.079 $\pm j0.789$	−0.092 $\pm j0.559$
						−0.114 $\pm j0.437$	−0.108 $\pm j0.196$

b. T_n oscillates with an equal ripple between -1 and +1 for $|\omega| \leq 1$.

c. $T_n(1) = 1$ for all n.

d. $T_n(-1) = 1$ for n even; $T_n(-1) = -1$ for n odd.

e. For $|\omega| > 1$, T_n approaches infinity as $2^{n-1}\omega^n$.

3. Performance Analysis

By performance analysis in this case it is meant the determination of the number of poles necessary on their respective locations on the s-plane, given an error criteria and the steepness of the "skirt" (in dB). For Butterworth case it has been discussed earlier, where the error criteria was the monotonic degradation of amplitude of the signals in the passband.

The following discussion will deal with the same thing but for the Chebyshev case, which deserves a separate section since a Chebyshev Filter will be chosen later. The error criteria here is the level of amplitude ripples of the signal in the passband.

Chebyshev polynomials are particularly suited for use in network theory because the approximation is uniform (although oscillatory) in the passband [15]. A Chebyshev polynomial provides the "best" approximation in the sense that it minimizes the maximum magnitude of the error. In other words, an error criterion that requires

$$\max |E| = \max |F - \tilde{F}| \tag{50}$$

to be made minimum yields a Chebyshev polynomial for $\tilde{F}$. That is, the maximum of the difference between a function F and its approximating polynomial $\tilde{F}$ is smaller for $\tilde{F} = T_n$ than for any other polynomial of the same degree n. By

extension, it is said then that [2] a function $\tilde{F}(\omega, a_1, a_2, \ldots, a_n)$ approximates a real function $F(\omega)$, given in the interval $\omega_1 \leq \omega \leq \omega_2$, in the Chebyshev sense, if the parameters $a_1, a_2, \ldots, a_n$ are determined such that the maximum magnitude of the error $|F - \tilde{F}|$ in this interval is minimized.

The use of Chebyshev polynomial for a rational function approximation is given by

$$|\tilde{Z}_{12}|^2 = \frac{1}{1 + \varepsilon^2 T_n^{\,2}(\omega)} \tag{51}$$

(compare with Eqs. (35)). Since $T_n^{\,2}(\omega)$ can reach the value 1 in the passband, a ripple factor ε^2 is introduced, ($\varepsilon^2 < 1$), to reduce the magnitude of the oscillation. Several typical plots of $|\tilde{Z}_{12}|^2$ are shown in Fig. 17. From the properties of $T_n(\omega)$ (Eqs. (37) and (49c) and Eq. (51)), two general features of these plots become evident:

a. $|\tilde{Z}_{12}|^2 = 1$ at $\omega = 0$ for all odd values of n, and $|\tilde{Z}_{12}|^2 = \frac{1}{1 + \varepsilon^2}$ at $\omega = 0$ for all even values of n.

b. The number of "valleys" and "troughs" in the passband is equal to n.

For small values of the ripple factor, the width of the ripple (peak to peak) in the passband is given by

$$1 - \frac{1}{1 + \varepsilon^2} \simeq \frac{\varepsilon^2}{2} \tag{52}$$

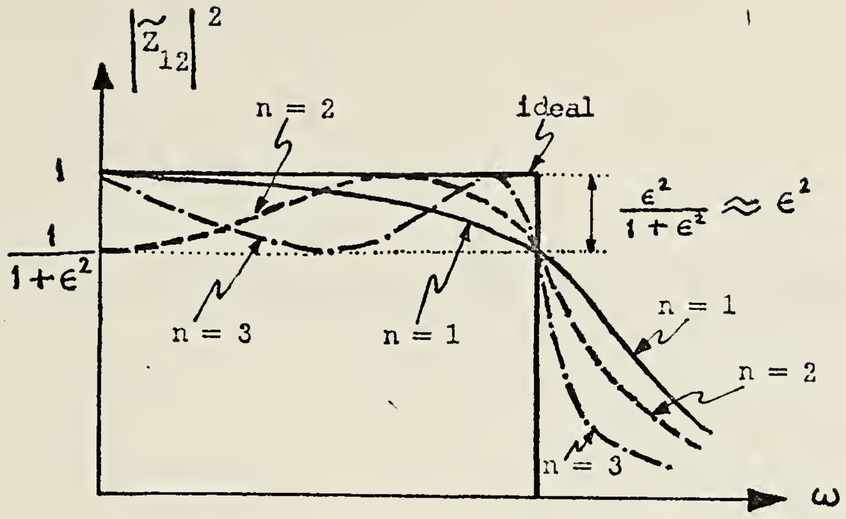

FIG. 17 Several Chebyshev Approximations

Also, for $\omega >> 1$, the magnitude $|\tilde{Z}_{12}|$ can be written as

$$|\tilde{Z}_{12}|_{\omega\to\infty} = \frac{1}{\varepsilon T_n} \tag{53}$$

From given specifications, the two parameters ε and n are determined. Then $|\tilde{Z}_{12}|^2$ can be written; then from it $\tilde{Z}_{12}(s)$ must be found. As in Butterworth function,

$$\tilde{Z}_{12}(s)\cdot\tilde{Z}_{12}(-s)\Big|_{s=j\omega} = \frac{1}{1+\varepsilon^2 T_n{}^2} = \frac{C(-s^2)}{B(-s^2)}\Big|_{s=j\omega} \tag{54}$$

Therefore, the roots of the equation

$$1 + \varepsilon^2 T_n{}^2(\omega) = 0 \tag{55a}$$

must be found, that is,

$$T_n(\omega) = \pm \frac{j}{\varepsilon} \tag{55b}$$

For this purpose, returning to the auxiliary parameter ϕ, Eq. (44b), and let it be complex,

$$\phi = \phi_1 + j\phi_2 \tag{56}$$

Eq. (44c) then becomes

$$T_n(\omega) = T_n(\tfrac{s}{j}) = \cos n\phi = \cos n(\phi_1 + j\phi_2) \tag{57}$$

$$= \cos n\phi_1 \cosh n\phi_2 - j\sin n\phi_1 \sinh n\phi_2$$

(recall that $\cos jx = \cosh x$; $\sin jx = j \sinh x$)

Eqs. (55b) and (57) yield

$$\cos n\phi_1 \cosh n\phi_2 - j\sin n\phi_1 \sinh n\phi_2 = \pm \frac{j}{\varepsilon} \tag{58}$$

Equating the real and imaginary parts of Eq. (58),

$$\cos n\phi_1 \cosh n\phi_2 = 0 \tag{59a}$$

$$\sin n\phi_1 \sinh n\phi_2 = \pm \frac{1}{\varepsilon} \tag{59b}$$

Eq. (59a) is satisfied only when

$$\cos n\phi_1 = 0 \tag{59c}$$

That is,

$$\phi_1 = (2k+1)\frac{\pi}{2n}, \quad k = 0,1,2,\ldots,(2n-1) \tag{59d}$$

These values of ϕ_1, when substituted into Eq. (59b), yield the result

$$\sinh n\phi_2 = \frac{1}{\varepsilon} \tag{59e}$$

That is,

$$\phi_2 = \frac{1}{n}\sinh^{-1}\frac{1}{\varepsilon} \tag{59f}$$

The desired roots are then by ($s=j\omega$)

$$s_{k+1} = j\cos(\phi_1+j\phi_2) = \sin\phi_1 \sinh\phi_2 + j\cos\phi_1 \cosh\phi_2 \tag{60}$$

where the values of ϕ_1 and ϕ_2 are given in Eq. (59d) and (59f). To find the locus of these roots, write

$$s_{k+1} = \sigma_{k+1} + j\omega_{k+1} \tag{61}$$

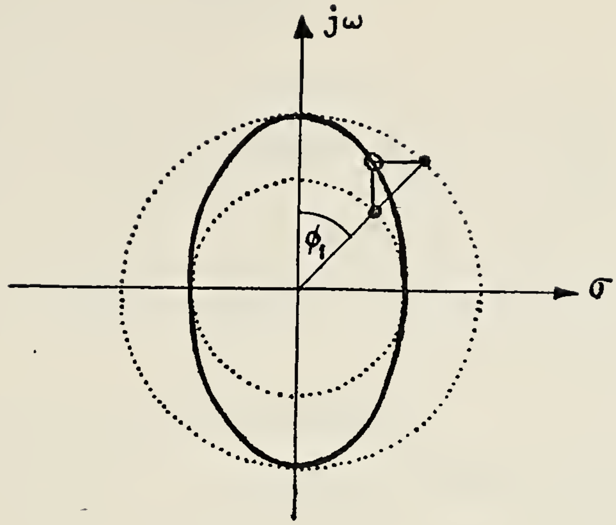

FIG. 18 Locus of Roots of the Denominator of a Chebyshev Transfer Function (Eq. (54))

Then Eq. (50) yields

$$\left(\frac{\sigma_{k+1}}{\sinh \phi_2}\right)^2 + \left(\frac{\omega_{k+1}}{\cosh \phi_2}\right)^2 = 1 \tag{62}$$

which is the equation of an ellipse with semiaxes $\sinh \phi_2$ and $\cosh \phi_2$, as shown in Fig. 18. This figure also shows the familiar graphical construction of an ellipse from its given semiaxes. In summary:

a. From the given specifications, fin n and ε.

b. Find ϕ_1 and ϕ_2 by Eqs. (59d) and (59f).

c. The poles of $\tilde{Z}_{12}(s)$ are the lhp (left hand plane) roots of Eq. 60. Explicitly, these are

$$s_{k+1} = -\sin(2k+1)\frac{\pi}{2n} \sinh \phi_2 + j\cos(2k+1)\frac{\pi}{2n} \cosh \phi_2$$
$$k = 0,1,2,\ldots,(n-1) \tag{63}$$

The resulting $\tilde{Z}_{12}(s)$ is then

$$\tilde{Z}_{12}(s) = \frac{1}{(s-s_1)(s-s_2)(s-s_3)\ldots.(s-s_n)} \tag{64}$$

$$= \frac{1}{s^n + b_{n-1}s^{n-1} + b_{n-2}s^{n-2} + \ldots. + b_1 s + b_o}$$

which has all its zeros at infinity.

Tables such as in the Butterworth case can also be set up, each for different ripple levels in the passband (Table 2). The following example should clarify the idea:

Suppose it is required to design a low-pass filter ($\omega_c = 1$) to the following specifications:

a. Peak-to-peak ripple in the passband must not exceed 2 dB.

b. At $\omega = 5\omega_c$, the response must be down at least 50 dB.

To solve this assignment, first it is necessary to obtain the ripple factor ε from the given ripple specification. It can be shown [6] that this relation is as follows:

$$\varepsilon^2 = 10^{0.1r} - 1 \tag{65}$$

where r is the ripple specification in dB.

Therefore in this problem,

$$\varepsilon^2 = 10^{(0.1)(2)} - 1$$

and it is found that $\varepsilon = 0.765$.

From the second specification, n can be found as follows:

$$\frac{1}{1 + \varepsilon^2 T_n^{\,2}(5)} = 10^{-5}$$

So,

$$\frac{1}{1 + 0.585\ T_n^{\,2}(5)} = 10^{-5}$$

and

$$T_n(5) = 413$$

It can also be shown [6], that $T_n(\omega)$ for $\omega > 1$ may be written as

$$T_n(\omega) = \frac{(\omega + \sqrt{\omega^2 - 1})^n + (\omega - \sqrt{\omega^2 - 1})^{-n}}{2} \qquad (66)$$

Therefore in this problem

$$(5 + \sqrt{24})^n + (5 + \sqrt{24})^{-n} = 413$$

So,

$$9.9^n \approx 413 \qquad\qquad n = 2.61$$

Rounding it up, n = 3 is chosen. Knowing n, then applying it into Eqs. (59d), (59f), and (63), the three pole locations can be determined and finally using Eq. (64), it turns out that

$$\tilde{Z}_{12}(s) = \frac{1}{s^3 + 0.738s^2 + 1.022s + 0.327}$$

Next task is of course, the realization of $\tilde{Z}_{12}(s)$ after finding its equation. The realization will be discussed later.

As a summary, it is worthwhile to make a comparison between Butterworth and Chebyshev approximation properties:

a. The Butterworth response is maximally flat and monotonic throughout. Chebyshev's is equiripple in the passband (minimizing the maximal error).

b. The Butterworth response is specified by one parameter, n. Chebyshev's is specified by two, ε and n.

c. The poles obtained from a Butterworth approximation lie on a unit circle (or, if ω_c is not scaled, on a circle with radius ω_c). The poles of a Chebyshev approximation lie on an ellipse. Comparing Eq. (43) with Eq. (63), the relation between these pole locations are:

-- the real part of a Chebyshev pole can be obtained by multiplying the real part of a Butterworth pole by sinh ϕ_2

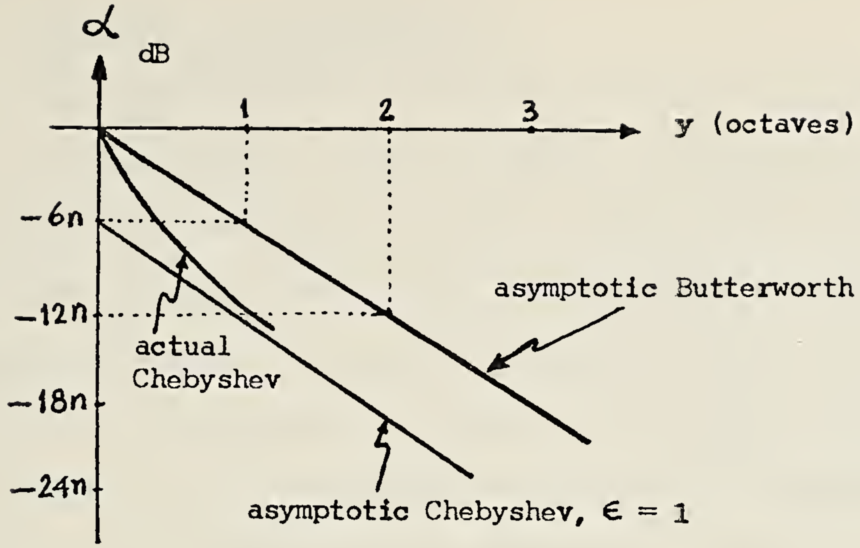

FIG. 19 Logarithmic Gain of a Chebyshev Function Compared with Butterworth's.

-- the imaginary part of a Chebyshev pole can be obtained by multiplying the imaginary part of a Butterworth pole by $\cosh \phi_2$

d. The logarithmic loss of a Butterworth response [6] is given by

$$\alpha_{dB} = -20\ n \log \omega \tag{67}$$

A computation for a Chebyshev response for very large ω [6] gives

$$\begin{aligned}\alpha_{dB} &= 20 \log \frac{1}{\varepsilon T_n} = -20 \log (\varepsilon T_n) \\ &= -20 \log \varepsilon - 20 \log(2^{n-1}\ \omega^n) \\ &\simeq -20 \log \varepsilon - 6(n-1) - 20\ n \log \omega \end{aligned} \tag{68}$$

This gain comparison is shown in Fig. 19.

4. Frequency Transformation

The discussions so far have involved characteristics of the low-pass filter. With suitable transformations of the independent frequency variable, other filter characteristics such as high-pass, band-pass and band-stop can be obtained. However, in the following discussions, only high-pass case will be exposed, because the type of filter desired is a band-pass and this can be achieved by a combination of low-pass and high-pass filters cascaded. Although a direct frequency transformation from low-pass to band-pass is also possible, but the frequency transformation parameter is more complicated than that in case of transforming a low-pass to high-pass filter. Therefore, the same band-pass arrangement is obtained through easier equation for the approximating transfer function.

It is important to note that the transformations of frequency do not affect the particular transfer function, that is, the dependent variable. Therefore, a given ripple in Z_{12} of a low-pass network will remain the same when, by suitable transformation of s, Z_{12} becomes the transfer function of a high-pass network. An introductory example should clarify these ideas.

Suppose it is required to find Z_{12} of a second order high-pass Butterworth (approximation) filter. From Table 1, a second-order low-pass Butterworth function is

$$\tilde{Z}_{12}(s) = \frac{1}{s^2 + 1.414s + 1}$$

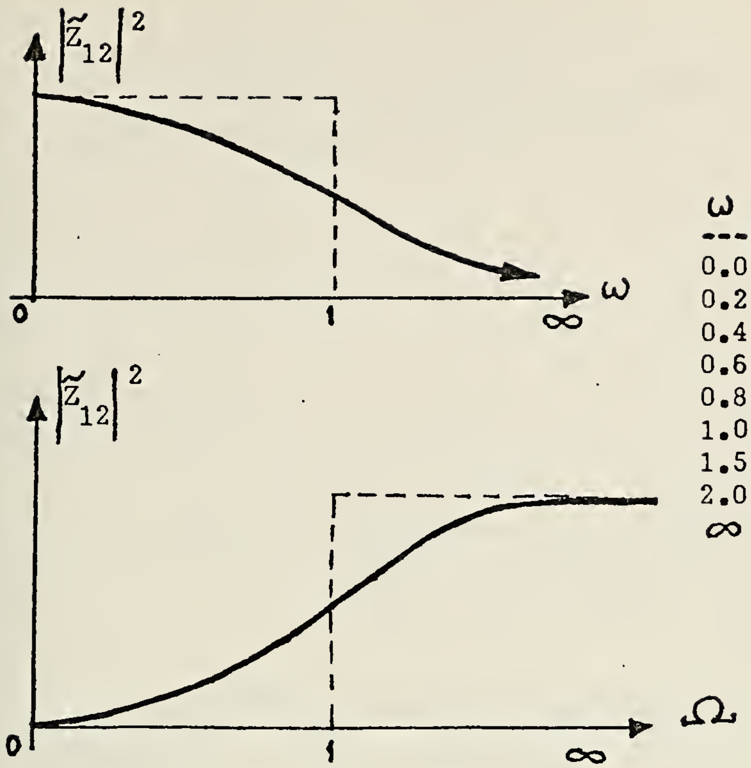

ω	$\lvert\tilde{Z}_{12}\rvert^2$	Ω
0.0	1.000	∞
0.2	0.9984	5.000
0.4	0.9750	2.500
0.6	0.8853	1.667
0.8	0.7094	1.250
1.0	0.5000	1.000
1.5	0.1649	0.667
2.0	0.0588	0.500
∞	0.0000	0.000

FIG. 20 Example of a Low-pass and a High-pass Characteristics

and therefore

$$|\tilde{Z}_{12}(\omega)|^2 = \frac{1}{1 + \omega^4} \quad \text{as in Eq. (41a).}$$

Several numerical values of this magnitude (square) are listed and plotted for comparison purposes in Fig. 20. Now introduce the frequency transformation:

$$\Omega = \frac{1}{\omega} \tag{69}$$

The corresponding values of Ω and $|\tilde{Z}_{12}|^2$ are also listed and plotted in Fig. 20.

Consider the general frequency variables $s = \sigma + j\omega$ and $p = \zeta + j\Omega$, then the following can be written

$$p = \frac{1}{s} \tag{70}$$

and therefore,

$$\tilde{Z}_{12}(p) = \frac{1}{(\frac{1}{p})^2 + 1.414(\frac{1}{p}) + 1} = \frac{p^2}{p^2 + 1.414p + 1} \tag{71}$$

The realization of the low-pass as well as the high-pass filters (hence the band-pass case, because the latter is a cascade of the two) is a different matter. This will be discussed later when a particular design for the hybrid side-band suppressor is under consideration; pertinent justifications regarding the circuit configurations satisfying the theoretical equations will be presented as the design process is gone through.

For the above example, several important observations can be made:

a. The transformation $p = \frac{1}{s}$ "reverses" the real frequency scale so that the low-pass band becomes the high-pass band, and vice versa.

b. The transformation $p = \frac{1}{s}$, for $\sigma = \zeta = 0$, yields $\Omega = -\frac{1}{\omega}$ rather than Eq. (69). However, since the magnitude function $|\tilde{Z}_{12}|$ is even, the results are not changed.

c. The error $|Z_{12}| - |\tilde{Z}_{12}|$ does not change. That is, its value at $\omega = \omega_i$ is the same as at $\Omega = \Omega_i = \frac{1}{\omega_i}$.

C. HYBRID METHOD

In the previous discussions, the components of the hybrid-method for SSB-generation have been introduced.

In the hybrid method, both phase-shift and filter methods are combined (cascaded) in order to achieve a high degree of sideband suppression with a more modest design. This is true, because the sideband suppression is carried out by a combination of the phase-shift and filter subsystems. The burden is now shared by the two; therefore their design can be made more modestly.

The phase-shift method alone could have done the job, but the error in phase-shift must be much less than 1°. Similarly, filter method alone could also have done it as well, but the number of poles of the transfer function would be too many to be practical and economical.

These constraints are actually the motivation of designing a hybrid method. With this method, phase-shift error of 2° might be considered which is relatively easier to implement and a network with transfer function having say 3 or 4 poles for the filter part (which is quite common) might be chosen; the overall performance is then still in accordance with the requirements.

There is another merit of using phase-shift subsystem here; with phase-shift method, the sideband suppression is independent of the frequency range where the unwanted sideband should start to take place. Therefore with the phase-shift method, a modulation frequency as low as several Hertz can be designed and implemented. With the filter-method, although theoretically it is also possible, the implementation (realization) is difficult. As it will be seen, the sideband suppression level in the filter method is directly related to the frequency range where the unwanted sideband is to start taking place. The lower this frequency range, the more poles are needed in the transfer function. Therefore, for operation at several Hertz the filter method is not practical.

These matters will be more clearly understood as the following design of ahybrid method is carried out.

Greater emphasis will be given to the design of the audio phase-shift and filter circuits, because these two are the crucial parts of the system.

III. DESIGN OF A HYBRID SSB SIGNAL GENERATOR

A. PERFORMANCE SPECIFICATIONS

It is required to design a hybrid SSB-signal generator with the following performance specifications:

Sideband suppression level	70 dB at least
Modulation frequency range	30 to 17,000 Hz
Carrier frequency	36,000 Hz
Guard band	4,000 Hz
Passband ripple through communication path	1.5 dB maximum

The design should be inductorless.

B. DESIGN OF THE PHASE-SHIFT SUBSYSTEM

1. The Audio Phase-shift Circuit

a. Time-constant Parameter Determination

This is the first step in the design. It involves mainly the computation of the time-constants which determine the all-pass characteristics for both transfer functions shifted 90° in their respective phases, given that the operating frequency range is 30 Hz to 17 kHz.

Computer aid analysis and the use of a log-log sheet to analyze the resulting phase response curves (Bode) gave a result where 7 (seven) cutoff frequencies (or the reciprocal of time constants) were necessary to cover the frequency range with the desired properties for each of the transfer functions. Note again that for each transfer

function (or also called "phase train"), each cutoff frequency is doubled (thus non-simple poles) to make it a second order all-pass function; therefore, there are a total of 14 poles or 7 pairs in each phase train.

The "best" phase-ripple in the passband was found equal to approximately 1.6°. This was obtained using the expression

$$e_{best} \cong \min\{\max |\Delta - 90°|\} \qquad (72)$$

where Δ is the phase difference of the two functions at a particular frequency. The word "best" means that the error was manipulated by adjusting the 14 cutoff frequencies (of the two phase trains) such that in the passband the maximum phase-shift error is closest to minimum, i.e. may not be a global minimum. This can be justified since digital computer analysis in this case is also an approximation; its accuracy depends on the frequency sample interval taken during the computation. Moreover, in this design one is not really interested in finding the global minimum of this phase-shift error (ripple), but rather, to find an error which is always less than a prescribed level. Achievement of the global minimum of this error itself is indicated by an equal maximum positive and negative swings of e_{best} in Eq. (72) throughout the frequency range [10].

Call the cutoff frequencies of the first phase-train $c_1, c_2, c_3, c_4, c_5, c_6, c_7$ and for the second phase-train (shifted 90° from the first) $d_1, d_2, d_3, d_4, d_5, d_6, d_7$. Note that the units of these cutoff frequencies were taken directly in Hertz instead of in radians; this should not be a problem as long as in the s-plane, in the equation $s = j\omega$, it is understood that ω is in Hz instead of in radians. Then according to Eq. (20a), the equations for the two phase-trains are

$$H_1(s) = \frac{(s-c_1)^2(s-c_2)^2(s-c_3)^2(s-c_4)^2(s-c_5)^2(s-c_6)^2(s-c_7)^2}{(s+c_1)^2(s+c_2)^2(s+c_3)^2(s+c_4)^2(s+c_5)^2(s+c_6)^2(s+c_7)^2} \tag{73}$$

and

$$H_2(s) = \frac{(s-d_1)^2(s-d_2)^2(s-d_3)^2(s-d_4)^2(s-d_5)^2(s-d_6)^2(s-d_7)^2}{(s+d_1)^2(s+d_2)^2(s+d_3)^2(s+d_4)^2(s+d_5)^2(s+d_6)^2(s+d_7)^2} \tag{74}$$

The s-plane configuration of these two functions are shown in Fig. 21 (a) and (b). Recall Eq. (21a) and the fact that the poles are non-simple, i.e. one on top of the other,

$$\begin{aligned}\arg H_1(j\omega) = -\ 4\{&\arctan \frac{\omega}{c_1} + \arctan \frac{\omega}{c_2} + \arctan \frac{\omega}{c_3} \\ &+ \arctan \frac{\omega}{c_4} + \arctan \frac{\omega}{c_5} + \arctan \frac{\omega}{c_6} \\ &+ \arctan \frac{\omega}{c_7}\}\end{aligned} \tag{75}$$

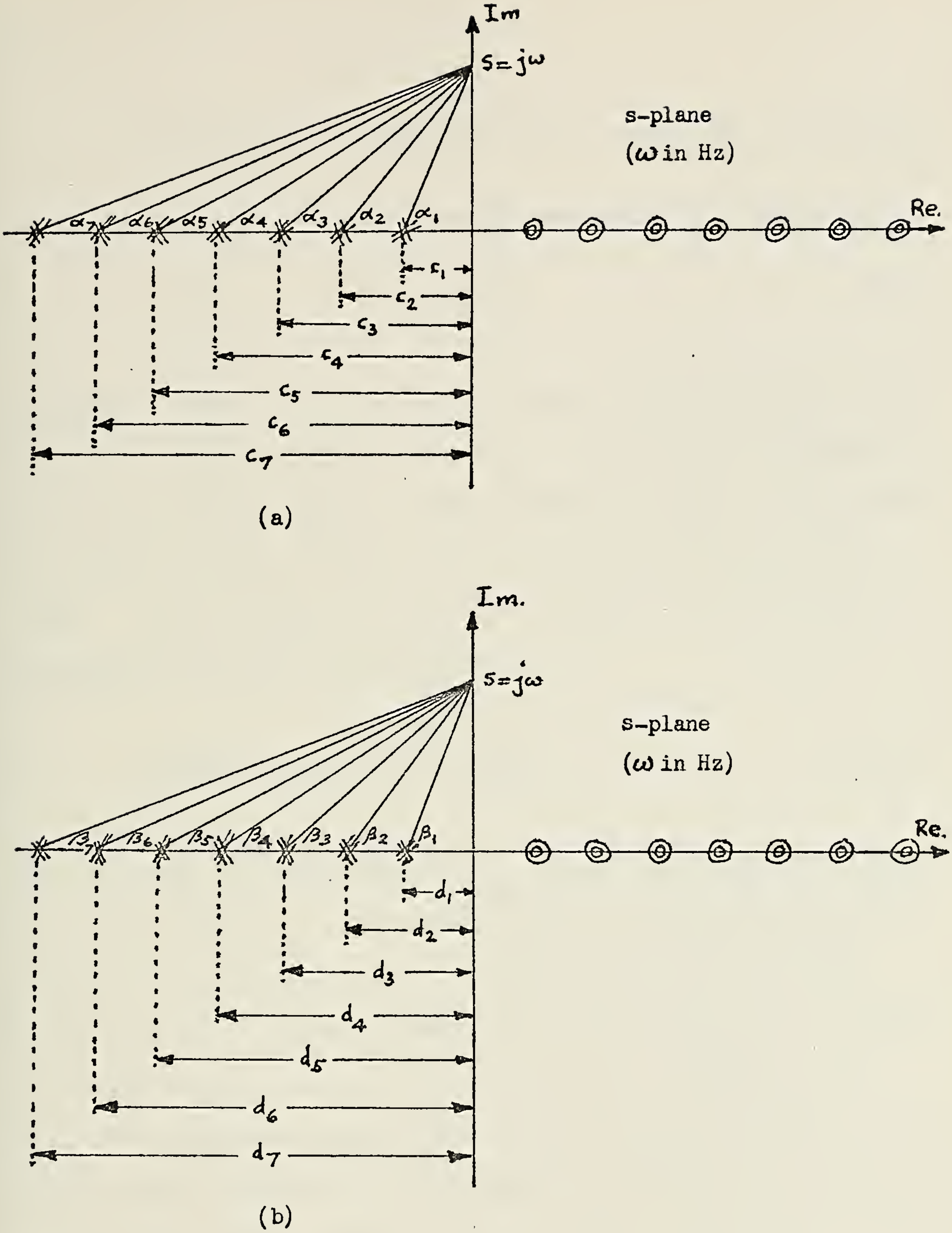

Fig.21 (a) Pole-zero configuration of $H_1(s)$ in eqn.(3.2.2). Note that the zeros are images of the poles for an all-pass function.
(b) Pole-zero configuration of $H_2(s)$ in eqn.(3.2.3). Note that the zeros are images of the poles.

and

$$\arg H_2(j\omega) = -4\{\arctan\frac{\omega}{d_1} + \arctan\frac{\omega}{d_2} + \arctan\frac{\omega}{d_3} + \arctan\frac{\omega}{d_4} + \arctan\frac{\omega}{d_5} + \arctan\frac{\omega}{d_6} + \arctan\frac{\omega}{d_7}\} \tag{76}$$

Appendix 1 shows the computer printout indicating the constant 90° phase-shift between $H_1(j\omega)$ and $H_2(j\omega)$ throughout 30 to 30,000 Hz frequency range (approximately). Note that this range is even better than up to 17,000 Hz specified range. The phase-shift error or "ripple" in this range is determined by the relationship:

$$\text{Phase-error } e = |\Delta - 90°| \tag{77}$$

The criteria of determining e_{best} is given in Eq. (72) and Fig. 21(c) shows the best phase-shift error obtained as a function of frequency in the specified frequency range (computer plot). The maximum phase error (best or smallest possible) e_{best} was found to be ~ 2.0°. Appendix 2 and Fig. 21(d) are the same computer printout and the best phase-shift error obtained as a function of frequency in the specified range for the case of a first order phase-shift network. It is clearly identified that although the frequency range is wider in the case of first-order phase-shift network, the

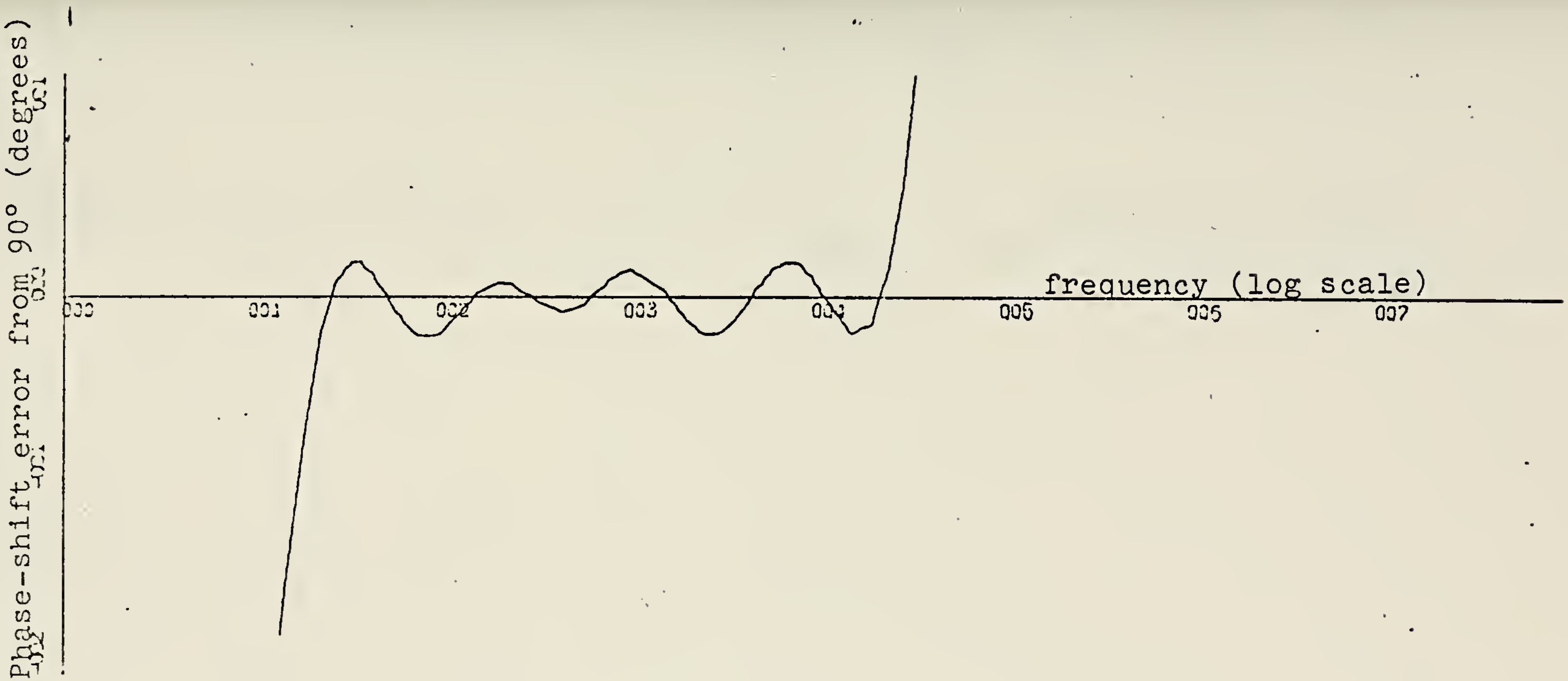

FIG. 21(c) Computer Plot

X-SCALE=1.00E+00 UNITS INCH.

Y-SCALE=1.00E+01 UNITS INCH.

KADARISMAN -- PH.SHIFT ERR.VS.FREQ.OF A 7-POLE

2-ND ORDER PH.SHIFT NETWORK FROM 0.03 TO 30 KHZ

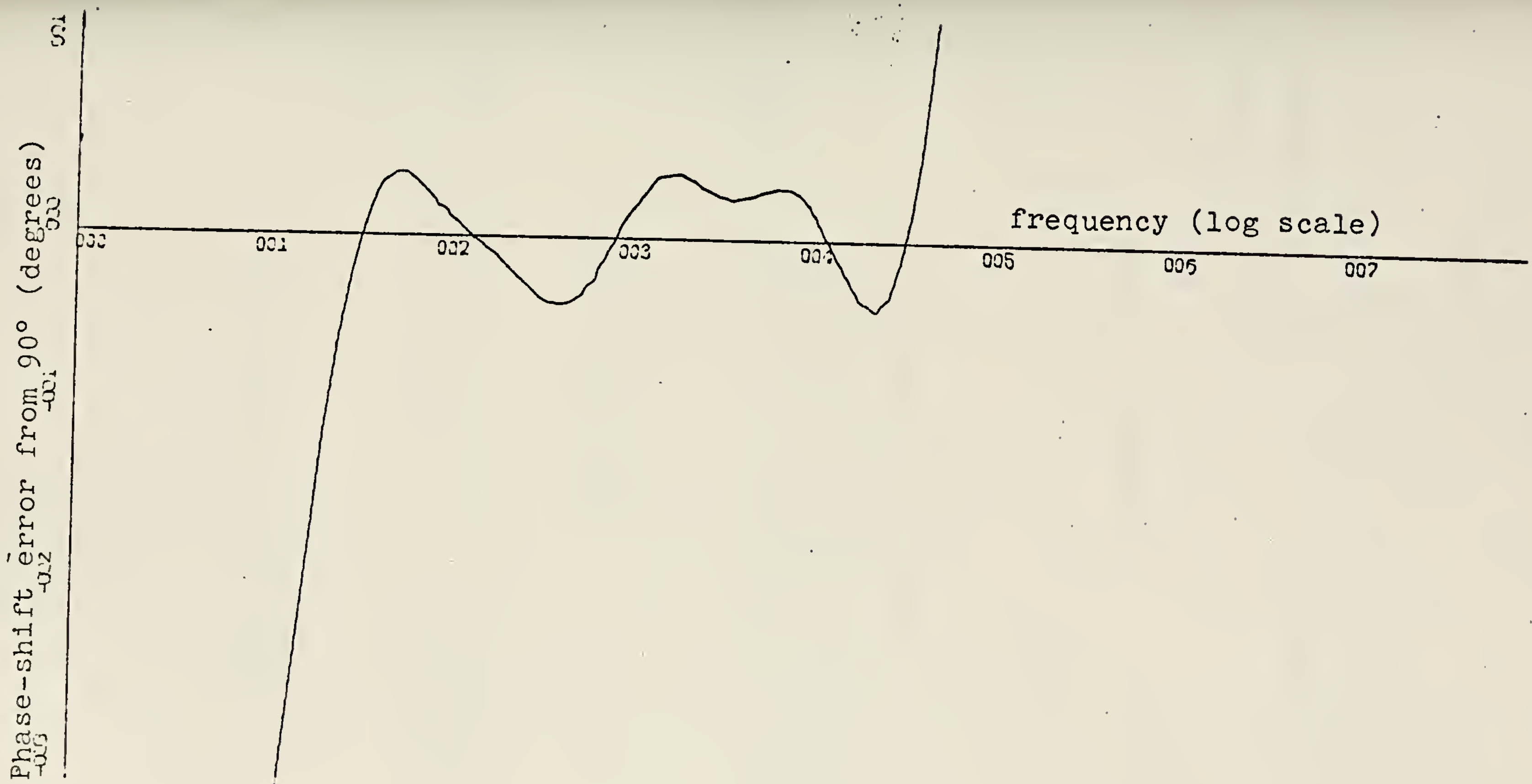

FIG. 21(d) Computer Plot

X-SCALE=1.00E+00 UNITS INCH.
Y-SCALE=1.00E+01 UNITS INCH.
KADARISMAN -- PH.SHIFT ERR.VS.FREQ.OF A 7-POLE
1-ST.ORDER PH.SHIFT NETWORK FROM 0.032 TO 44 KHZ

phase-shift error is about twice of that in the case of a second-order phase-shift network. Note also the low frequency characteristic is better with the second-order case.

According to Eq. (33), with the assumption that the two signal components are perfectly balanced, the sideband suppression that the phase-shift subsystem is capable to perform is

$$\text{Sideband Suppression} = 20 \log \cot \frac{2.0°}{2}$$

$$= 35.16 \text{ dB} \tag{78}$$

b. A Proposed Realization

Consider Eq. (73). To realize this transfer function, one needs to cascade seven phase-trains, each of the form:

$$F(s) = \frac{(s - f_c)^2}{(s + f_c)^2} \tag{79}$$

where f_c may be $c_1, c_2, c_3, c_4, c_5, c_6$, or c_7. Eq. (79) may be regarded as a cascade of two first order all-pass functions, that is,

$$F(s) = \frac{(s - f_c)}{(s + f_c)} \cdot \frac{(s - f_c)}{(s + f_c)} \tag{80}$$

Next call,

$$F_1(s) = \frac{s - f_c}{s + f_c} \tag{81}$$

The realization of Eq. (73) may start with the realization of Eq. (81). Eq. (81) can be written as

$$F_1(s) = 1 - \frac{2\ f_c}{s + f_c} \tag{82}$$

Therefore, Eq. (80) becomes

$$F(s) = (1 - \frac{2\ f_c}{s + f_c}) \cdot (1 - \frac{2\ f_c}{s + f_c}) \tag{83}$$

and the realization of $H_1(s)$ is now focused on finding a certain circuit arrangement which will satisfy Eq. (83).

Consider the circuit arrangement in Fig. 22. In this figure, section I represents the realization of Eq. (81), as a first order all-pass network. To make a second order all-pass network (Eq. (83)), section II in Fig. 22, which is identical to section I is connected in cascade with section I.

Consider now only section I in Fig. 22, with signal applied at its input (ac condition). The purpose of using an FET for F_1 in the circuit is primarily to provide a very high impedance between the incoming audio signal and ground which is made possible by the FET's extremely high

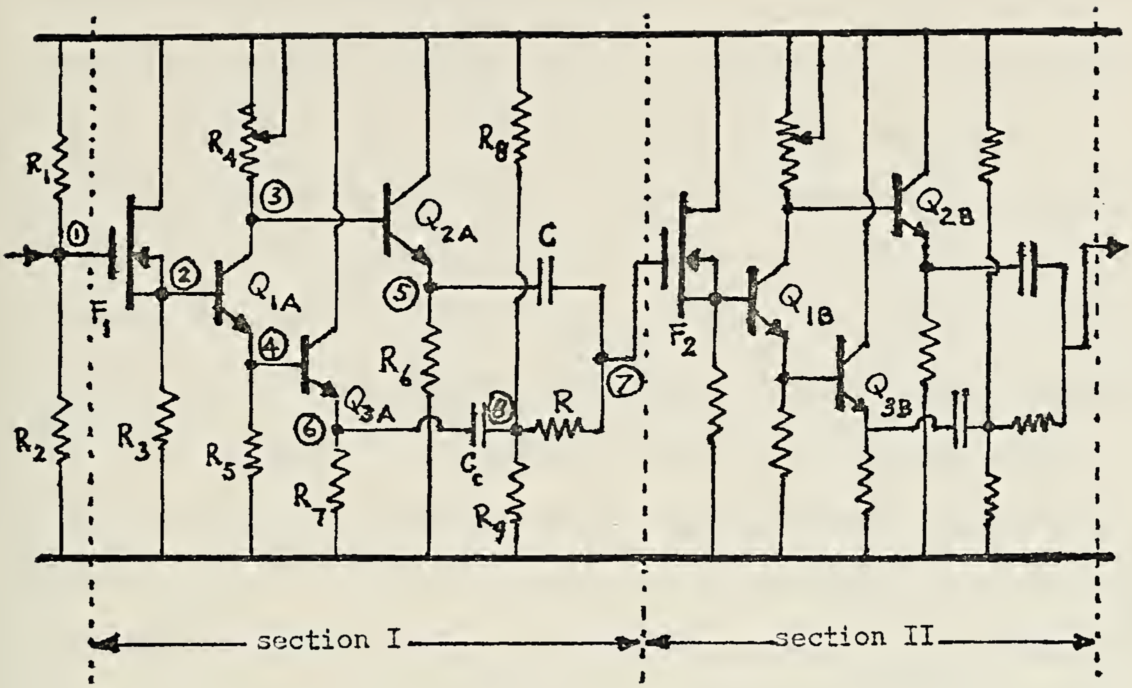

FIG. 22 Circuit arrangement for the realization of Eq. (83)

input impedance characteristic. Another important factor in choosing FET here is its low noise - figure characteristic, which makes it very suitable for this purpose.

The FET is CD (common drain) connected. Therefore, it acts as a buffer stage between the audio signal input at point 1 and the phase-splitter input at point 2. Since F_1 is CD connected, the voltage gain between its output and input is practically unity and no phase inversion occurs. Hence, $v_{1} \approx v_{2}$ (inphase).

The signal voltage v_{2} is now split into two equal voltages v_{3} and v_{4}, but they are 180° out of phase. To do this, the arrangemement of Q_{1A} transistor, R_4 and R_5

resistors acts as a phase-splitter. Q_{1A} is basically CC (common collector) connected, but in addition to the normal output terminals across R_5, a second output terminals are taken across R_4 which is inserted between Q_{1A}'s collector and the dc-supply line (ac ground). The ac-output voltages are then $v_{③}$ and $v_{④}$. If Q_{1A} is viewed to have $v_{③}$ as the only output voltage, then the circuit is actually CE (common emitter) configurated with a resistance (R_5) present in Q_{1A}'s emitter circuit. In this case the output voltage $v_{③}$ is 180° out of phase from the input voltage $v_{②}$. On the other hand, if Q_{1A} is viewed to have $v_{④}$ as the only output voltage then the circuit is actually CC configurated with a resistance (R_4) present in Q_{1A}'s collector circuit. In this case the output voltage $v_{④}$ is inphase with the input voltage $v_{②}$. By using a potentiometer, R_4 is adjusted such that $v_{③} = v_{④}$ (in magnitude). This can be achieved by making $R_4 = R_5$. To prove this statement, consider next only the circuit consisting of Q_{1A} transistor, R_4 and R_5 resistors in Fig. 22 as shown (redrawn) by Fig. 23. The two output voltages are

$$v_E = i_E R_E = i_E R_5 \tag{84}$$

and

$$v_C = i_C R_C = i_C R_4 \tag{85}$$

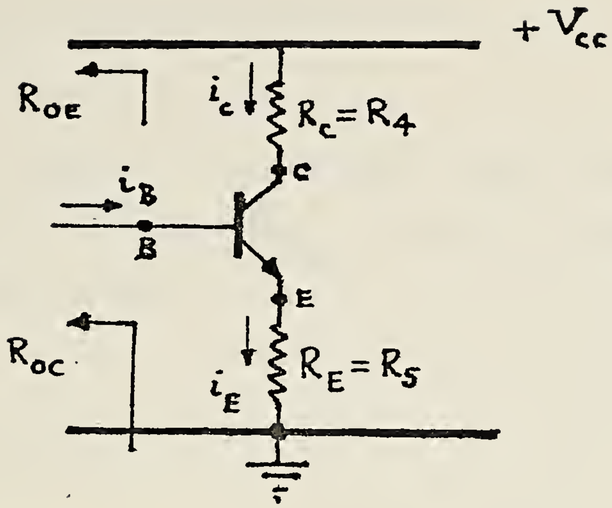

FIG. 23 The Phase-splitter

It is desired that v_E be equal to v_C (in magnitude). To achieve this, a relationship between R_4 and R_5 must be found such that the condition $v_C = v_E$ or consequently,

$$i_C R_4 = i_E R_5 \tag{86}$$

or

$$i_C R_4 = (i_C + i_B) R_5 \tag{87}$$

is satisfied.

From Eq. (87),

$$\left(\frac{i_C}{i_C + i_B}\right) R_4 = R_5 \tag{88}$$

but $\left(\frac{i_C}{i_C + i_B}\right)$ in practice approaches unity because $i_B << i_C$ for a good transistor (large h_{FE}). Provided that Q_{1A} is chosen from a high beta transistor type (typical h_{FE} 200), the assumption that $\left(\frac{i_C}{i_C + i_B}\right) \approx 1$ can be strongly justified. Eq. (88) then becomes

$$R_4 \approx R_5 \tag{89}$$

This proves the earlier statement that if $R_4 = R_5$, then $v_{3} = v_{4}$. This explanation has clarified the phase-splitting action of the phase splitter circuit, i.e. one signal is split into two of the same voltage but one is 180° out of phase from the other. However, the two split signals, while experiencing the same high impedance R_{oC} looking into the emitter terminal at point 4 and ground is low, characterized by the CC configuration and that looking into the collector terminal at point 3 and ground, R_{oE}, is high, characterized by the CE configuration.

The next step is to drive the time constant RC-circuit from the two output terminals of the phase-splitter. It is desired that the time constant circuit of RC be driven by low output impedances of the phase-splitter. Also desired is that the operation of R and C be contained from the effects of adjacent elements at all frequencies (to preserve the time constant value RC). In addition, an undesired signal feedback

from the direction of RC into Q_{1A}'s output terminals need to be avoided.

To achieve low impedance drive and isolation, Q_{2A} transistor stage is introduced. Q_{2A} stage is also CC connected, therefore it provides low output impedance across point (5) and ground (R_6 excluded) driving the RC-circuit while at the same time blocks the RC-circuit from the effects of the circuitry connected to Q_{2A}'s input.

The RC-circuit is isolated from the loading effects coming from next stage (section II in Fig. 22) by the high input impedance of FET F_2. The connection of the RC-circuit directly to point (4) could have been done, because a low output impedance (R_5 excluded) of Q_{1A} stage looking into this point and ground has been provided. However, with this arrangement there is still a path for undesired signal feedback from the RC-circuit direction coming to point (4). Therefore, Q_{3A} transistor stage (CC configurated) is inserted as a buffer stage. The driving impedance of the RC-circuit is now still low, but there will be no feedback signal coming back to interfere at Q_{1A} stage. Summarizing, the purpose of Q_{2A} and Q_{3A} stages is to provide low impedance at points (5) and (6) driving the RC-circuit, while at the same time to provide isolation for the RC-circuit and to prevent signal feedback between points (3) and (4). The driving impedances of the RC-circuit are R_6

in parallel with R_{oE} of Q_{2A} at point 5 and R_7 in parallel with R_{oC} of Q_{3A} at point 6.

A coupling capacitor C_c is connected between point 6 and resistor R. The value of C_c is chosen very large compared to that of C ($C_c >> C$) such that at the lower edge of the passband (30 Hz in this case) it is already essentially short circuited. For low frequencies of the passband then, Q_{1A}, Q_{3A}, C_c and R constitute the signal path from point 2 to point 7 which is the input of next stage's FET. This is the case, since capacitor C is practically open circuited for low frequencies. For higher frequencies in the passband, although C_c is still short circuited, C is practically short circuited also, and now the signal from point 2 almost entirely flows through Q_{1A}, Q_{2A}, directly to point 7. This is caused by the fact that with C short circuited, points 5 and 7 are short circuited.

The biasing of FET F_2 is done through the resistances R_8 and R_9. The fact that R_8 and R_9 are not connected directly to F_2's gate, but through the time constant element R is important, because the parallel combination of these two resistors (in ac operation) would still be a high impedance relatively across the output terminals of Q_{3A} stage, which has a very low impedance driving the RC-circuit. The values of R_8 and R_9 are of the order of several Megohms, therefore they certainly do not effect the low impedance

drive of RC-circuit, and at the same time the high input impedance of FET F_2 (almost infinity) is looked from point 8 as an even higher impedance, because R is now a part of it (in series). Thus, the desired operation of RC (value of time constant preserved at all frequencies) is not jeopardized.

While in ac-condition this arrangement is significant, in dc-condition the analysis is the same as if $R_8||R_9$ were connected directly to F_2's gate (as normally done), because with FET's practically no current flows in the gate circuit, or if there is any, it is a leak current between gate and source which for very good quality FET's is very small.

So far, a proof has not been presented which shows the validity of Eq. (83) in the circuit arrangement of Fig. 22. This will be done in the following analysis.

Fig. 24 shows an ac-equivalent circuit for the portion in Fig. 22 between points 2 and 7. Note that v_{2} is equal in magnitude to v_{1}, v_{3}, v_{4}, v_{5} and v_{7}, because of the CC configuration of F_1, Q_{1A}, Q_{2A} and Q_{3A} and the fact that $R_4 = R_5$.

Applying Kirrchoff's Law in Laplace Transform,

$$V_{2}(s) = RI(s) + \frac{I(s)}{s\ C} - V_{2}(s) \tag{90}$$

Therefore,

$$I(s) = \frac{2\ V_{2}(s)}{R + \frac{1}{sC}} \tag{91}$$

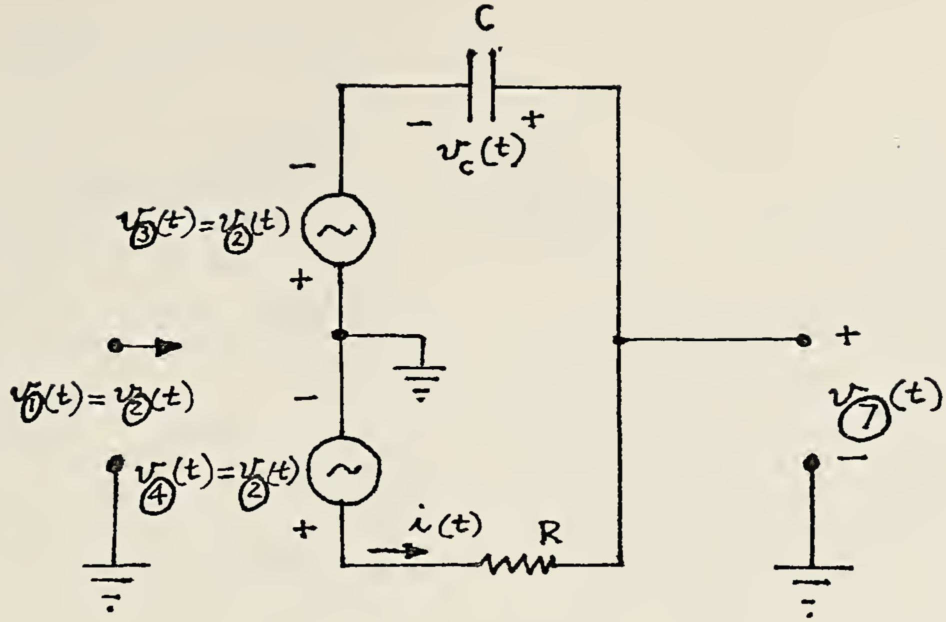

FIG. 24 Ac-equivalent circuit for analyzing the performance of the circuit in Fig. 22

Note: $L\{v_{2}(t)\} = V_{2}(s)$
$L\{i(t)\} = I(s)$

The output voltage,

$$V_{7}(s) = V_{2}(s) - RI(s)$$

$$= V_{2}(s) - \frac{2RV_{2}(s)}{R + \frac{1}{sC}} \qquad (92)$$

The transfer function,

$$F_1(s) = \frac{V_{7}(s)}{V_{2}(s)} = 1 - \frac{2\ R}{R + \frac{1}{sC}}$$

$$= 1 - \frac{2RCs}{RCs + 1}$$

$$= 1 - \frac{2s}{s + \frac{1}{RC}}$$

$$= \frac{s + \frac{1}{RC} - 2s}{s + \frac{1}{RC}}$$

$$= - \frac{s - \frac{1}{RC}}{s + \frac{1}{RC}} \tag{93}$$

Since $\frac{1}{RC} = f_c$,

$$F_1(s) = - \frac{s - f_c}{s + f_c} \tag{94}$$

In Fig. 22, two identical networks described by Eq. (94) are cascaded (sections I and II in the figure). Hence the equation,

$$H_1(s) = F_1(s)^2 = \left\{\frac{s - f_c}{s + f_c}\right\}^2$$

according to Eq. (83) has been satisfied by the circuit arrangement in Fig. 22. To recheck the amplitude requirement, which should be constant (all-pass), consider the function

$$F_1(s) = \pm \frac{s - f_c}{s + f_c}$$

$$= \pm 1 - \frac{2 f_c}{s + f_c} \qquad (95)$$

For zero frequency or s = 0, $F_1(s) = \pm 1$ and for infinite frequency or $s = \infty$, $F_1(s) = \pm 1$. So, there is a sign change of $F_1(s)$. However, for a second order all-pass function, since Eq. (95) is squared, $H_1(s)$ has always the same sign (positive) for all frequencies. This clarifies the previous discussion regarding Eqs. (18a) and (21a).

c. DC and AC Analysis

The details of the proposed all-pass network in Fig. 22 (only one phase-train is considered) will now be presented. Particular FET and transistor types are chosen. Given their characteristic data one can now start to do the design and conduct dc and ac analyses. These consist of determining the element values at a certain operating (bias) condition of the FET;s and transistors. The cutoff frequencies found by the digital computer analysis are implemented as RC-circuit at each phase train stage.

In choosing the type of transistors, the important criteria used are:

- high h_{fe} (small signal current gain) and h_{FE} (dc current gain), typically greater than 200 for both of them. Thus, a high input impedance, i.e. good isolation properties can be achieved (this will be evident later).

- small h_{oe} (output conductance), thus the effect of stray conductances at the transistor output can be minimized.

- small stray capacitances between the transistor terminal such that in the operating frequency range there is no shorting effects between them.

- maximum collector-to emitter voltage must be at least equal to the planned supply voltage V_{cc}. In this case V_{cc} = + 20 volt will be chosen (for NPN transistors only).

In choosing the type of FET's, the important criteria are

- high transconductance (10,000 - 20,000 μohms are typical)

- very low input capacitance (1 to 4 pF are typical)

- very low feedback capacitance (0.1 to 0.2 pF are typical)

- drain to source voltage (maximum) is greater than V_{cc}; in this case + 20 volt is planned.

The FET type chosen was SD-200; actually it is a MOS Field Effect Transistor/n-channel enhancement type. Its important data are:

g_m (forward transconductance)	15,000 μohms
r_d (drain to source resistance)	> 10 k-ohmns (typical)
gate leakage current I_{GSS}	0.001 nA (typical)
input small signal stray capacitance C_{iss}	2 pF (typical)

Its characteristic curves are shown in Fig. 25 (a) and (b).

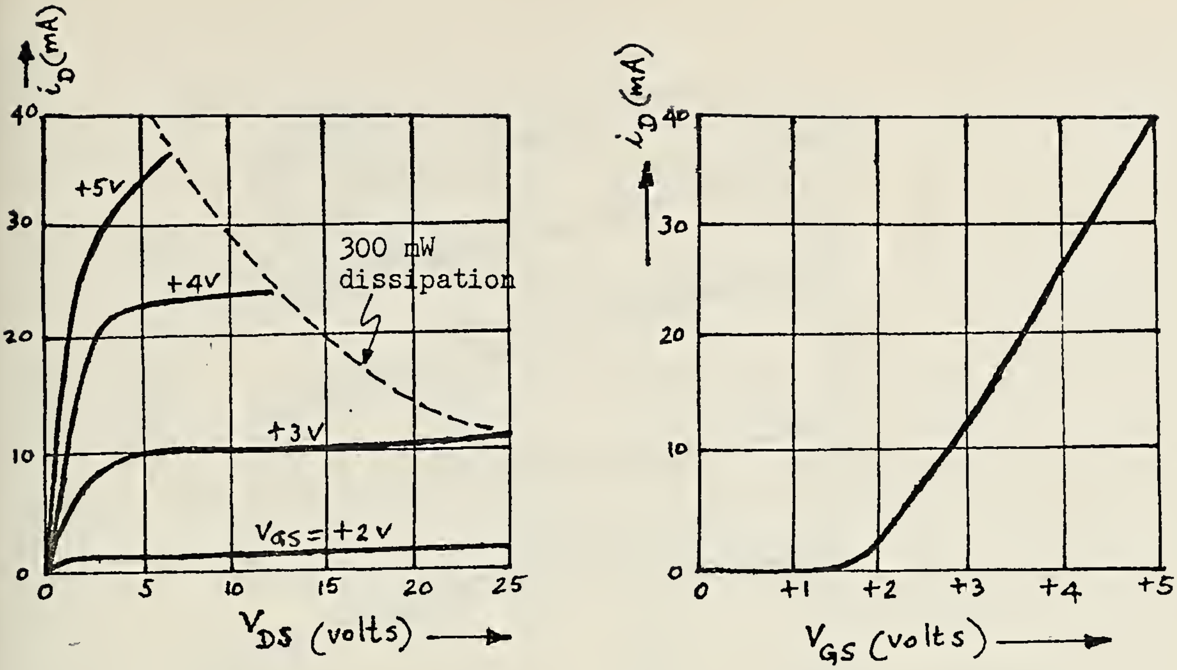

FIG. 25 The characteristic curves of SD-200 MOS-FET
(a) output characteristic curves
(b) transfer characteristic curve

The transistors chosen for Q_{1A} as well as Q_{2A} and Q_{3A} are all of the same type, namely BC-113, which is of low noise/small signal NPN diffused silicon planar epitaxial transistor with high beta characteristics. The output characteristic curves of BC-113 transistors for BC-113 are shown in Fig. 26. The important data of BC-113 transistor are:

V_{CEO} (collector to emitter voltage)	25 volts max. (at least)
h_{FE} (dc current gain)	350 typical
V_{BE} (base to emitter voltage)	0.64 typical
h_{fe} (small signal current gain)	400 typical
h_{ie} (input resistance)	10 k-ohms typical

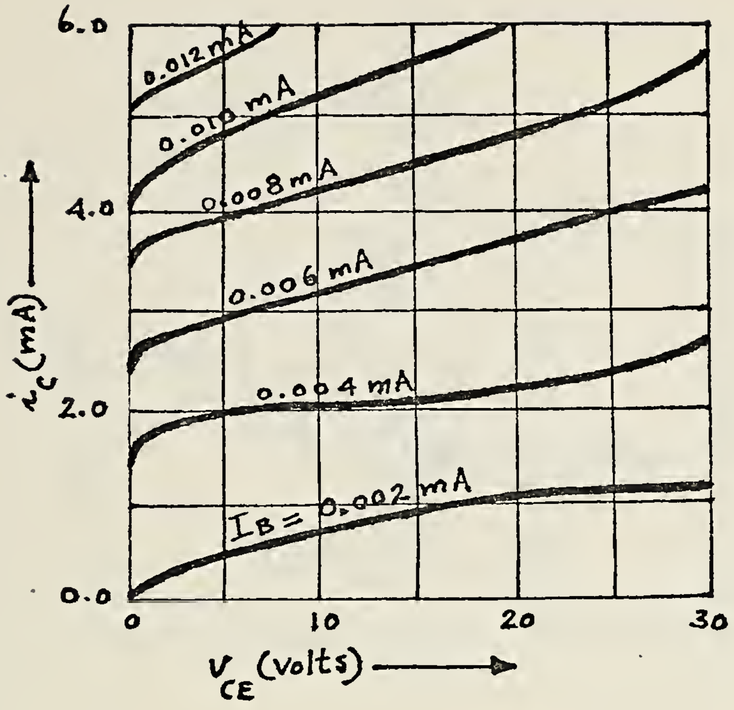

FIG. 26 The output characteristic curves of BC-113 transistor (T = 25°C)

h_{re} (voltage feedback ratio)	4.2×10^{-4} typical
h_{oe} (output conductance)	20 μ-ohms typical

Note the word "typical" for these data means that the values specified were taken at typical operating conditions of the transistor and FET.

(1) DC analysis. As a first step, an analysis (dc) on the phase-splitter is carried out yielding correct values of R_4 and R_5.

Consider the phase-splitter section only in Fig. 22, which is redrawn in Fig. 23. A quiscient point

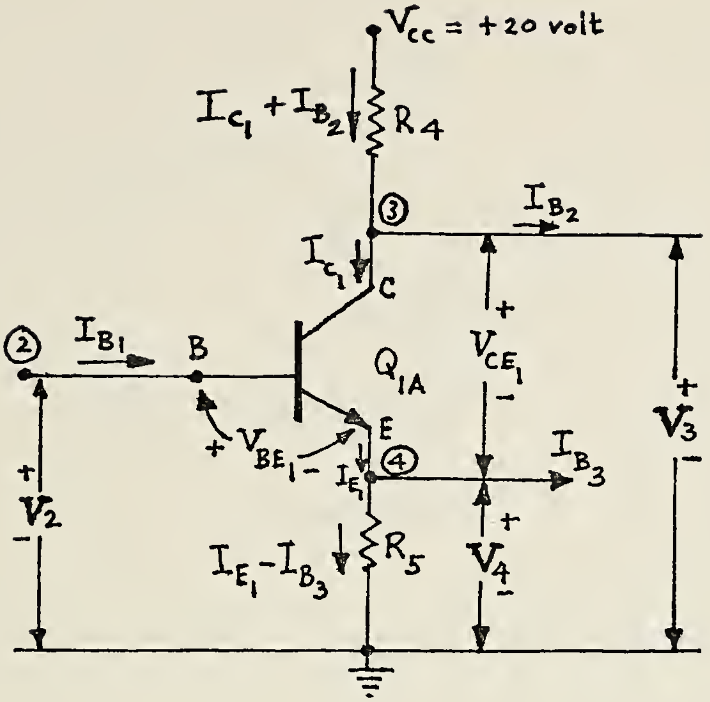

FIG. 27 The phase-splitter section in Fig. 22

(dc condition) must be chosen for Q_{1A}. Let I_c = 1.3 mA and V_{CE} = 10 volts be the values at quiscient condition (Q-point). Also let V_{cc} = + 20 volts, a value which is safe for the transistor since V_{CEO} = 25 volts max. (at least) according to given data. The Q-point is located on Fig. 26 and for this point, a corresponding base current $I_B \simeq 0.0028$ mA is found. Since the transistor types are taken the same for Q_{1A}, Q_{2A} and Q_{3A}, let the I_B's for the three at quiscient condition be the same. Therefore, $I_{B_1} = I_{B_2} = I_{B_3} = 0.0028$ mA in Fig. 27. Applying Kirchoff's Law on Fig. 27 (dc condition),

$$(I_{C_1} + I_{B_2})R_4 + V_{CE_1} + (I_{E_1} - I_{B_3})R_5 = V_{CC} \qquad (96)$$

where in this case,

$$I_{C_1} = 1.3 \text{ mA}$$

$$I_{B_2} = I_{B_3} = 0.0028 \text{ mA}$$

$$V_{CE_1} = +\ 10 \text{ volts}$$

$$V_{CC} = +\ 20 \text{ volts}$$

The emitter current I_E can be expressed as

$$I_{E_1} = I_{B_1} + I_{C_1} \qquad (97a)$$

$$= \frac{I_{C_1}}{h_{FE}} + I_{C_1} \qquad (97b)$$

$$= \frac{1 + h_{FE}}{h_{FE}} I_{C_1} \qquad (97c)$$

Since the operating condition here, namely quiscient values of V_{CE_1} and I_{C_1}, are chosen as typical, the hybrid parameters in the data given may be used. Note that these values can be determined using the given characteristic curves.

Eq. (95) then becomes

$$(1.3 + 0.0028)R_4 + 10.0 + \{[(\frac{1+350}{350})(1.3)]$$

$$- 0.0028\}R_5 = +\ 20$$

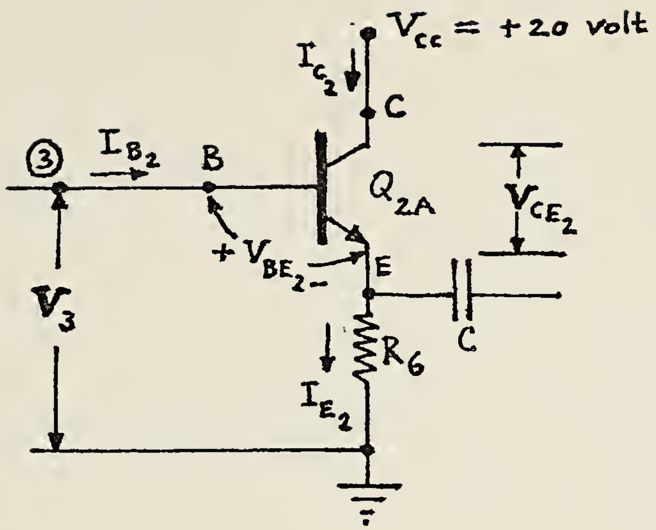

FIG. 28 Q_{2A} transistor stage in Fig. 22

Since $R_4 = R_5$ is the required condition for the phase-splitter,

$$1.3028\ R_4 + 10.0 + 1.3009\ R_4 = 20$$

$$2.6037\ R_4 = 10$$

$$R_4 = 3.841 \text{ k-ohms} = R_5 \qquad (98)$$

To make a fine adjustment to balance $v_{③}$ and $v_{④}$, a potentiometer is connected to R_4 as shown in Fig. 22. Therefore, in actual realization R_4 is not exactly equal to R_5; the requirement to achieve $v_{③} = v_{④}$ is a more dominating factor.

As a second step, the resistance value of Q_{2A} stage will be determined. Consider the Q_{2A} stage shown in Fig. 28. Applying Kirrchoff's voltage law to the

base-emitter circuit,

$$V_{③} = V_{BE_2} + I_{E_2} R_6 \tag{99}$$

where

$$V_{③} = V_{CE_1} + I_{E_1} R_5 \tag{100a}$$

or

$$V_{③} = V_{CE_1} + \frac{1 + h_{FE}}{h_{FE}} I_{C_1} - I_{B_3} R_5 \tag{100b}$$

$$= 10.0 + \frac{351}{350} 1.3 - 0.0028 (3.841)$$

$$= 14.996 \text{ volts} \approx 15 \text{ volts}$$

Typical value of V_{BE} for BC-113 transistor is 0.64 volt. Therefore, V_{BE_2} = 0.64 volt, and

$$I_{E_2} = I_{B_2} + I_{C_2} \tag{101a}$$

(no current flows through the capacitor C at dc-condition) or

$$I_{E_2} = I_{B_2} + h_{FE} I_{B_2} \tag{101b}$$

Since $I_{B_2} = I_{B_1} = 0.0028$ mA was assumed,

$$I_{E_2} = 0.0028 + (350)(0.0028) = 0.983 \text{ mA}$$

Eq. (99) then becomes

$$15 = 0.64 + (0.983)\, R_6$$

or

$$R_6 = 14.60 \text{ k-ohms} \tag{102}$$

The Q-point of Q_{2A} transistor is at:

$$I_{C_2} = h_{FE}\, I_{B_2} = (350)(0.0028) = 0.98 \text{ mA}$$

and

$$V_{CE_2} = V_{CC} - I_{E_2} R_6 = 20 - (0.983)(14.60)$$

$$= 5.64 \text{ volts.}$$

As a third step, the resistance value of Q_{3A} transistor stage will be determined. Consider Q_{3A} stage shown in Fig. 29. Applying Kirrchoff's law to the base-emitter circuit,

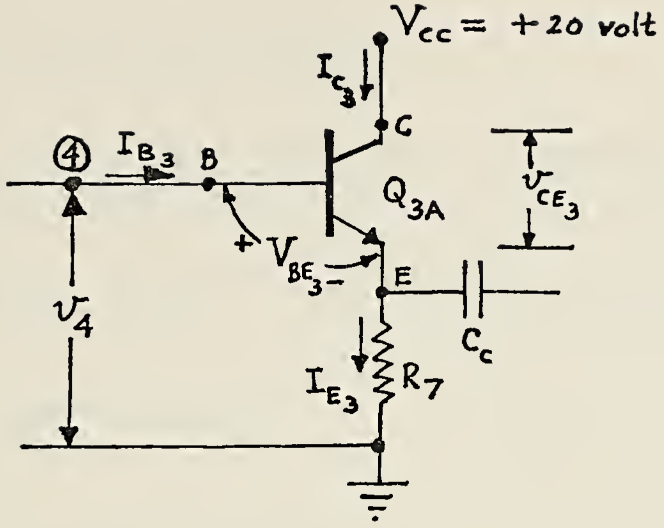

FIG. 29 Q_{3A} transistor stage in Fig. 22

$$V_4 = V_{BE_3} + I_{E_3} R_7 \tag{103}$$

where

$$V_4 = (I_{E_1} - I_{B_3}) R_5 = [(\frac{1 + h_{FE}}{h_{FE}}) I_{C_1} - I_{B_3}] R_5$$

$$= 4.996 \text{ volts} \approx 5 \text{ volts}$$

$$V_{BE_3} = 0.64 \text{ volt}$$

$$I_{E_3} = I_{B_3} + I_{C_3} \tag{104a}$$

(no current flows through capacitor C_c at dc condition)

or

$$I_{E_3} + I_{B_3} + h_{FE}\, I_{B_3} \tag{104b}$$

Since $I_{B_3} = I_{B_2} = I_{B_1} = 0.0028$ mA was assumed,

$$I_{E_3} = 0.0028 + (350)(0.0028) = 0.983 \text{ mA}$$

Eq. (103) then becomes

$$5 = 0.64 + (0.983)\, R_7$$

or

$$R_7 = 4.431 \text{ k-ohms} \tag{105}$$

The Q-point of Q_{3A} transistor is at:

$$I_{C_3} = h_{FE}\, I_{B_3} = (350)(0.0028) = 0.98 \text{ mA}$$

and

$$V_{CE_3} = V_{CC} - I_{E_3}\, R_7 = 20 - (0.983)(4.431) = 15.64 \text{ volts}$$

As a fourth step, the values of R_1, R_2 and R_3 will be determined. Consider F_1 (FET) circuit in Fig. 22, which is redrawn in Fig. 30.

D = drain
S = source
G = gate

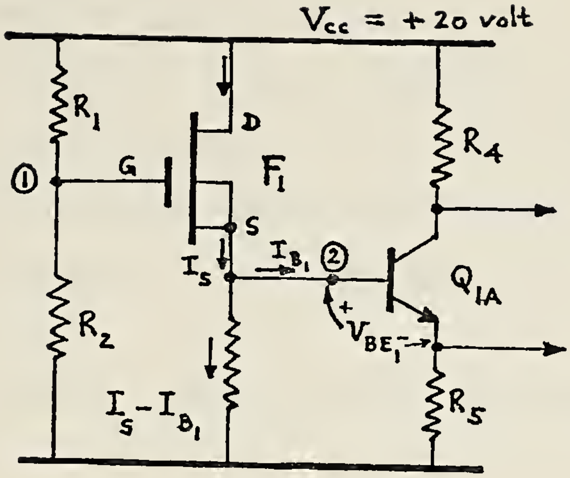

FIG. 30 The FET and phase-splitter circuit in Fig. 22

The voltage V_{DS} (drain to source voltage),

$$V_{DS} = V_{CC} - V_{②} \tag{106}$$

where

$$V_{②} = V_{BE_1} + (I_{E_1} - I_{B_3})\, R_5 \tag{107}$$

$$= 6.4 + [\tfrac{351}{350}\,(1.3) - 0.0028]\,(3.841)$$

(refer to previous calculations)

$$= 11.40 \text{ volts}$$

Therefore according to Eq. (106), $V_{DS} = 20 - 11.40 = 8.60$ volts. The voltage drop across R_3 is practically $= V_{②}$ because I_{B_2} is very small (= 0.0028 mA) and the resistance

of the wire connecting point 2 and Q_{1A}'s base is negligible. Now, to find the value of R_3, a drain current (dc) must be chosen, i.e. I_D at Q-point of the SD-200 MOS-FET. On the SD-200 MOS-FET output characteristic curves are shown in Fig. 25, a convenient Q-point is chosen at:

$$V_{DS} = 8.60 \text{ volts (which has been computed)}$$

and

$$I_D = 2 \text{ mA (chosen conveniently)}.$$

Since $I_D = I_S$, the current flowing through R_3 can be found as

$$R_3 = \frac{V_2}{I_S - I_{B_2}} = \frac{11.40}{1.997} = 5.71 \text{ k-ohms} \tag{108}$$

Next, to find R_1 and R_2, the FET portion of Fig. 30 can be represented by a Thevenin equivalent circuit shown in Fig. 31. In this equivalent circuit,

$$V = \frac{R_2 \ V_{CC}}{R_1 + R_2} \tag{109}$$

and

$$R_b = \frac{R_1 \ R_2}{R_1 + R_2} \tag{110}$$

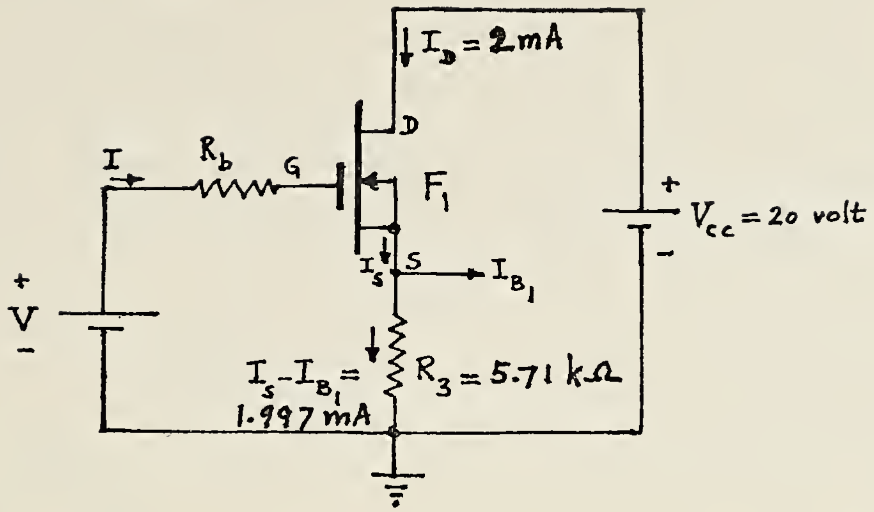

FIG. 31 Thevenin equivalent circuit for bias resistance calculations of the FET circuit in Fig. 22

V_{GS_1} is the gate to source voltage of FET F_1 at quiscient condition. With the given Q-point on Fig. 25(a) (I_D = 2mA), the corresponding V_{GS_1} is determined from Fig. 25(b) and found as V_{GS_1} = + 2 volts. The voltage at the gate terminal V_G is equal to the sum of V_{GS_1} and the voltage drop across R_3

$$V_G = V_{GS_1} + V_{2} \tag{111}$$

$$= 2.0 + 11.40$$

$$= 13.40$$

For an FET, the gate current is the gate leakage current. Ideally, it is desired to be zero. The SD-200 MOS-FET data gives this current as 0.001 nA which is practically negligible. Hence, in Eq. (109) $V = V_G$ and R_1 and R_2 act merely as a voltage divider. Eq. (109) then becomes

$$13.40 = \frac{R_2}{R_1 + R_2} (20)$$

$$\frac{R_2}{R_1 + R_2} = 0.6698$$

or

$$R_2 = 0.6698\ R_1 + 0.6698\ R_2$$

$$0.3302\ R_2 = 0.6698\ R_1$$

$$R_2 = 2.0285\ R_1 \qquad (112)$$

R_1 may be chosen arbitrarily large. The resistance $R_1||R_2$ does not effect the FET's input impedance, because there is practically no current in the gate circuit. The only consideration in choosing the value of R_1 and R_2 is isolation of the incoming signal from shunting to ground with the presence of these resistors. Therefore, let R_1 be chosen as

$$R_1 = 5.0 \text{ Meg-ohms (large enough)} \qquad (113a)$$

then from Eq. (112)

$$R_2 = (2.0285)(5.0) = 10.143 \text{ Meg-ohms} \tag{113b}$$

Since section II is identical to section I in Fig. 22, the bias resistances of the FET F_2 are calculated in the same way. Hence

$$R_8 = 5.0 \text{ Meg-ohms} \tag{114a}$$

$$R_9 = 10.0 \text{ Meg-ohms.} \tag{114b}$$

Note the fact that for the first stage of the phase train only F_1 has the bias resistances connected directly to its gate. The rest of the FET's will have the respective time constant resistance R connected between their gate and bias resistances.

(2) AC Analysis. In the previous discussions, the performance of the circuit in Fig. 22 when signal is present has been analysed qualitatively. A quantitative analysis will now be presented to completely evaluate the performance of the circuit and to see that the circuit is really performing as an all-pass network.

As a first step in the ac-analysis, consider the phase-splitter in Fig. 22 as if it were a CE-amplifier with an emitter resistance (R_5) connected. It is

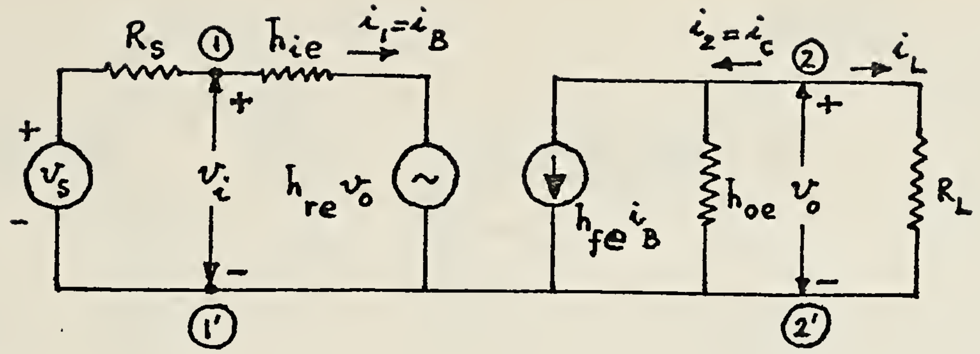

FIG. 32 The ac-hybrid-equivalent circuit of a CE-amplifier (no emitter resistance)
R_s is the signal source internal resistance
R_L is the load resistance

known that a CE-amplifier (without emitter resistance) can be represented by the ac-hybrid-equivalent circuit shown in Fig. 32.

The current gain A_i for the CE-amplifier is

$$A_i = \frac{i_L}{i_1} = \frac{-\ i_2}{i_1} \tag{115}$$

From the equivalent circuit in Fig. 32,

$$i_2 = h_{fe}\ i_1 + h_{oe}\ v_o \tag{116}$$

Substituting

$v_o = -\ i_2R_L$ in Eq. (116),

$$A_i = -\ \frac{i_2}{i_1} = -\ \frac{h_{fe}i_1 - h_{oe}i_2R_L}{i_1}$$

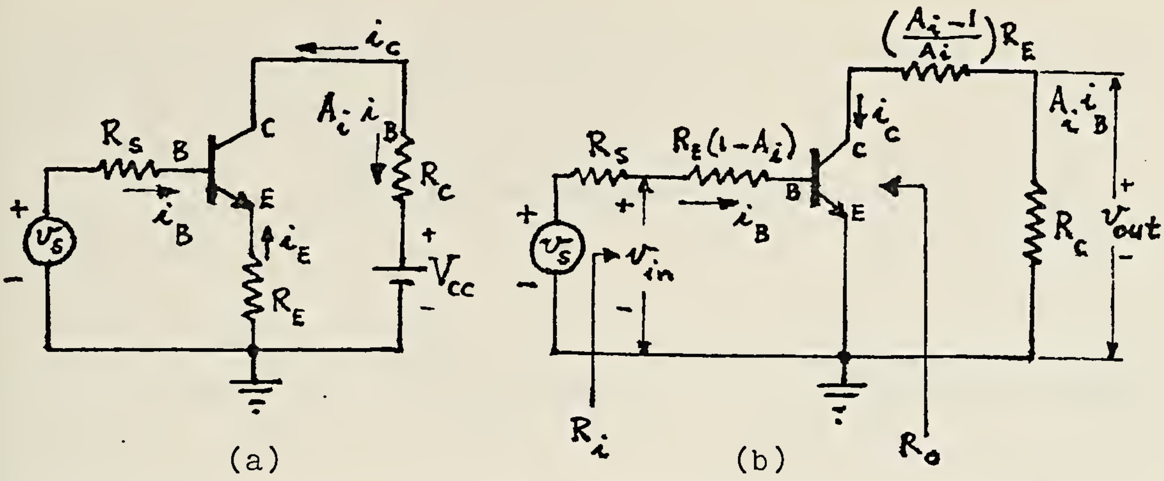

FIG. 33 (a) CE-amplifier with emitter resistance R_E
(b) Small-signal equivalent circuit

or

$$A_i = - h_{fe} - A_i h_{oe} R_L$$

$$A_i(1 + h_{oe}R_L) = - h_{fe}$$

or

$$A_i = - \frac{h_{fe}}{1 + h_{oe}R_L} \tag{117}$$

Consider now the case where the phase splitter is a CE-amplifier with a resistance in its emitter circuit. The phase splitter is redrawn in Figs. 33(a) and its equivalent circuit is shown in Fig. 33(b). Note that the equivalent circuit in Fig. 33(b) was derived using the dual of Miller's theorem [8]. The two amplifiers in Fig. 33(a) and (b) are

equivalent in the sense that the base and collector currents are the same in the two circuits.

The effective load impedance R_L is from Fig. 33(b)

$$R_L = R_C + (\frac{A_i - 1}{A_i})\ R_E \tag{118}$$

An analysis consistent with the circuit in Fig. 32 is now possible. Using Fig. 33(b), Eqs. (117) and (118) the current gain is now,

$$A_i = \frac{-\ h_{fe}}{1 + h_{oe}R_L} = \frac{-\ h_{fe}}{1 + h_{oe}\{R_C + (\frac{A_i - 1}{A_i})\ R_E\}} \tag{119}$$

For the above equation, A_i can be solved explicitly,

$$A_i = \frac{h_{oe}\ R_E - h_{fe}}{1 + h_{oe}(R_C + R_E)} \tag{120}$$

The input resistance can be evaluated using Fig. 33(b) and its hybrid ac equivalent circuit in Fig. 32 (with $R_E(1-A_i)$ resistance in series with h_{ie}),

$$R_{in} = \frac{v_{in}}{i_b} = (1 - A_i)R_E + h_{ie} + h_{re}\ \frac{v_{out}}{i_b} \tag{121}$$

Since

$$v_{out} = -\ i_C R_L = A_i\ i_B\ R_L \tag{122}$$

Eq. (121) can be expressed by

$$R_{in} = \frac{v_{in}}{i_B} = (1 - A_i)R_E + h_{ie} + h_{re} A_i R_L \qquad (123)$$

where R_L is given by Eq. (118) and A_i is given by Eq. (120). Usually the third term on the right hand side of Eq. (123) can be neglected (very small compared with the other two terms).

The voltage gain is expressed by

$$A_{V_E} = \frac{A_i R_C}{R_{in}} \qquad (124)$$

where A_i is given by Eq. (120), R_{in} is given by Eq. (123). The subscript E for A_V indicates that the voltage gain is for CE-configuration of the amplifier.

The output resistance (with R_L considered external to the amplifier) looking into the output terminals can be evaluated using the same equivalent circuit and the equations that have been derived, v_{in} set to zero and a voltage is applied across the output terminals. The evaluation yields

$$R_{o_{CE}} = \frac{1}{h_{oe}} \frac{(1+h_{fe})R_E+(R_s+h_{ie})(1+h_{oe}R_E)}{R_E+R_s+h_{ie}-h_{re}h_{fe}/h_{oe}} \qquad (125)$$

Note that if $R_E >> R_s + h_{ie}$, then

$$R_{o_{CE}} \approx \frac{1 + h_{fe}}{h_{oe}} + \frac{(R_s + h_{ie})(1 + h_{oe}R_E)}{h_{oe}R_E} \tag{126}$$

As a second step, consider now the phase-splitter circuit as if it were CC-configurated with a resistance (R_4) in its collector circuit. From Fig. 33, it is seen that the relationship between the CE-current gain A_{i_E} (designated simply by A_i in the figure) and the CC-current gain A_{i_C} is

$$A_{i_C} = 1 - A_{i_E} \tag{127}$$

where

$$A_{i_C} = - \frac{i_E}{i_B}$$

and

$$A_{i_E} = - \frac{i_C}{i_B}$$

Substituting Eq. (120) into Eq. (127), the expression for the current gain is

$$A_{i_C} = \frac{1 + h_{oe} R_C + h_{fe}}{1 + h_{oe}(R_C + R_E)} \tag{128}$$

The input resistance R_{in} is obtained from Eq. (121), with A_i replaced by A_{i_E}. The voltage gain of the

CC circuit with R_C present in the collector circuit is obtained as follows:

$$A_{V_C} = \frac{v_{out}}{v_{in}} = A_{i_C} \frac{R_E}{R_{in}} \tag{129}$$

As a third step, the actual values evaluated using these formulas with the given transistor data are pursued. These values are required to base a judgment which will be made in the conclusion of this analysis, whether or not the phase-splitter and the related transistor and FET stages have met the performance requirements.

From Eq. (120),

$$A_i = \frac{h_{oe} R_E - h_{fe}}{1 + h_{oe}(R_C + R_E)}$$

$$= \frac{(20)(10^{-6})(3841) - 400}{1 + (20)(10^{-6})(3841 + 3841)}$$

$$= - \frac{399.92}{1.154} = - 346.66$$

$$A_i \approx 347 \tag{130}$$

From Eq. (118)

$$R_L = R_C + \frac{A_i - 1}{A_i} R_E = 3.841 + \frac{348}{347} (3.841)$$

$$= 7.69 \text{ k-ohms}$$

and from Eq. (123)

$$R_{in} = (1 - A_i)\ R_E + h_{ie} + h_{re}\ A_i\ R_L$$

$$= (348)(3.841) + 10 + (4.2)(10^{-4})(-347)(7.69)$$

$$R_{in} = 1.34 \text{ Meg-ohms} \tag{131}$$

From Eq. (124)

$$A_{V_E} = \frac{A_i\ R_C}{R_{in}}$$

$$= \frac{(-347)(3.841)}{1.34} = -\ 0.9906$$

$$A_{VE} = -\ 0.99 \tag{132}$$

From Eq. (128)

$$A_{i_C} = \frac{1 + h_{oe}\ R_C + h_{fe}}{1 + h_{oe}(R_C + R_E)}$$

$$= \frac{1 + (20)(10^{-6})(3841) + 400}{1 + (20)(10^{-6})(3841 + 3841)}$$

$$= \frac{401.077}{1.154} = 347.67$$

$$A_{i_C} = 348 \tag{133a}$$

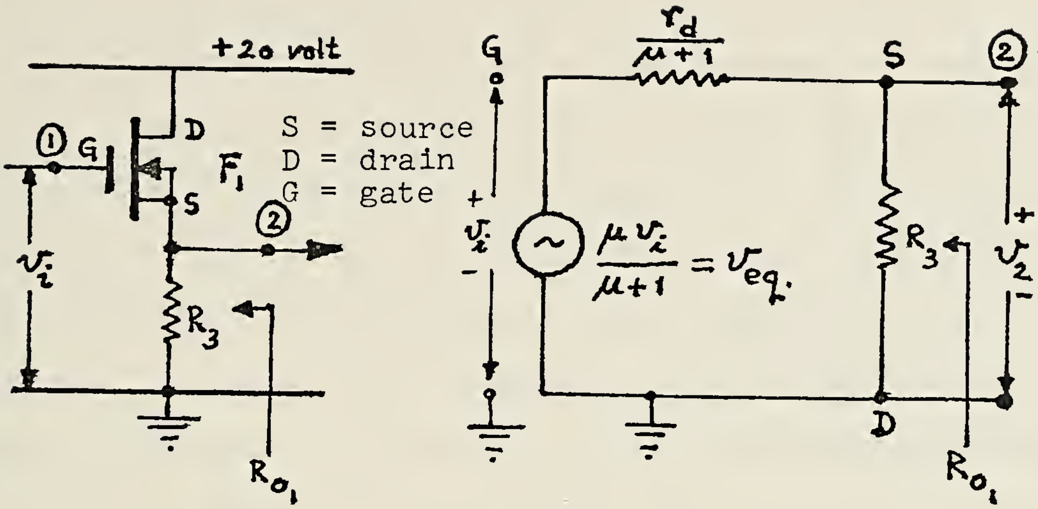

FIG. 34 (a) The FET F_1-stage of the circuit in Fig. 22
(b) Its small-signal equivalent circuit

and from Eq. (129),

$$A_{V_C} = A_{i_C} \frac{R_E}{R_{in}} = (348) \frac{(3.841)}{(1344.1)} = +\ 0.9935$$

or

$$A_{V_C} = +0.99 \tag{133b}$$

As a fourth step, an equation of the resistance in the input circuit of Q_{1A} stage, namely R_s, must be established. The value of R_s is needed in order to evaluate the output resistance of Q_{1A}-stage (using Eq. (125)). R_s is the output resistance of the FET F_1-stage. The FET stage is redrawn in Fig. 34(a) and its small-signal equivalent circuit is shown in Fig. 34(b). Note that the gate leakage

current (gate to source) is practically non-existent (0.001 nA typical) such that the gate terminal in the equivalent circuit can be considered unconnected to the rest of the circuit like an ideal FET should be. The output resistance then is always independent of the bias resistances; looking into the output terminals the resistance seen is always R_{o_1} because it is buffered with an infinite resistance of the input. According to the definition, the output resistance R_{o_1} is a parallel combination of the load (R_3 in this case) and the resistance looking into the output terminals (S-D open, without R_3) and with input voltage source short circuited (i.e. $v_{eq} = 0$ in this case). Hence,

$$R_{o_1} = R_3 \; // \; \frac{r_d}{\mu + 1} \tag{134}$$

where $\mu = g_m \, r_d$.

The value of R_3 has been found earlier, namely $R_3 = 5.71$ k-ohms. Now, the value of r_d need to be determined first. Referring to the characteristic curves of SD-200 MOS-FET in Fig. 25(a), with $I_D = 2$ mA at Q-point, it is hard to obtain r_d (the slope of the curve at that point); so, one can do a good estimate of r_d by evaluating the slope at Q-point with larger I_D, say $I_D = 15$ mA, and at $V_{DS} = 10$ volts, and find that the value of r_d at this particular Q-point to be approximately 10 k-ohms. If now the desired Q-point location is at $I_D = 2$ mA and at $V_{DS} = 15$ volts

(chosen conveniently), it is reasonable to estimate the value of r_d at this point to be 15 k-ohms. Therefore,

$$r_d = 15 \text{ k-ohms}$$

$$g_m = 15{,}000 \ \mu\text{-ohms}$$

$$\mu = g_m \, r_d = (15{,}000)(15{,}000)(10^{-6})$$

$$\mu = 225$$

and Eq. (134) gives

$$R_{o_1} = (5710) \ // \ [\frac{15{,}000}{225 + 1}]$$

$$= (5710) \ // \ (66.37)$$

$$= \frac{(5710)(66.37)}{5710 + 66.37}$$

$$R_{o_1} = 65.61 \text{ ohms} \qquad (135)$$

The input resistance of the FET stage must be very high. This is indeed the case, since there is practically no current flowing between the gate and source.

Consider now Eq. (135). The output resistance R_{o_1} of the F_1-stage acts as the effective R_s resistance in the input circuit of Q_{1A} transistor stage. Therefore,

evaluating Eq. (119) for this stage is now possible, with $R_s = R_{o_1} = 65.61$ ohms. Eq. (119) gives

$$R_{o_{③}} = \frac{1}{20 \times 10^{-6}} \; \frac{(1+400)(3841)+(65.61+10000)(1+(20)(10^{-6})(3841)}{3841+65.61+10000-(4.2)(10^{-4})(400)/(20x10^{-6})}$$

$$\approx (0.05)(10^{-6}) \; \frac{(1.54)(10^{6}) + (10065.61)(1.0768)}{22306.61}$$

$$\approx (0.05)(10^{-6}) \; \frac{(1.551)(10^{6})}{(0.0223)(10^{6})}$$

$$R_{o_{③}} \approx 3.476 \text{ Meg-ohms} \tag{136}$$

Note that $R_{o_{③}}$ is the output resistance looking into Q_{1A} across R_4 but R_4 is considered external to $R_{o_{③}}$. The value of $R_{o_{③}}$ is much different from its counterpart $R_{o_{④}}$ across R_5. The output resistance $R_{o_{④}}$, which is that of a CC-transistor circuit can be evaluated using a corresponding (CC) hybrid small-signal equivalent circuit similar to that in Fig. 32 and the equations that have been found, in terms of CE-parameters. The evaluation yields a reasonable approximation for the output resistance,

$$R_{o_{CC}} \approx \frac{R_s + h_{ie}}{1 + h_{fe}} \tag{137}$$

Again as before, R_5 is considered external to $R_{o_{CC}}$. In this case, R_4 acts as a protection resistor and has almost no

effect on the small-signal operation of the emitter follower. The value of R_s is the same as before. Hence,

$$R_{o_{4}} \approx \frac{65.61 + 10000}{1 + 400}$$

or

$$R_{o_{4}} \approx 25.10 \text{ ohms} \tag{138}$$

As a fifth step, one would like to evaluate the output resistances $R_{o_{5}}$ and $R_{o_{6}}$ looking into the output terminals of Q_{2A} and Q_{3A} stages respectively. This is a step needed to verify that eventually the impedances driving the time constant elements R and C are indeed low, such that the desired operation condition may take place. Q_{2A} and Q_{3A} are CC-configurated, therefore, their input impedances are high and their output impedances are low; thus they act as good buffer (isolation)-stages between their inputs and outputs. The expression in Eq. (137) in this case is again applicable. For Q_{2A}-stage, Eq. (137) gives

$$R_{o_{5}} \approx \frac{R_{s_{3}} + h_{ie}}{1 + h_{fe}} \tag{139}$$

where $R_{s_{3}}$ is the effective resistance in the Q_{2A} input circuit, namely,

$$R_{s③} = R_4 \mathbin{//} R_{o③}$$

$$= (3841) \mathbin{//} ((3.476)(10^6))$$

$$= \frac{(3841)(3.476)(10^6)}{(3.476)(10^6) + 3841}$$

$$R_{s③} = 3.836 \text{ k-ohms}$$

and Eq. (139) gives

$$R_{o⑤} \approx \frac{3836 + 10000}{1 + 400}$$

$$R_{o⑤} \approx 34.51 \text{ ohms} \tag{140}$$

and the resistance driving the RC-circuit at point ⑤ is

$$R'_{o⑤} = R_6 \mathbin{//} R_{o⑤} = \frac{(14600)(34.51)}{14600 + 34.51}$$

$$R'_{o⑤} = 34.43 \text{ ohms} \tag{141}$$

For Q_{3A}-stage, Eq. (137) is also applied, and

$$R_{o⑥} \approx \frac{R_{s④} + h_{ie}}{1 + h_{fe}} \tag{142}$$

where $R_{s④}$ is the effective resistance in Q_{3A} input circuit,

namely

$$R_{s④} = R_5 \,//\, R_{o④}$$

$$= \frac{(3841)(25.10)}{3841 + 25.10}$$

$$R_{s④} = 24.84 \text{ ohms}$$

and Eq. (142) now gives

$$R_{o⑥} = \frac{24.84 + 10000}{1 + 400}$$

$$R_{o⑥} = 25.0 \text{ ohms} \qquad (143)$$

and the resistance driving the RC-circuit at point ⑥ is

$$R_{o⑥}' = R_7 \,//\, R_{o⑥}'$$

$$= \frac{(4431)(25)}{(4431 + 25)} = 24.86$$

$$R_{o⑥}' = 24.86 \text{ ohms} \qquad (144)$$

As a sixth step, a review is conducted on the circuit parameters which have been computed and a judgment is made whether or not the particular circuit (Fig. 22) satisfies the requirements of an all-pass network.

Starting at the FET(F_1) input at point 1,
the input signal must be isolated between point 1 and ground. This is provided by the high ohm values of R_1 and R_2 (R_1 = 5.0 Meg-ohm and R_2 = 10.143 Meg-ohm), satisfactorily. Also, the isolation between the input and output circuits of the FET is well served. Since F_1 is CC-configurated, $v_{1} \approx v_{2}$ (inphase) and the resistance driving the signal at point 2 is R_{o_1} = 65.61 ohms, which is quite low hence satisfactory. The output resistance of Q_{2A}-stage, however, was found high as expected, namely R_{o_3} = 3.476 Meg-ohms, because of the CE-configuration seen at point 3. The voltage gain A_{V_E} has been shown in Eq (132) to be $\approx$ -0.99 and A_{V_C} in Eq. (133b) to be $\approx$ + 0.99. Thus, the phase-splitter operation of Q_{1A}-stage has been confirmed, $v_{2} \approx - v_{3}$ and $v_{2} \approx v_{4}$. The output resistance of Q_{1A}-stage driving Q_{3A}-stage at point 4 was found about 25.10 ohms, which is low as desired. Q_{2A}-stage has the task to transform the high driving resistance at its input (R_{o_1} // R_4) to low resistance and thus enabling a low resistance drive for the RC-circuit eventually. It was found in Eq. (141) that R_{o_5}' = 34.43 ohms, which is low as desired.

Q_{3A}-stage would not have been inserted if it was not for the purpose of blocking any signal-feedback, because actually the driving resistance at point 4 is already low. With the introduction of Q_{3A}-stage, the driving resistance at point 6 was found as R_{o_6}' = 24.86 ohms, which is low as desired .

Hence, it may be concluded that the circuit as far as the portion before the RC-circuit is concerned should work properly. Although at points 5 and 6 the driving resistances were not found to be exactly equal, they are of low level values of the same order. What is important is the low value of these resistances.

As a seventh (final) step, the values of R, C and C_c must be determined. There are six circuits like the one in Fig. 22, in cascade to form one phase train, each with different RC value. The RC values are determined by the computer simulation whose results are shown in Fig. 21(c). As an example to show the R and C computation, let the first time constant (cutoff frequency) of the first stage of the first train be picked, namely 19.5 Hertz. Then,

$$RC = \frac{1}{\text{cutoff frequency (in radians)}} \tag{145a}$$

or in this case,

$$RC = \frac{1}{2\pi\ (19.5)}$$

$$RC = 0.0082 \tag{145b}$$

Now, suitable R and C values must be chosen which satisfy Eq. (145b). There is a criteria for choosing these component values, namely the value of R must be much greater than R_s

(or the resistance driving the RC-circuit) and also the size of C should not be too large. Let the value of R be

$$R = 2 \text{ Meg-ohms} \tag{146}$$

then from Eq. (145b),

$$C = 0.0041 \ \mu\text{-Farad} \tag{147}$$

which in this case is not very small but also not very large. C could have been chosen smaller, but then R would become larger.

The value of R_s in this case is given by Eq. (141) or Eq. (144) and it is quite obvious that R is much greater than R_s. Therefore, the criteria above is reasonably satisfied. For the other time constant realizations with higher cutoff frequencies, one expects smaller values of R and C. The cutoff frequency of 19.5 Hz above is indeed unusually low, so that the values of R and C should not be surprising. In choosing the value of C_c, the guidelines are that its value must be much larger than C and that its reactance X_{C_c} at the lower edge of the passband (30 Hz in this case) must be much smaller than R. Let $C_c = 0.04$ μF be chosen. Then X_{C_c} at 30 Hz is 0.133 ohm, which is obviously much smaller than R; however, C_c is not very small but not very large either compared to C, but can be reasonably accepted

here. Again, the values of C_c for the other stages of the phase train can be better evaluated, since they have higher cutoff frequencies. Thus,

$$C_c(1^{st}\text{-stage of } 1^{st} \text{ phase train}) = 0.04\ \mu F \quad (148)$$

The constraint of choosing C_c is also its size. A size of 0.04 μF is already considered rather large.

2. The R.F. Phase-Shift Subsystem Components

The R.F. Phase-shift Subsystem Components are not crucial parts which are difficult to design as in the case of the audio phase phase-shift circuit. Instead of working over a range of frequencies, the carrier frequency phase-shift circuit works only at a single fixed frequency, thus it does not present difficulties in the design. A simple circuit consisting of only R and C components will suffice. An arrangement of two RC circuits giving +45° and -45° can easily be built. As for the balanced-modulators, they may be chosen from packages offered by various integrated circuit (IC) manufacturers.

C. DESIGN OF THE FILTER SUBSYSTEM

1. General

The band-pass filter which is to be designed has the frequency characteristics as shown in Fig. 35(a). Fig. 35(b) shows how the band-pass (BP) filter can actually be regarded. The 30-dB suppression as shown is contributed by

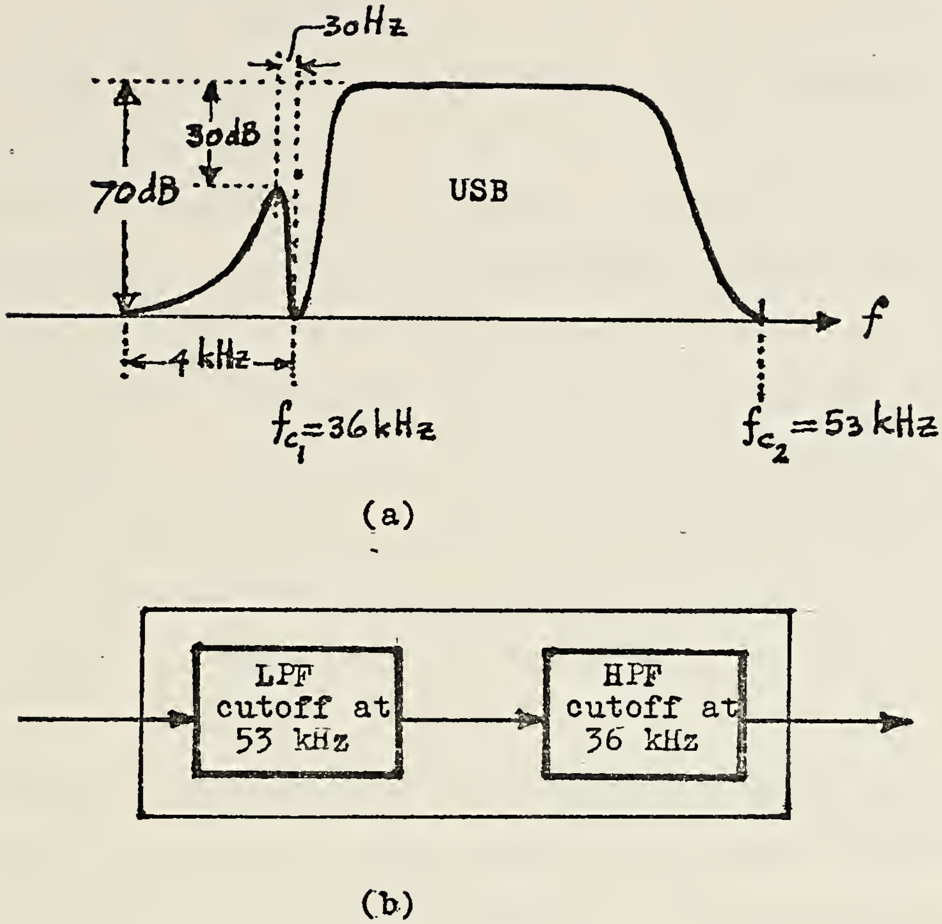

FIG. 35 (a) Frequency characteristics of the filter subsystem
(b) The filter may be regarded as a cascade of an LPF and an HPF

the phase-shift subsystem. After passing the filter, the sideband suppression must be 70-dB at least at 4 kHz distance from the carrier frequency. Let the USB be chosen.

The choice of the carrier frequency is based on the following considerations:

- it must be greater than at least twice the upper edge of the baseband signal (17 kHz in this case) to avoid second

harmonic interference; the effect of higher harmonics has been assumed insignificant in this case; recall that these interferences are caused by imperfection in the balanced modulator or mixer operation.

- choosing a lower frequency implies less poles required in the realization (compared with choosing a higher frequency), thus making it easier to design.

- the frequency chosen should be less than 108 kHz, the upper limit recommended by CCITT for program-channel broadcasting (note that the sideband suppressor has been intended for application in broadcasting); and usually the carrier frequency chosen is an integer multiplication of 4-kHz.

Based on these considerations, the frequency configuration in Fig. 35(a) is chosen. USB in this case is more favorable. The band from 36 to 53 kHz can be used as a program channel in a broadcasting system. If a stereo-broadcasting system were desired, another program channel may be placed in the region between 53 kHz and 108 kHz (may be USB or LSB); as a consequence however, its design is more elaborate than the first, because of the higher frequency where the baseband is translated (with the same suppression specification) needs more poles. Let the discussions from hereon be focused on the realization of Fig. 35.

2. Pole Locations (Chebyshev Approximation)

First, the pole locations of the LPF (low-pass filter) with $f_{c_2} = 53$ kHz are determined. Let these assumptions be made: The sideband suppression level must be at least 30 dB (or the filter's frequency response is 30 dB down) at $f = 2f_{c_1}$ and the maximum peak-to-peak ripple in the passband 0.25 dB. It is noted here that the above 30 dB specification is only to account the effect of the second harmonic f_{c_1}, i.e. 72 kHz, the effect of higher harmonics for practical purposes may be neglected; moreover, the signal itself is already bandlimited between 0.03 to 17 kHz, therefore a suppression level of 30 dB would suffice thus makes the design easier (less poles involved). It is also noted from the overall hybrid system's specifications that the passband ripple is not to exceed 1.5 dB (peak-to-peak). This specification is actually the allowed total ripple contributed by the filters in the transmitter as well as in the receiver. Since the complete filter is a combination or a cascade of LPF and an HPF, each having ripple, the worst total ripple may be the algebraic sum of them, because they may be inphase or out of phase. This consideration applies to both the transmitter and receiver. Therefore, the choice to specify 0.25 dB for each the filters is quite safe in order to fulfill the overall passband ripple specification.

According to Eq. (65), the ripple factor ε can be found.

$$\varepsilon^2 = 10^{(0.1)(0.25)} - 1$$

or

$$\varepsilon = 0.243$$

With 30 dB suppression specified and using Eq. (54),

$$\frac{1}{1 + \varepsilon^2 T_n{}^2(\omega)} = 10^{-1.5}$$

$$\frac{1}{1 + (0.243)^2 T_n{}^2(\omega)} = 10^{-1.5}$$

$$10^{-1.5} + 0.059\, T_n{}^2(\omega)\, 10^{-1.5} = 1$$

$$0.059\, T_n{}^2(\omega)\, 10^{-1.5} = 0.968$$

$$T_n{}^2(\omega) = \frac{(10^{1.5})(1.03)}{0.059} = 518.8$$

or

$$T_n(\omega) = 22.78$$

The suppression should take place effectively at $f = 2\, f_{c_1}$; since $f_{c_1} = 36 \text{ kHz} = \frac{36}{53} f_{c_2}$, then $f = \frac{72}{53} f_{c_2} = 1.358\, f_{c_2}$. Therefore,

$$T_n(\omega) = T_n(1{,}358) = 23.5$$

Using Eq. (66),

$$T_n(1,358) = \frac{(1.358 + \quad (1.358)^2-1)^n + (1.358 - \quad (1.358)^2-1)^{-n}}{2}$$

$$22.78 = \frac{(2.277)^n + (0.439)^{-n}}{2}$$

$$45.56 = (2.277)^n + (0.439)^{-n}$$

$$n = 380$$

or round up

$$n = 4$$

Hence, there are 4 poles required for the LPF section of the filter. The locations of these 4 poles are now determined. Since Table 2 does not provide them, they must be evaluated using Eq. (59) and ((63). Using Eq. (59),

$$\phi_2 = \frac{1}{n} \sinh^{-1} \frac{1}{\varepsilon}$$

$$\phi_2 = \frac{1}{4} \sinh^{-1} \frac{1}{0.243}$$

$$\phi_2 = 0.5306$$

$$\sinh \phi_2 = 0.5558 \tag{149a}$$

$$\cosh \phi_2 = 1.1441$$

and using Eq. (63),

$$s_{k+1} = -\sin(2k+1)\frac{\pi}{8}\sinh \phi_2 + j\cos(2k+1)\frac{\pi}{8}\cosh \phi_2$$
$$k = 0,1,2,\ldots,7$$

the following 4-pole locations are obtained:

$$s_{1,4} = -\ 0.2127 \pm j\ 1.0570 \tag{149b}$$

$$s_{2,3} = -\ 0.5135 \pm j\ 0.4378$$

Second, the pole locations of the HPF are determined. According to the discussions in Section III.B.4, in order to do this, an LPF with the same specifications may be designed first, then using the frequency transformation method the HPF is obtained without changes in the filter characteristics whatsoever, i.e. the same cutoff frequency, sideband suppression level, passband ripple etc.). The specifications for the filter in this case are: 50 dB sideband suppression level at a frequency of 4 kHz from cutoff (f_{c_1}) and maximum peak-to-peak ripple of 0.25 dB in the passband. Note that the total sideband suppression level including the phase-shift

sybsystem's contribution would be about (30 + 50) dB = 80 dB, a figure well above the (at least) 70 dB specified. This is necessary for safety performance. With maximum peak-to-peak passband ripple of 0.25 dB, the ripple factor is the same as before, namely $\varepsilon = 0.243$. Using Eq. (51),

$$\frac{1}{1 + (0.243)^2\, T_n^{\,2}(\omega)} = 10^{-2.5}$$

$$10^{-2.5} + (0.059)\, 10^{-2.5}\, T_n^{\,2}(\omega) = 1$$

$$(0.059)\, 10^{-2.5}\, T_n^{\,2}(\omega) = 0.997$$

$$T_n^{\,2}(\omega) = \frac{(10^{2.5})(0.997)}{0.059} = 5343.71$$

$$T_n(\omega) = 73.10$$

or rounded up

$$T_n(\omega) = 74 \tag{150a}$$

In this case ω is the frequency where the sideband suppression level of 50 dB starts to take place, namely $f_{c_1} + \frac{4}{36} f_{c_1} = 1.11\, f_{c_1}$ (LPF case), and since $T_n(\omega)$ is scaled to f_{c_1} then $\omega = 1.11$ and

$$T_n(1.11) = 74 \tag{150b}$$

Applying this result to Eq. (66) gives

$$T_n(1.11) = \frac{(1.11 + \sqrt{(1.11)^2 - 1}\,) + (1.11 - \sqrt{(1.11)^2 - 1}\,)^{-n}}{2}$$

$$74 = \frac{(1.59)^n + (0.63)^{-n}}{2} \tag{151a}$$

$$148 = (1.59)^n + (0.63)^{-n}$$

$$n = 9.3$$

or rounded up

$$n = 10 \tag{151b}$$

To find the 10 pole locations, Eqs. (59f) and (63) are evaluated because Table-2 does not provide them.

Evaluating Eq. (59f) gives

$$\phi_2 = \frac{1}{n} \sinh^{-1} \frac{1}{\varepsilon} = \frac{1}{10} \sinh^{-1} \frac{1}{0.243} = 0.2122 \tag{152a}$$

$$\sin \phi_2 = 0.2138$$

$$\cos \phi_2 = 1.0226 \tag{152b}$$

Evaluating Eq. (63) gives

$$\begin{aligned} s_{1,10} &= -\ 0.0334 \pm j\ 1.0100 \\ s_{2,9} &= -\ 0.0971 \pm j\ 0.9111 \\ s_{3,8} &= -\ 0.1512 \pm j\ 0.7231 \\ s_{4,7} &= -\ 0.1905 \pm j\ 0.4643 \\ s_{5,6} &= -\ 0.2112 \pm j\ 0.1560 \end{aligned} \tag{152c}$$

(all poles scaled to 36 kHz)

3. A Proposed Realization

To realize the filter with pole locations found in Section 2, consider the circuit arrangment shown in Fig. 36(a) which is an active-filter circuit using only R,C and OPAMP (operational amplifier) components. This circuit is a realization of a pair of (conjugate) poles only in the case of the filter is an LPF. A generalized relation will be established regarding the poles of this circuit and the circuit parameter(s) which are variable. It will be shown that by varying the gain of the circuit or the time constants of the two stages, or the combination of them (within the stable condition limits of the circuit), one could obtain the desired pole locations.

The two OPAMPs are connected in non-inverting configuration, thus the time constant elements R_1,C_1 and R_2,C_2 face high (almost infinite) input impedance of the first and second OPAMPs respectively. This situation is desirable such that there will be no loading effects influencing the operation of R_1,C_1,R_2 and C_2. In fact, it is for this reason that the non-inverting configuration was chosen for the OPAMPs. Because the OPAMPs are non-inverting, the phase of v_x will be the same with that of v_3 and v_4, hence no phase inversion problem arises. All of these make the OPAMP application for this purpose quite favorable.

Provided that the gain of the first OPAMP-stage is unity, the essential ac-equivalent circuit will be that shown in Fig. 36(b). The analysis of the circuit arrangement is based on this equivalent circuit.

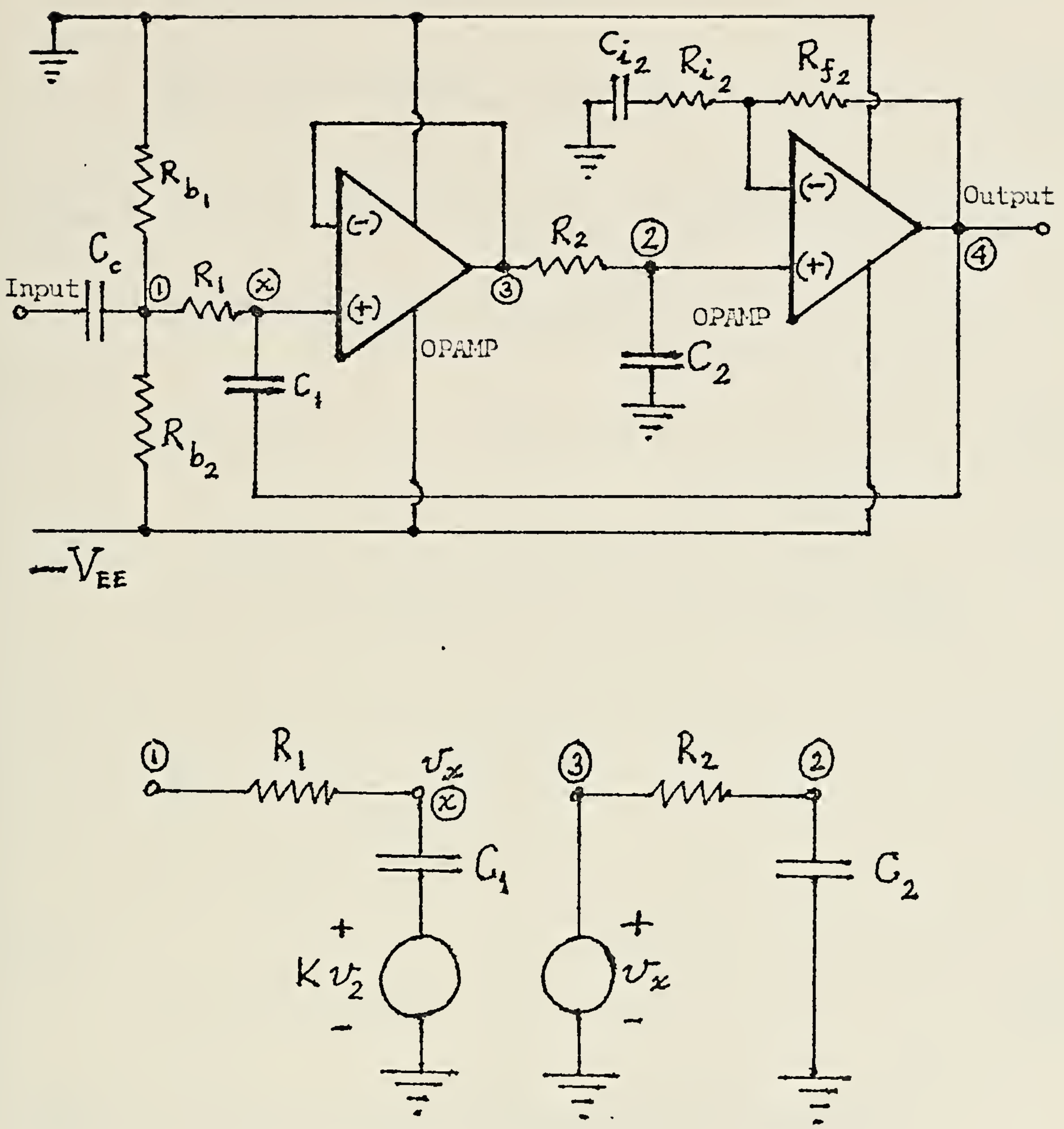

FIG. 36 (a) A proposed realization of a pair of conjugate poles (LPF case)

(b) The essential ac equivalent circuit

Applying Kirchhoff's law to the first stage,

$$\frac{1}{R_1}(v_x - v_1) + sC_1(v_x - Kv_2) = 0 \tag{153a}$$

where K is the gain of the circuit received at point x

$$v_x - v_1 + sC_1R_1v_x - SC_1R_1Kv_2 = 0$$

or

$$(1 + s\tau_1)v_x - v_1 - s\tau_1Kv_2 = 0 \tag{153b}$$

where $\tau_1 = R_1C_1$ is the first stage time constant.

Applying Kirchhoff's law to the second stage,

$$\frac{1}{R_2}(v_2 - v_x) + sC_2v_2 = 0 \tag{154a}$$

$$v_2 - v_x + sC_2R_2v_2 = 0$$

or

$$v_x = (1 + s\tau_2)v_2 \tag{154b}$$

where $\tau_2 = R_2C_2$ is the second stage time constant.

Substituting Eq. (154b) into Eq. (153b),

$$(1 + \tau_1s)(1 + \tau_2s)v_2 - \tau_1sKv_2 = v_1 \tag{155a}$$

$$\frac{v_2}{v_1} = \frac{1}{(1+\tau_1 s)(1+\tau_2 s) - \tau_1 sK}$$

$$\frac{v_2}{v_1} = \frac{1}{\tau_1\tau_2 s^2 + \tau_1 s + \tau_2 s + 1 - \tau_1 sK}$$

$$\frac{v_2}{v_1} = \frac{1}{\tau_1\tau_2 s^2 + (\tau_1 - K\tau_1 + \tau_2)s + 1}$$

$$\frac{v_2}{v_1} = \frac{\frac{1}{\tau_1\tau_2}}{s^2 + (\frac{1}{\tau_1} + \frac{1}{\tau_2} - \frac{K2}{\tau_2})s + \frac{1}{\tau_1\tau_2}} \qquad (155b)$$

The pole locations of the transfer function expressed by Eq. (155b)

$$s^* = -\frac{1}{2}\left(\frac{1}{\tau_1} + \frac{1}{\tau_2} - \frac{K}{\tau_2}\right) \pm \sqrt{\left(\frac{\frac{1}{\tau_1} + \frac{1}{\tau_2} - \frac{K}{\tau_2}}{2}\right)^2 - \frac{1}{\tau_1\tau_2}} \qquad (156a)$$

Since $\frac{1}{\tau_1\tau_2} > \frac{\frac{1}{\tau_1} + \frac{1}{\tau_2} - \frac{K}{\tau_2}}{2}$, then

$$s^* = -\left[\frac{\frac{1}{\tau_1} + \frac{1}{\tau_2}(1-K)}{2}\right] \pm j\sqrt{\frac{1}{\tau_1\tau_2} - \left[\frac{\frac{1}{\tau_1} + \frac{1}{\tau_2}(1-K)}{2}\right]^2} \quad (156b)$$

or for K >> 1,

$$s^* = -\left[\frac{\frac{1}{\tau_1} - \frac{1}{\tau_2}(K-1)}{2}\right] \pm j\sqrt{\frac{1}{\tau_1\tau_2} - \left[\frac{\frac{1}{\tau_1} - \frac{1}{\tau_2}(K-1)}{2}\right]^2} \quad (156c)$$

By now, it can already be seen that s* or the pole location is a function of the time constants τ_1 and τ_2 and the gain K. The variable function can be chosen τ_1, τ_2 or K individually or a combination of them.

As a first step, let K be chosen as the variable, τ_1 and τ_2 fixed and $\tau_1 = \tau_2 = \tau$ is set, where τ is the circuit time constant. Note the time constant of the circuit is the inverse of the cutoff frequency and can be obtained by calculating the modulus of the vector s* expressed in Eq. (156c), this being the square root of the sum of the square of the real component plus the square of the imaginary component; if $\tau_1 = \tau_2$, it will turn out that $\tau_1 = \tau_2 = \tau$, the circuit time constant.

For the active LPF described by Eq. (156c), one must now find the complex pole locations as a function of the gain K. Eq. (156c) becomes

$$s^* = -\frac{1}{\tau}\left[\frac{1-(K-1)}{2}\right] \pm j\sqrt{\frac{1}{\tau^2} - \frac{1}{\tau^2}\left[\frac{1-(K-1)}{2}\right]^2} \tag{157a}$$

$$s^* = -\frac{1}{\tau}\left(1-\frac{K}{2}\right) \pm j\,\frac{1}{\tau}\sqrt{1-\left(1-\frac{K}{2}\right)^2}$$

or

$$s^* = \frac{1}{\tau}\left[-\left(1-\frac{K}{2}\right) \pm j\sqrt{1-\left(1-\frac{K}{2}\right)^2}\,\right] \tag{157b}$$

Now, find the value of K such that

$$\sqrt{\frac{1-\left(1-\frac{K}{2}\right)^2}{1-\frac{K}{2}}} = b \tag{158}$$

namely the absolute value of the ratio of the imaginary to real components of the pole.

Eq. (158) becomes

$$1-\left(1-\frac{K}{2}\right)^2 = b^2\left(1-\frac{K}{2}\right)^2$$

$$1-\left(1-\frac{K}{2}\right)^2 - b^2\left(1-\frac{K}{2}\right)^2 = 0$$

$$(1 - \frac{K}{2})^2(1 + b^2) = 1$$

$$(1 - \frac{K}{2})^2 = \frac{1}{1 + b^2}$$

$$1 - \frac{K}{2} = \frac{1}{1 + b^2}$$

$$\frac{K}{2} = 1 - \frac{1}{1 + b^2}$$

or $$K = 2(1 - \frac{1}{\sqrt{1 + b^2}}) \tag{159}$$

However, the value of K in Eq. (159) must be such that the circuit does not oscillate. For this reason, let the critical gain K_{crit} be found.

By inspection of Eq. (156c), oscillation occurs when $\frac{1}{\tau} - \frac{1}{\tau}(K-1) = 0$, i.e. when the poles are all located on the imaginary axis.

Then,

$$1 - (K_{crit} - 1) = 0 \tag{160a}$$

$$1 - K_{crit} + 1 = 0$$

or $$K_{crit} = 2 \tag{160b}$$

Therefore, the allowed value for K is

$$1 \leq K < 2 \tag{161}$$

(with $\tau_1 = \tau_2 = \tau$)

The pole locations already found in Eq. (149b) and (152c) are now listed again but with corresponding values of b also give.

53 kHz filter	$s_{1,4} = -0.2127 \pm j\,1.0570$	$b = 4.9694$
	$s_{2,3} = -0.5135 \pm j\,0.4378$	$b = 0.8526$
36 kHz filter	$s_{1,10} = -0.0334 \pm j\,1.0100$	$b = 30.2395$
	$s_{2,9} = -0.0971 \pm j\,0.9111$	$b = 9.3831$
	$s_{3,8} = -0.1512 \pm j\,0.7231$	$b = 4.7824$
	$s_{4,7} = -0.1905 \pm j\,0.4643$	$b = 2.4373$
	$s_{5,6} = -0.2112 \pm j\,0.1560$	$b = 0.7386$

For each value of b, the corresponding K is computed using Eq. (159). The results are tabulated in Table-3.

Hence, the setup should work since the values of K are still less than 2, therefore no oscillation will take place. However, since many poles imply that there must be some poles very closely located to the imaginary axis (in this case $s_{1,11}$ and $s_{2,10}$), care must be taken in choosing

Table-3 b and K values for the poles of the 53 kHz and 36 kHz filters

	Pole	b	K
53 kHz filter	$s_{1,4}$	4.9694	1.6054
	$s_{2,3}$	0.8526	0.4780
36 kHz filter	$s_{1,10}$	30.2395	1.9339
	$s_{2,9}$	9.3831	1.7880
	$s_{3,8}$	4.7824	1.5906
	$s_{4,7}$	2.4373	1.2408
	$s_{5,6}$	0.7386	0.3912

the components of R and C for the realization of these poles; they must be made of very high precision components. Note that the choice of $\tau_1 = \tau_2 = \tau$ was done for convenience in the realization, namely R_1C_1 of the first stage can be made identical to R_2C_2 of the second stage (using the same components for both stages). τ_1 could have been chosen different from τ_2 with the consequence of different K_{crit} and different K and b relationship, but this step is not regarded necessary since one can not avoid the closeness of some poles to the imaginary axis (closeness to oscillation at K_{crit}), unless a particular K_{crit} other than 2 is desired for some reason.

As a second step, the method of how to go about varying K is discussed. Refer to Fig. 36(a). It is noted that the use of OPAMPs is very suitable for isolation (buffering) purposes between stages. OPAMPs have almost infinite input impedance and very low output impedance, thus making them very favorable for driving next stage circuit. The problems of connecting stages in the phase-shift subsystem are all nicely taken care of by the use of OPAMPs. From the theory of OPAMPs, the gain of an OPAMP connected like in the second stage is

$$K = \frac{R_i + R_f}{R_i} = 1 + \frac{R_f}{R_i} \tag{162}$$

where R_f is the OPAMP feedback resistance and R_i is the resistance connected in the OPAMP's input circuit.

From Fig. 36(b), the voltage source KV_2 is equal to the voltage at point 2 multiplied by the gain K_2 of the second OPAMP-stage and it is also noted that in order for the analysis using the equivalent circuit to be valid, the voltage at the first OPAMP output at point 3 must be equal to v_x, or in other words the first OPAMP must have unity gain. In order the first OPAMP stage has unity gain, its input and output are shorted, i.e., $R_{f_1} = 0$; and with R_{i_1} infinite (open), Eq. (162) reduces to

$$K_1 = 1 \tag{163}$$

The gain of the second OPAMP stage is according to Eq. (162)

$$K_2 = 1 + \frac{R_{f_2}}{R_{i_2}} \tag{164a}$$

Since $K_2 = K$,

$$R_{f_2} = (K - 1)R_{i_2} \tag{164b}$$

Hence, in order to vary the pole location, K is varied by varying the ratio of R_{f_2} to R_{i_2}, with R_{f_1} set equal to R_{i_1}. The values of K have been prescribed and can be found in Table-3 for each of the pole locations.

As a third step, now the realization of the circuit is conducted, i.e. the values of the components are determined. A sample calculation will be presented to realize a pair of

poles and the complete result for the entire pole realizations are tabulated in Table-4. Let $s_{3,8}$ of the 36 kHz filter be chosen for this purpose.

From Eq. (152c)

$$s_{3,8} = -\ 0.1512 \pm j\ 0.7231$$

The distance from one of these pair of poles to the s-plane origin is

$$h = \sqrt{(Re)^2 + (Im)^2} \tag{165}$$

where Re is the real component and Im is the imaginary component of the pole.

For $s_{3,8}$ Eq. (165) gives

$$h = \sqrt{(0.1512)^2 + (0.7231)^2}$$

$$h = 0.7387$$

Since h is equal to the cutoff frequency and the time constant is the inverse of cutoff frequency

$$\tau = \frac{1}{h} \tag{166}$$

Note that h in the above expression is scaled to a frequency $f_{c_1} = 36$ kHz. The actual value of h is then

$$h' = (0.7387)(2\ )(36)(10^3)$$

$$h' = 167090.0035$$

Plugging this value into Eq. (166) gives

$$\tau = 0.0000059847 \text{ second} \tag{167}$$

Since in this case $\tau = R_1C_1 = R_2C_2$ then

$$0.0000059847 = R_1C_1 \tag{168}$$

Choosing a realistic size of C_1, say

$$C_1 = 0.0002\ \mu F = C_2 \tag{169}$$

then

$$R_1 = \frac{0.0000059847}{(0.0002)(10^{-6})}$$

$$= 29923.99$$

or

$$R_1 = 29.924 \text{ k-ohms} = R_2 \tag{170}$$

Note that to make $K_1 = 1$,

$$R_{i_1} = 0 \quad \text{and} \quad R_{f_1} = \infty \tag{171}$$

For this pole pair, according to Table-3 the value of K is 1.5906. Therefore according to Eq. (164b),

$$R_{f_2} = (1.5906 - 1)R_{i_2} = 0.5906\ R_{i_2} \tag{172}$$

Choosing

$$R_{i_2} = 10 \text{ k-ohms} \tag{173}$$

gives

$$R_{f_2} = 5.906 \text{ k-ohms} \tag{174}$$

Similar calculations are done on the other poles and the results are tabulated in Table-4.

Up to this point, only the LPF filter with 36 kHz cutoff frequency has been designed. However, it is not the kind of filter which is desired, but a HPF with the same cutoff frequency is to be designed. To do this, a simple step needs only to be taken, namely interchanging the connection of R_1 and C_1, and also of R_2 and C_2. The HPF will perform exactly the same unwanted sideband suppression as its LPF counterpart. The realization of a pair of poles for the HPF case looks then like the one shown in Fig. 37(a). Note that in addition to the interchanging of the resistors and capacitors mentioned above, the bias resistor arrangement which was previously (in Fig. 36(a)) connected in front of the first OPAMP is now connected in front of the second OPAMP;

Table-4 Circuit components for the 53 kHz/4-pole and 36 kHz/10-pole Chebyshev Filters

	Pole	h	K	R_{i_2} (k-ohm)	R_{f_2} (k-ohm)	C_1 (μF)	R_1 (k-ohm)	C_2 (μF)	R_2 (k-ohm)
53 kHz filter	$s_{1,4}$	1.0782	1.6054	10.0	6.064	0.0002	13.926	0.0002	13.926
	$s_{2,3}$	0.6748	0.4780	10.0	4.780	0.0002	22.251	0.0002	22.251
36 kHz filter	$s_{1,10}$	1.0105	1.9339	10.0	9.339	0.0002	21.875	0.0002	21.875
	$s_{2,9}$	0.9163	1.7830	10.0	7.830	0.0002	24.124	0.0002	24.124
	$s_{3,8}$	0.7387	1.5906	10.0	5.906	0.0002	29.924	0.0002	29.924
	$s_{4,7}$	0.5019	1.2408	10.0	2.408	0.0002	44.042	0.0002	44.042
	$s_{5,6}$	0.2626	0.3912	10.0	3.912	0.0002	84.177	0.0002	84.177

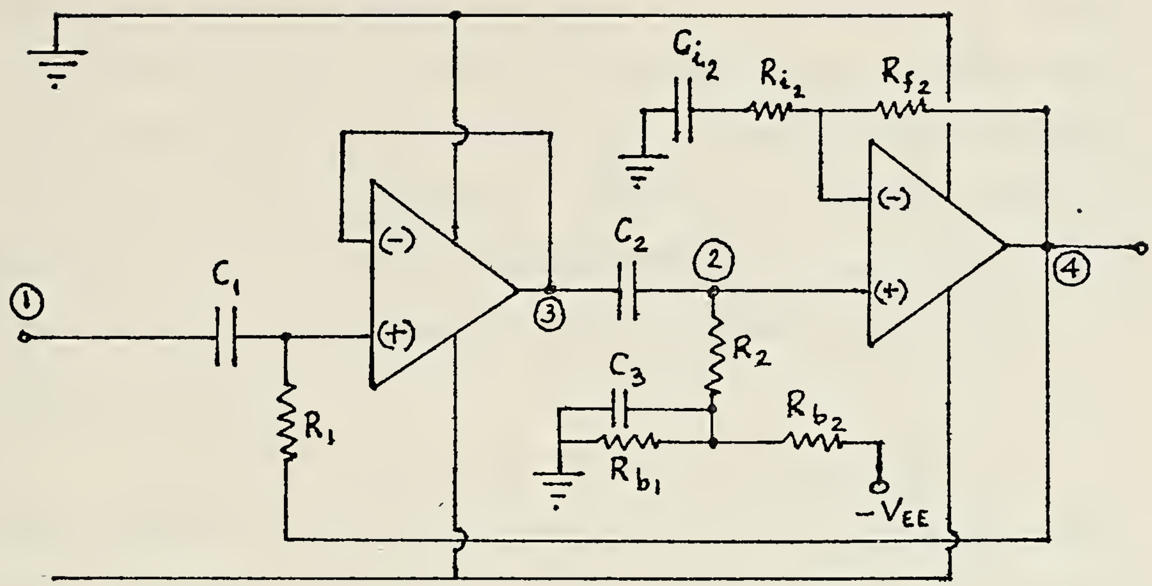

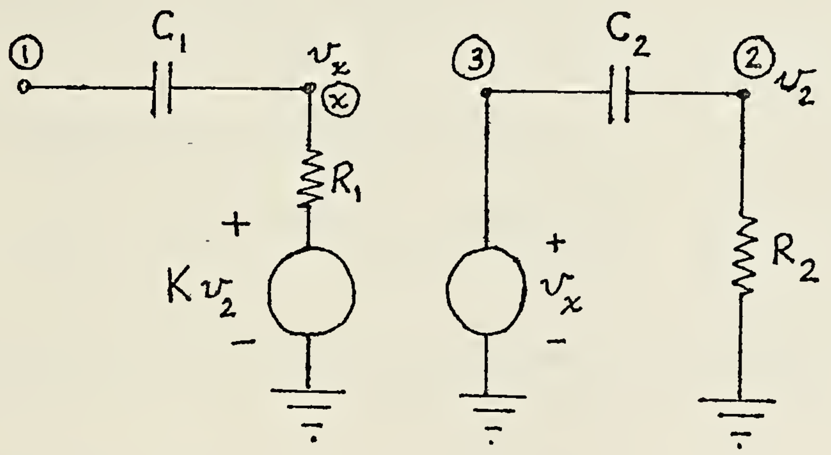

FIG. 37 (a) Realization of a pair of conjugate poles of an HPF

(b) Its equivalent circuit

by this new arrangement, the two OPAMPS still get the proper bias; the coupling capacitor C_c is no longer needed, because C_1 can now act also as a coupling capacitor. A proof needs to be presented here, to show that by doing these interchanges in resistors and capacitors connection, an equation similar to that in Eq. (71) will be obtained, i.e. in accordance with the principle of frequency transformation outlined in Section II.B.4.

With the connections of R_1 and C_1, R_2 and C_2 interchanged respectively, the equivalent circuit in Fig. 36(b) becomes that shown in Fig. 37(b). Applying Kirchhoff's law on the first stage yields

$$sC_1(v_x-v_1) + \frac{1}{R_1}(v_x-Kv_2) = 0 \qquad (175a)$$

$$sC_1R_1(v_x-v_1) + (v_x-Kv_2) = 0$$

or

$$(sC_1R_1+1)v_x - sC_1R_1v_1 - Kv_2 = 0 \qquad (175b)$$

Applying Kirchhoff's law on the second stage yields

$$sC_2(v_2-v_x) + \frac{v_2}{R_2} = 0 \qquad (176a)$$

$$R_2sC_2v_2 - sC_2R_2v_x + v_2 = 0$$

or

$$v_x = \frac{(sC_2R_2+1)v_2}{sC_2R_2} = 1 + \left(\frac{1}{sC_2R_2}\right)v_2 \qquad (176b)$$

Substituting Eq. (176b) into Eq. (175b) gives

$$(sC_1R_1 + 1)(1 + \frac{1}{sC_2R_2})v_2 - sC_1R_1v_1 - Kv_2 = 0 \qquad (177a)$$

$$\frac{v_2}{v_1} = \frac{sC_1R_1}{(sC_1R_1 + 1)(1 + \frac{1}{sC_2R_2}) - K}$$

Since $R_1C_1 = \tau_1$ and $R_2C_2 = \tau_2$ then

$$\frac{v_2}{v_1} = \frac{\tau_1\tau_2}{\tau_1\tau_2 + \frac{1}{s}(\tau_1 + \tau_2 - K\tau_2) + \frac{1}{s^2}} \qquad (177b)$$

Eq. (177b) has the form similar to that in Eq. (71) and if compared to Eq. (155b), its LPF counterpart, is its "dual", i.e. everything in Eq. (155b) is upside down, all variables related to frequency; namely s, $\frac{1}{\tau_1\tau_2}$, $\frac{1}{\tau_1}$, $\frac{1}{\tau_2}$ become $\frac{1}{s}$, $\tau_1\tau_2$, τ_1 and τ_2 respectively. All of these are in agreement with the principle of frequency transformation. Hence, the HPF design has been carried out.

4. The Complete Filter Subsystem

The complete filter subsystem will then consist of a cascade of 5 (five) circuit arrangement such as that in Fig. 37(a), each representing a realization of a pair of poles listed in Table-3. The values of the components are tabulated in Table-4. This stack of circuits is further cascaded with the LPF consisting of 4-poles which has been

designed earlier with cutoff-frequency at 53 kHz. This LPF-section consists of two circuits as in Fig. 36(a) cascaded.

Suitable OPAMPs can be chosen from packages offered by manufacturers ("off the shelf"). A package called the "QUAD" consists of 4 (four) OPAMPs, therefore it can be used for realizing two pairs of poles. The entire circuit should now simulate or resemble the Chebyshev approximation function with a total of 14 poles.

D. THE HYBRID SSB-GENERATOR

Having completed the designs of the phase-shift and filter subsystems, one is now ready to combine or cascade them and obtain the Hybrid SSB signal-generator.

The overall system can be depicted by the block diagram and the frequency plan shown in Fig. 38. The phase-shift subsystem performs about 30 dB suppression of the undesired sideband while the filter subsystem performs the remaining 40 dB suppression. Hence, a total of about 70 dB suppression of the undesired sideband is achieved.

There is a major advantage here to employ the phase-shift method in SSB-generation, namely its ability to suppress the undesired sideband with 30 dB at a frequency as low as 30 Hz, which the filter method cannot do economically. Although this characteristic is insignificant as far as the SSB-generation is concerned, it plays an important role in the SSB signal reception (demodulation). It is understood that in the SSB

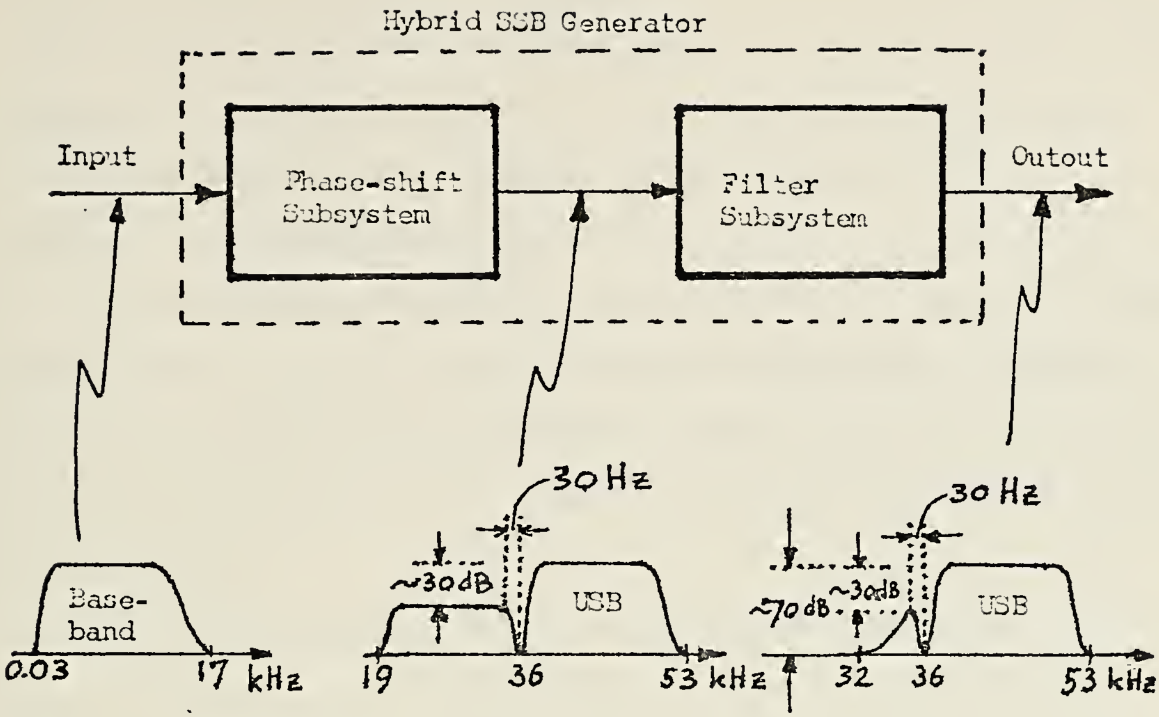

FIG. 38. The Hybrid SSB-Generator and Its Frequency Plan

signal demodulation process, a reconstructed carrier frequency from a local source with the same frequency as that of the incoming signal is reinserted, causing the audio frequency (AF) signal to be recovered at the domodulator's output terminals. This process could be regarded as translating the received signal down to zero frequency, hence recovering the AF band containing the transmitted information.

However, due to incomplete suppression of the undesired sideband, the AF baseband signal recovered at the demodulator's outputs will consist of two components, namely the AF component corresponding to the undesired sideband (LSB in this case) which was incompletely suppressed during the signal transmission.

This undesired sideband AF component may be viewed as being "folded back" at zero frequency, since no negative frequency signal is possible to exist; therefore, both desired and undesired sideband AF components now occupy the same (positive frequency) baseband.

The undesired situation is inevitable, and obviously one would like to recover the transmitted information contained in the AF baseband corresponding to the desired sideband and to have the effect of the undesired sideband AF component to be negligible.

The interaction of these two components is mainly felt at low frequencies of the AF band. This is caused by the unideal transition ("skirt") of any sideband suppression system to pass the desired signals within the passband and at the same time only within several Hz distance from the passband's edge it must completely suppress the undesired signal.

However, with hybrid-SSB generated signals, before they arrive at the demodulator's input, a sharp drop (30 dB in this case) within Hz-range from the carrier frequency (30 Hz in this case) has been provided by the phase-shift subsystem of the hybrid SSB-signal generator in the transmitter. Due to the combined action of the phase-shift and filter subsystems in the transmitter, the received signal has thus a negligible level of undesired sideband AF component in the recovered signal.

If the phase-shift subsystem in the transmitter were not used, the sideband suppression would have been carried out by the filter alone, and an overall sharp drop like mentioned above could not have been achieved, due to the fact that the filter can not attenuate these low frequency signals sufficiently. Thus, in the reception or demodulation process, the effect of the undesired signal would still be potentially interfering with the desired signal in the AF band, especially in the lower frequencies. This is a definite advantage of the phase-shift method over the filter method in SSB-signal generation.

Regarding this matter, the following analysis should clarify the statements that have been made, thus making the significance of the phase-shift presence in the hybrid SSB-signal generator be more clearly appreciated.

In the demodulation process (reception of the signal), the signal detection is usually not phase-coherent, such that not only amplitude distortion is encountered, but also phase-distortion. Phase distortion can cause the detected USB and LSB signal components in the recovered AF baseband (which appear after a carrier from the reconstructed source has been applied to the demodulator translating the baseband down to "zero frequency") interact with each other. They either cancel or add to each other (vectorially), depending on their relative phase difference. The phase relationship between these two components is unpredictable. In addition, the phase instability of the reinserted carrier also

contributes to this unpredictable interaction. This phase-"jitter" is felt mainly at low frequencies of the AF band because of the reasons which have been mentioned earlier.

The following vector analysis explains why it is desirable to have a 30 dB attenuation (or more if possible) of the unwanted sideband signal at ~ 30 Hz (or less if possible) and above, thus making the phase-"jitter" effect negligible. A comparison is made between the case where the phase-shift subsystem is absent and the case where it is present in the hybrid SSB-signal generator.

First, if in Fig. 38 the phase-shift subsystem was not present, there would not have been a 30 dB suppression of the undesired sideband signal (LSB in this case) at 36 kHz. At 36 kHz then, a considerable undesired signal would still have been encountered due to the filter's skirt which is not sharp within 30 Hz. Figure 39(a) shows the received SSB signal at the demodulator's input, and Fig. 39(b) shows the recovered AF baseband at the demodulator's output which consists of desired and undesired sideband AF components (note the "fold-back" of the undesired sideband AF component). Within the 30 Hz, the undesired AF component is practically equal in magnitude with the desired AF component (and decays thereafter). These two interacting components can be described by a vector $\underline{a}$ of the desired AF component and a vector $\underline{b}$ of the undesired AF component; vector $\underline{b}$ varies with respect to vector $\underline{a}$ in a manner (randomly, according to a

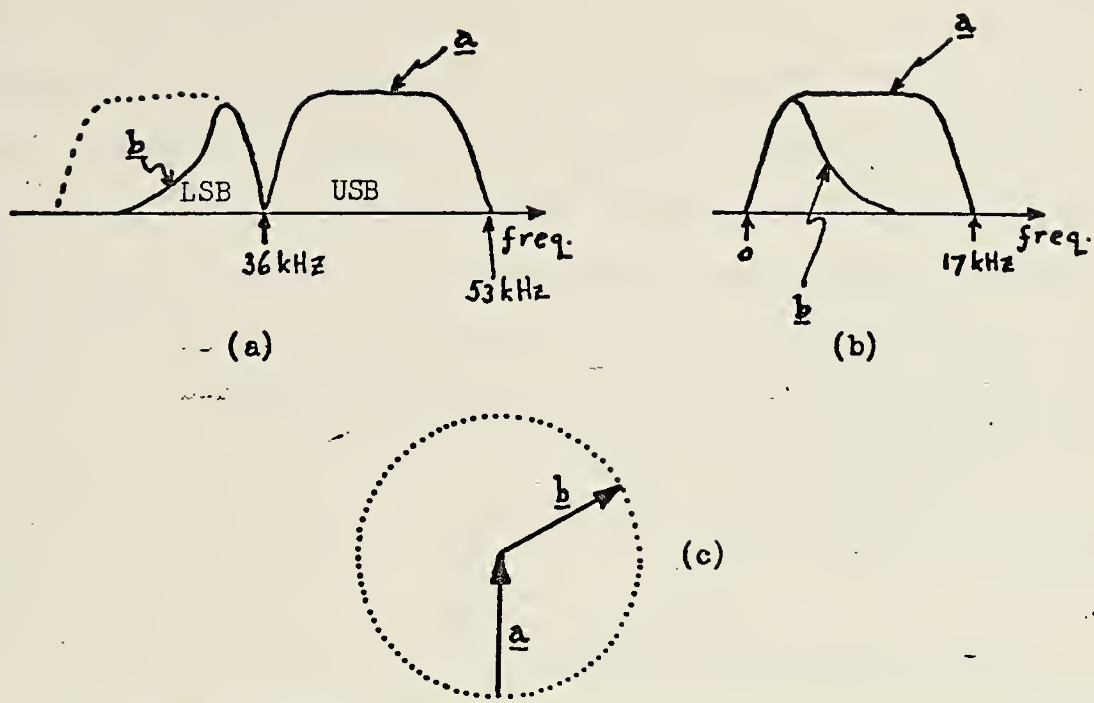

FIG. 39 (a) The received filter generated signal at demodulator's input
(b) The desired (a) and undesired (b) AF components at the demodulator's output
(c) Vectors a and b variation with respect to each other

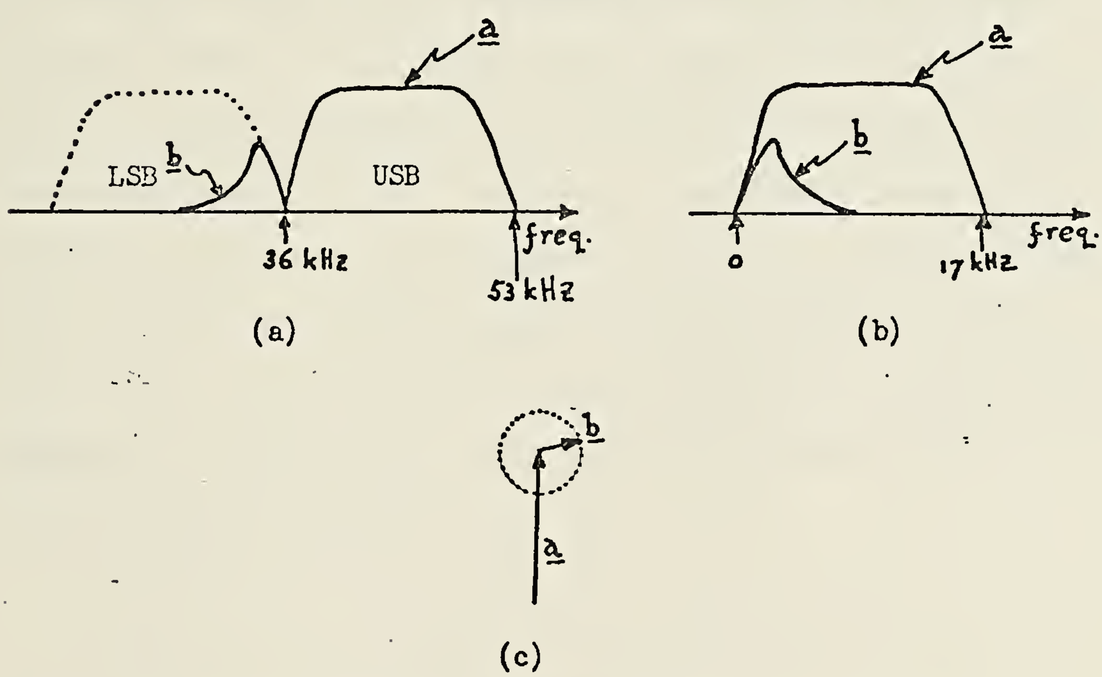

FIG. 40 (a) The received hybrid generated SSB signal at the demodulator's input
(b) The desired (a) and undesired (b) AF components at the demodulator's output
(c) Vectors a and b variation with respect to each other

circle path) such as shown in Fig. 39(c). Since the magnitudes of a and b are equal, the effect of the interaction between them is damaging to the demodulator's output. The worst situation is when both vectors are inphase or 180° out of phase. In case they are inphase, the demodulator will produce two AF components, namely the desired and the undesired components, each with the same level. If both vectors are 180° out of phase, they cancel to each other and no signal at all would be recovered at the demodulator's output. This is one of the reasons why the filter method is not suitable for low frequency operation.

Secondly, consider the case where a phase-shift unit is present in Fig. 38. Figure 40(a) shows the received SSB signal at the demodulator's input and Fig. 40(b) shows the recovered AF band at the demodulator's output as before. However, due to the action of the phase-shift unit, the undesired AF component is now 30 dB below the desired AF component within 30 Hz. This is a considerable drop in vector b magnitude with respect to vector a. The variation of the two vectors with respect to each other is shown in Fig. 40(c). The circle with radius $|b|$ is now very small compared to that before. To show this quantitatively, a 30 dB drop means that

$$20 \log \frac{|\underline{a}|}{|\underline{b}|} = 30 \tag{178a}$$

$$\log \frac{|\underline{a}|}{|\underline{b}|} = 1.5$$

$$\frac{|\underline{a}|}{|\underline{b}|} = 31.6$$

or $$|\underline{b}| = 0.0316\ |\underline{a}| \tag{178b}$$

If both vectors happen to be inphase, i.e. they add each other algebraically, the signal at the demodulator's output is then

$$\frac{\underline{a} + \underline{b}}{\underline{a}} = \frac{1 + 0.0316}{1} = 1.0316 = 0.27 \text{ dB} \tag{179}$$

Hence, the fluctuation of the desired signal at the demodulator's output caused by the presence of the unwanted sideband AF component is only about ± 0.27 dB, which is still tolerable for practical purposes.

Therefore, this analysis has clarified the previous statements saying that the phase-shift method has a significant advantage over the filter method in the low frequency range.

To mention one more advantage of employing the phase-shift method in the context of SSB-reception is the very short distance between the lower edges of the resulting LSB and USB bands, i.e. twice of 30 Hz or 60 Hz in this case, where a 30 dB suppression has been provided; one that any filter system can not do economically. Therefore, more efficient utilization of the frequency spectrum can be achieved. Adjacent channels may be assigned even closer to each other.

IV. APPLICATION

The use of carrier telephone networks or other telecommunication paths for sound program transmission has increased recently. For example the frequency spectrum between 36 and 84 kHz may be utilized for a single program channel with 15 kHz bandwidth (monoaural system) as well as for two such program channels for simultaneous transmission. In the latter, the two channels contain "high-fidelity" band respectively, hence a stereophonic sound transmission is obtained. Instead of utilizing the spectrum for 2 program channels, one could also put 1 program channel and 6 voice channels in the spectrum (6 channels of about 2.5 kHz bandwidth each). The information contained in these channels are then transmitted through carrier telephone networks, thus high quality sound program transmission over long distances is possible and this technique may receive a potential application in stereo-broadcasting in the future.

In the building of a monaural program channel system, SSB technique is employed in conjunction with frequency spectrum conservation. In the building of a 2-program channel system, the SSB technique is mandatory, because of the limited frequency spectrum (recommended by CCITT).

It is in this context that the hybrid SSB-signal generator discussed earlier, comes into play. In the following

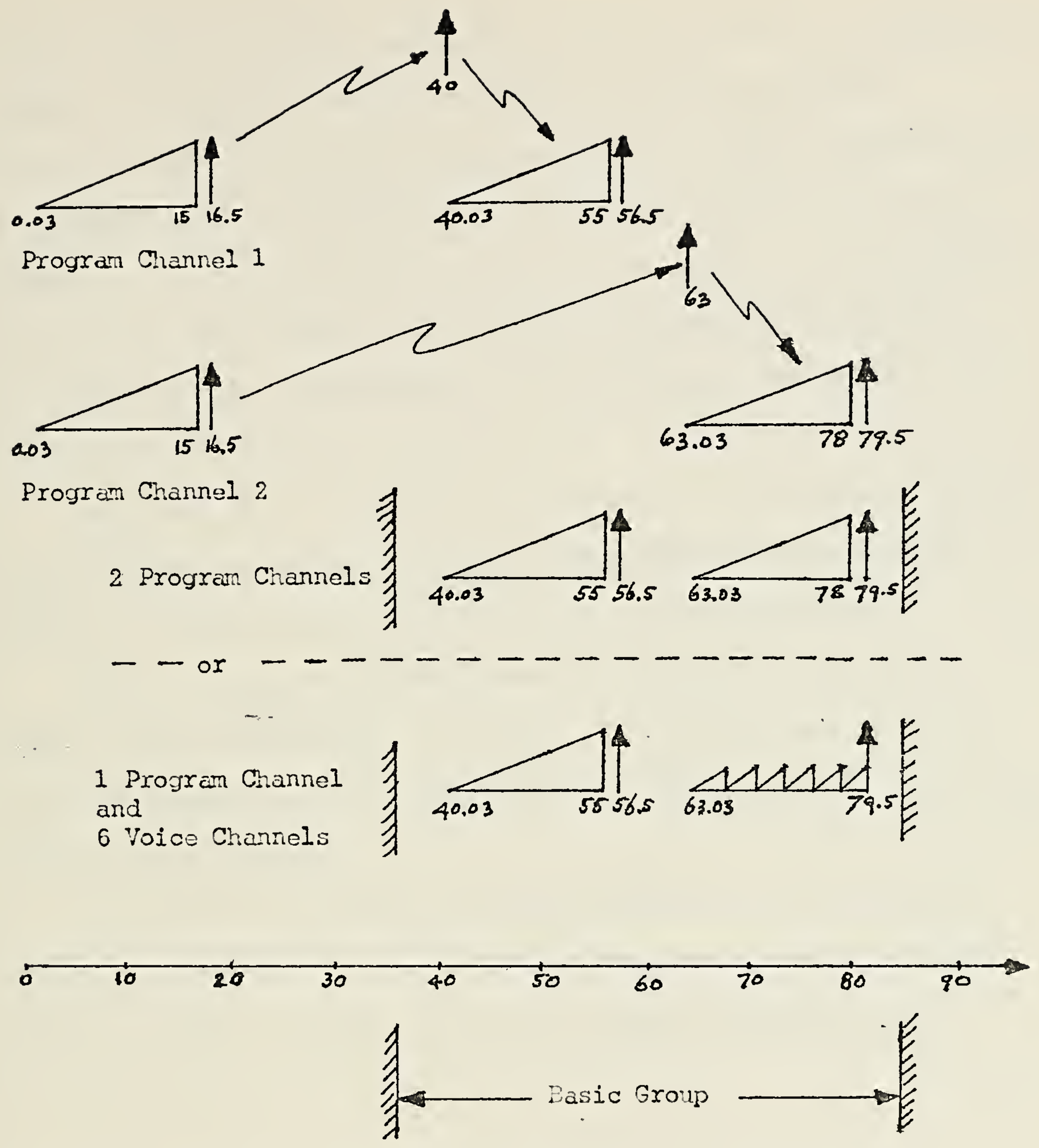

FIG. 41 Frequency allocation plan for a 2-program channel transmission

example, a frequency allocation plan for 2-program channel system will be presented. This is illustrated in Fig. 41.

Program channel 1 and program channel 2 have a bandwidth (baseband) from 0.03 to 15 kHz respectively. At the upper

edge of each of these basebands a pilot tone of 16.5 kHz is added to make the reception easier. Program channel 1 is translated to 40 kHz frequency and the upper sideband is selected (LSB is suppressed). Program channel 2 is translated to 63 kHz and also the USB is selected. In these two operations, the hybrid SSB-signal generator is employed. It must provide a passband of approximately 17 kHz wide to include also the pilot tone.

The fact that the USB was chosen in both program channel translation is due to reasons discussed earlier, namely to make the filter design easier (less poles involved).

The two program channels are then placed within the basic group between 36 - 84 kHz. The guard band between the two channels is 6.5 kHz which is quite safe to accomodate channel overlappings.

Instead of utilizing the basic group for two program channels, it can also be utilized for one program channel and six voice channels of about 2.5 kHz bandwidth each.

V. CONCLUSIONS

To conclude, the important features of the last discussions will be outlined:

a. The crucial part in designing a phase-shift SSB-signal generator is the design of the audio-phase shift circuit. To be effective, the audio phase-shift circuit must have a phase-shift error maintained less than 2° throughout the operating band, 17 kHz in this case. Without using computers, it is almost impossible to determine the time constants of the all-pass networks involved to meet these requirements. Therefore, the phase-shift method which has been considered unpopular in the past, may now be reconsidered as a potential method. Moreover, the high accuracy circuit components required can be met today, due to sophisticated technology.

b. The smaller the phase-shift error, the higher the side-band suppression level. It turned out that the smaller the phase-shift error specified, the higher the order of all-pass networks are necessary (with non-simple poles), but as a consequence the price is higher. It has been shown that with second-order all-pass networks cascaded to cover 17 kHz frequency range, a phase shift error less than 2° could be obtained.

c. Many all-pass networks are necessary for a wideband signal, e.g. in this case 7 stages were necessary to satisfy the above specifications.

d. The sideband suppression of the phase-shift suppressor takes place almost immediately; it can be designed down to several Hz. This is a great advantage over its counterpart system, namely the filter system.

e. This characteristic is very important in the SSB-signal demodulation (reception) process, with regard to the suppression of the unwanted signal reappearance in the passband, spectrum efficiency and reducing phase distortion effects.

f. In the design of the filter part, the Chebyshev approximation function may be used to realize the filter; the smaller the passband ripple and the steeper the "skirt", the more poles are necessary in the Chebyshev function.

g. The suppression of the signal by the filter does not result immediately as in the phase-shift system. The best "skirt" still has a frequency range of the order of several kHz before the suppression effectively takes place.

h. The Hybrid SSB-signal generation method is a combination of the two methods, thus enabling a design with reasonable degree of complexity for each of them and still obtain a high degree overall suppression performance. Furthermore, due to the use of the phase-shift method, a better characteristic at lower audio frequencies (of the order of several Hz) is obtained.

i. In the particular design undertaken, a sideband suppression level of 70 dB (at least) was specified, but actually more than 80 dB was theoretically possible (50 dB contributed by the filter and more than 30 dB by the phase-shift unit).

The way is still open to design an even higher dB specification, if only one is willing to pay higher price. He could either design a better phase-shift unit with higher order all-pass circuits (higher order here implies more non-simple poles), but with the provision of a high degree of time constant stability - or he can design a better filter unit with more poles, but with the provision of a high degree of gain stability to prevent the filter circuit from oscillation.

j. The Hybrid-SSB-signal generation may become a potential technique in the future for sound transmission through international telecommunication paths. It can be applied for monaural (1 program channel) broadcast or stereophonic (2 program channels) broadcast or a mixture of a monaural band and several voice channels utilization.

k. Inductorless realization makes it very attractive and compatible with miniaturization.

VI. APPENDIX

COMPUTER PRINTOUT FOR SECOND ORDER 90° PHASE-SHIFT NETWORK (APPENDIX 1)

CUTOFF-FREQS OF F1 = 19.5 166.0 946.0 6190.0 126530.9 174370.4 237031.6 HZ

CUTOFF-FREQS OF F2 = 37.6 258.0 1487.0 10232.0 209669.8 327421.4 1076572.0 HZ

FREQ-HZ	ANGLE1-DEG	ANGLE2-DEG	PH.SHIFT ERR.-DEG
0.500	-6.708	-3.585	-86.877
1.000	-13.408	-7.168	-83.760
1.500	-20.092	-10.749	-80.657
2.000	-26.754	-14.327	-77.573
2.500	-33.385	-17.901	-74.516
3.000	-39.979	-21.469	-71.490
3.500	-46.529	-25.031	-68.502
4.000	-53.028	-28.586	-65.558
4.500	-59.469	-32.132	-62.662
5.000	-65.848	-35.668	-59.820
5.500	-72.159	-39.194	-57.035
6.000	-78.397	-42.709	-54.312
6.500	-84.557	-46.211	-51.653

7.000	-90.636	-49.700	-49.063
7.500	-96.630	-53.174	-46.544
8.000	-102.536	-56.634	-44.098
8.500	-108.351	-60.078	-41.727
9.000	-114.073	-63.505	-39.432
9.500	-119.700	-66.915	-37.215
10.000	-125.231	-70.306	-35.075
15.000	-175.191	-103.078	-17.887
20.000	-216.064	-133.453	-7.389
25.000	-249.542	-161.209	-1.667
30.000	-277.399	-186.364	1.035
35.000	-301.063	-209.087	1.976
40.000	-321.587	-229.620	1.967
45.000	-339.723	-248.227	1.496
50.000	-356.010	-265.163	0.847
55.000	-370.835	-280.658	0.177
60.000	-384.483	-294.913	-0.431
65.000	-397.160	-308.102	-0.941
70.000	-409.028	-320.368	-1.341
75.000	-420.204	-331.837	-1.633
80.000	-430.783	-342.608	-1.826
85.000	-440.839	-352.769	-1.930
90.000	-450.431	-362.393	-1.962

95.000	-459.607	-371.539	-1.933
100.000	-468.405	-380.260	-1.855
105.000	-476.861	-388.599	-1.738
110.000	-484.999	-396.593	-1.594
160.000	-553.004	-462.883	0.121
210.000	-604.216	-513.330	0.886
260.000	-644.819	-554.061	0.758
309.999	-678.290	-588.000	0.289
359.999	-706.753	-616.928	-0.175
409.999	-731.557	-642.046	-0.490
459.999	-753.583	-664.206	-0.624
509.998	-773.425	-684.024	-0.600
559.998	-791.500	-701.957	-0.457
609.998	-808.109	-718.343	-0.234
659.998	-823.473	-733.443	0.031
709.997	-837.765	-747.455	0.310
759.997	-851.118	-760.535	0.583
809.997	-863.640	-772.808	0.832
859.997	-875.420	-784.371	1.049
909.996	-886.533	-795.304	1.229
959.996	-897.043	-805.675	1.368
1009.996	-907.005	-815.538	1.467
1059.996	-916.466	-824.940	1.526

1109.995	-925.469	-833.921	1.548
1609.995	-996.906	-906.399	0.507
2109.995	-1047.296	-958.250	-0.954
2609.995	-1086.248	-997.982	-1.734
3109.994	-1118.178	-1029.986	-1.808
3609.994	-1145.351	-1056.767	-1.416
4109.992	-1169.046	-1079.837	-0.791
4609.988	-1190.050	-1100.151	-0.101
5109.984	-1208.885	-1118.337	0.547
5609.980	-1225.919	-1134.825	1.094
6109.977	-1241.430	-1149.917	1.513
6609.973	-1255.634	-1163.835	1.798
7109.969	-1268.703	-1176.748	1.955
7609.965	-1280.781	-1188.782	1.999
8109.961	-1291.987	-1200.042	1.945
8609.957	-1302.422	-1210.611	1.811
9109.953	-1312.173	-1220.559	1.615
9609.949	-1321.316	-1229.943	1.373
10109.945	-1329.914	-1238.816	1.097
10609.941	-1338.023	-1247.221	0.802
11109.938	-1345.693	-1255.195	0.498
16109.934	-1405.637	-1317.384	-1.747
21109.930	-1448.313	-1359.581	-1.268

26109.926	-1482.677	-1391.060	1.617
31109.922	-1512.389	-1416.247	6.142
36109.918	-1539.182	-1437.460	11.722
41109.914	-1563.972	-1456.012	17.961
46109.910	-1587.281	-1472.690	24.591
51109.906	-1609.421	-1487.993	31.428
56109.902	-1630.596	-1502.250	38.346
61109.898	-1650.938	-1515.685	45.253
66109.875	-1670.538	-1528.458	52.080
71109.813	-1689.461	-1540.682	58.779
76109.750	-1707.757	-1552.442	65.315
81109.688	-1725.461	-1563.801	71.660
86109.625	-1742.604	-1574.807	77.797
91109.563	-1759.211	-1585.497	83.714
96109.500	-1775.304	-1595.903	89.401
101109.438	-1790.900	-1606.047	94.853
106109.375	-1806.018	-1615.949	100.069
111109.313	-1820.674	-1625.625	105.049

COMPUTER PRINTOUT FOR FIRST ORDER 90° PHASE-SHIFT NETWORK (APPENDIX 2)

CUTOFF-FREQS OF F1 = 19.5 166.0 946.0 6190.0 126531.0 174371.0 237032.0 HZ

CUTOFF-FREQS OF F2 = 76.9 345.8 2621.0 17440.0 347959.0 543373.0 1786626.0 HZ

FREQ-HZ	ANGLE1-DEG	ANGLE2-DEG	PH.SHIFT ERR.-DEG
0.500	-3.354	-0.936	-87.582
1.000	-6.704	-1.872	-85.169
1.500	-10.046	-2.809	-82.762
2.000	-13.377	-3.744	-80.368
2.500	-16.693	-4.680	-77.987
3.000	-19.990	-5.615	-75.626
3.500	-23.264	-6.550	-73.286
4.000	-26.514	-7.485	-70.971
4.500	-29.735	-8.419	-68.684
5.000	-32.924	-9.352	-66.428
5.500	-36.080	-10.285	-64.205
6.000	-39.198	-11.217	-62.019
6.500	-42.279	-12.148	-59.870
7.000	-45.318	-13.079	-57.761
7.500	-48.315	-14.008	-55.694

8.000	-51.268	-14.937	-53.669
8.500	-54.175	-15.865	-51.690
9.000	-57.036	-16.791	-49.755
9.500	-59.850	-17.717	-47.867
10.000	-62.615	-18.641	-46.026
15.000	-87.595	-27.808	-30.213
20.000	-108.032	-36.798	-18.766
25.000	-124.771	-45.564	-10.793
30.000	-138.700	-54.070	-5.371
35.000	-150.532	-62.289	-1.757
40.000	-160.793	-70.200	0.593
45.000	-169.861	-77.795	2.067
50.000	-178.005	-85.069	2.936
55.000	-185.418	-92.026	3.392
60.000	-192.241	-98.672	3.569
65.000	-198.580	-105.019	3.561
70.000	-204.514	-111.079	3.435
75.000	-210.102	-116.866	3.236
80.000	-215.391	-122.395	2.997
85.000	-220.419	-127.682	2.738
90.000	-225.215	-132.741	2.474
95.000	-229.803	-137.587	2.216
100.000	-234.203	-142.235	1.968

105.000	-238.430	-146.696	1.734
110.000	-242.499	-150.984	1.515
160.000	-276.502	-186.467	0.035
210.000	-302.108	-212.999	-0.891
260.000	-322.409	-234.137	-1.727
309.999	-339.145	-251.620	-2.475
359.999	-353.376	-266.432	-3.056
409.999	-365.778	-279.207	-3.428
459.999	-376.791	-290.380	-3.590
509.998	-386.712	-300.275	-3.563
559.998	-395.750	-309.131	-3.381
609.998	-404.054	-317.134	-3.080
659.998	-411.736	-324.429	-2.693
709.997	-418.882	-331.130	-2.248
759.997	-425.559	-337.328	-1.769
809.997	-431.820	-343.096	-1.276
859.997	-437.710	-348.493	-0.783
909.996	-443.266	-353.568	-0.302
959.996	-448.521	-358.361	0.160
1009.996	-453.502	-362.906	0.597
1059.996	-458.233	-367.228	1.005
1109.995	-462.734	-371.353	1.381
1609.995	-498.453	-404.960	3.493

2109.995	-523.647	-429.985	3.663
2609.995	-543.124	-449.922	3.202
3109.994	-559.089	-466.367	2.722
3609.994	-572.676	-480.260	2.416
4109.992	-584.523	-492.226	2.297
4609.988	-595.025	-502.704	2.321
5109.984	-604.442	-512.011	2.430
5609.980	-612.959	-520.382	2.578
6109.977	-620.715	-527.989	2.726
6609.973	-627.817	-534.966	2.850
7109.969	-634.351	-541.416	2.936
7609.965	-640.390	-547.416	2.974
8109.961	-645.993	-553.030	2.963
8609.957	-651.211	-558.308	2.903
9109.953	-656.087	-563.290	2.796
9609.949	-660.658	-568.010	2.648
10109.945	-664.957	-572.494	2.462
10609.941	-669.011	-576.766	2.245
11109.938	-672.846	-580.845	2.001
16109.934	-702.818	-613.747	-0.929
21109.930	-724.156	-637.220	-3.063
26109.926	-741.338	-655.005	-3.667
31109.922	-756.194	-669.078	-2.884

36109.918	-769.591	-680.616	-1.025
41109.914	-781.986	-690.365	1.621
46109.910	-793.640	-698.813	4.827
51109.906	-804.710	-706.287	8.424
56109.902	-815.298	-713.017	12.281
61109.898	-825.469	-719.165	16.304
66109.875	-835.269	-724.850	20.419
71109.813	-844.730	-730.160	24.570
76109.750	-853.878	-735.162	28.716
81109.688	-862.730	-739.906	32.824
86109.625	-871.302	-744.434	36.868
91109.563	-879.605	-748.776	40.829
96109.500	-887.651	-752.957	44.694
101109.438	-895.449	-756.999	48.451
106109.375	-903.009	-760.917	52.092
111109.313	-910.336	-764.725	55.612

LIST OF REFERENCES

1. Albersheim, W. and Shirley, F.R., "Computation Methods for Broadband 90° Phase-difference Networks", IEEE Transaction on Circuit Theory, May 1969, pp. 189-196.

2. Cauer, W., Synthesis of Linear Communication Networks, pp. 738-741, McGraw-Hill Book Co., Inc. New York 1958.

3. Collins Radio Corporation, Cedar Rapids, Iowa 1959, "Fundamentals of Single Side Band".

4. Discrete Products Handbook, Fairchild Semiconductor, 1973.

5. DMOS Catalogue by Signetics Corp. 1973.

6. Karni, S., Network Theory: Analysis and Synthesis, Allyn and Bacon, Inc. 1966.

7. Kennedy, G., Electronic Communication Systems, McGraw-Hill Book Company 1970.

8. Millman, J. and Halkias, C.C., Integrated Electronics: Analog and Digital Circuits and Systems, McGraw-Hill Book Company 1972.

9. Mottershead, A., Electronic Devices and Circuits, Goodyear Publishing Company, Inc., 1973.

10. Norgaard, D.E., "The Phase-Shift Method of Single Sideband Signal Generation", Proceedings of the IRE, 1956, pp. 1718-1743.

11. Pappenfus, E.W., Bruene, W.B. and Schoenike, E.O., Single Sideband Principles and Circuits, McGraw-Hill Book Company, 1964.

12. Seshu, S. and Balabanian, N., Linear Network Analysis, John Wiley & Sons, Inc. 1959.

13. Shirley, F.R., "Shift Phase Independent of Frequency", Electronic Design, 18 September 1970.

14. Taub, H. and Schilling, D.L., Principles of Communication Systems, McGraw-Hill Book Company, Inc. 1971.

15. Winkler, S., "The Approximation Problem of Network Synthesis", IRE Trans. on Circuit Theory, CT-1 pp. 5-20, September 1954.

INITIAL DISTRIBUTION LIST

		No. Copies
1.	Defense Documentation Center Cameron Station Alexandria, Virginia 22314	2
2.	Library, Code 0212 Naval Postgraduate School Monterey, California 93940	2
3.	Department Chairman, Code 52 Department of Electrical Engineering Naval Postgraduate School Monterey, California 93940	1
4.	Asst. Professor G. D. Ewing, Code 52Ew Department of Electrical Engineering Naval Postgraduate School Monterey, California 93940	2
5.	Asst. Professor R. W. Adler, Code 52Ab Department of Electrical Engineering Naval Postgraduate School Monterey, California 93940	1
6.	LCDR Sugihono Kadarisman Indonesian Navy Communication Center Jakarta, Indonesia c/o U.S. Defense Liaison Group Indonesia APO San Francisco 96356	1

23 MAR 76
25 JAN 77
S 9364
24420

156861
Thesis
K106 Kadarisman
c.1 Hybrid method of
single sideband signal
generation.